IRE
Transactions
on Microwave Theory and Techniques

Volume MTT-4 APRIL, 1956 Number 2

TABLE OF CONTENTS

PUBLISHED BY THE
essional Group on Microwave Theory and Techniques

IRE PROFESSIONAL GROUP ON

MICROWAVE THEORY AND TECHNIQUES

The Professional Group on Microwave Theory and Techniques is an association of IRE members with professional interest in the field of Microwave Theory and Techniques. All IRE members are eligible for membership and will receive all Group publications upon payment of the prescribed annual assessment of $2.00.

PGMTT Chapters

Baltimore	H. E. Schrank
Boston	Walter Rotman
Buffalo-Niagara	Frank Pelton
Albuquerque-Los Alamos	Sheldon H. Dike
Long Island	Robert Wegenroth
Philadelphia	S. M. King
Los Angeles	C. W. Chandler
Chicago	Clarence Arnow
Northern New Jersey	T. N. Anderson
San Francisco	K. Tomiyasu

IRE TRANSACTIONS

on Microwave Theory and Techniques

Published by the Institute of Radio Engineers, Inc., for the Professional Group on Microwave Theory and Techniques, at 1 East 79th Street, New York 21, New York. Responsibility for the contents rests upon the authors, and not upon the IRE, the Group, or its members. Prices per copy: IRE PGMTT members, $1.70; IRE members, $2.55; nonmembers, $5.10. Annual subscription price: IRE members, $8.50; colleges and public libraries, $12.75; nonmembers, $17.00.

Address all manuscripts to Theodore S. Saad, Sage Laboratories, 30 Guinan St., Waltham, Mass.

H. A. Wheeler

H. A. Wheeler was born in St. Paul, Minn., on May 10, 1903. In 1925, he received the degree of B.S. in Physics from George Washington University, and from 1925 to 1928 engaged in post-graduate study in the Physics Department of Johns Hopkins University.

After summer work with Professor Alan Hazeltine, Mr. Wheeler joined Hazeltine Corporation at its beginning in 1924, where he worked on the design of radio receivers. In 1926, he originated the diode detector and avc that came into common use in broadcast receivers. Later he specialized in fm and TV receivers; the latter work was awarded the Morris Liebmann Prize by the IRE in 1940. In 1939, he was appointed Vice-President and Chief Consulting Engineer of Hazeltine Electronics Corporation. During World War II, he worked on iff radar, for which he received the Navy Certificate of Commendation. Also he was active in the microwave developments that were later adopted in the dme sets now used for air navigation. He has more than 150 U. S. patents and many foreign patents.

In 1946, Mr. Wheeler started an independent engineering group, which in 1947 became Wheeler Laboratories, Inc., in Great Neck, N. Y. He is President of this company and the director of their activities. This group has specialized in the development and design of microwave components, assemblies and antennas, mainly for radar and guided missiles.

From 1929 to 1935, Mr. Wheeler computed and put into use various forms of the piston attenuator in a waveguide below cutoff. In those days before waveguides, he may have been the first to use the TE-10 mode in a rectangular pipe, now the most common mode in waveguides.

In that period, he also became active in the field of antennas. This led to the presentation of the principles of small antennas, and to such concepts as the "radiation power factor," the "radianlength," the "radiancircle" (the interception area of an isotropic radiator), and the "radiansphere" (the region in which the "near field" predominates).

In 1942, he published a study of the skin effect, including a simple derivation and some charts and rules that have come into common use.

His interest in transmission lines led to his early use of circle diagrams and reflection charts. One of those was his transition-loss chart published in 1936. Later he promoted the use of the "loss circle" for measuring the attenuation in either a linear network or a superheterodyne converter. About 1942, he computed and designed strip lines between parallel planes and put them into service in trombones.

Mr. Wheeler's more recent interest in waveguides has led to various developments, such as the step twist (fixed or rotary) and the waveguide spark gap (hemispheres). He introduced the term "port" to describe either a hole in a waveguide or a pair of terminals in a wire circuit.

In a series entitled "Wheeler Monographs," he has presented various topics related to circuit theory, circle diagrams, powdered iron, transmission lines, and other subjects. The first collection of these papers was published as Volume I in 1953.

During the past few years, Mr. Wheeler has been devoting some attention to the conformal mapping of fields, in an effort to present the subject in more useful forms. This places emphasis on the equivalence of various contours, and on ways of expressing their simplest properties.

He is a Fellow of IRE and has served on the Board of Directors. He is also a Fellow of AIEE and an Associate Member of IEE. He is now a member of the Administrative Committee of the PGMTT.

Microwave Engineering—Is It Specialization or Diversification?

H. A. WHEELER*

When a college graduate is considering employment in the field of microwaves, he often asks us, "Wouldn't it be a mistake to specialize so early in my career?"

Before World War I, when I was a boy, I decided to "specialize" in "wireless." I don't know why. No one conceived that wireless would blossom out into the tremendous field that today is embraced in the Institute of Radio Engineers. By the time I graduated from engineering school in 1925, radio broadcasting had already got out of hand and was being brought under control. But all frequencies above 1.5 megacycles were relegated to the amateurs because "they had no practical value."

The field of microwaves today probably occupies the attention of more engineers than did radio broadcasting in its period of most active growth. The microwave professional group has 2,000 members, which places it among the top 6 of the 24 "specialized" groups now active (the top one is that of electronic computers, with 4,000 members). The microwave group has as many members and as diversified activities as the entire IRE had 30 years ago. We have only the faintest conception of the future of microwaves.

The engineering graduate, embarking on his career, is going to do his first useful work on a specific problem. In proportion to his abilities and opportunities, he will become more productive and more versatile. His tools are his method of thinking and the principles he will come to appreciate. He will try to apply his talents where the results will be most satisfying.

He will do his best in a stimulating environment, working on a fascinating subject. Microwaves is a fascinating subject that has brought together many talented workers to form the stimulating environment. They have just enough specialization to be recognized as a fraternity with a common denominator.

The field of microwaves may be identified with either of two physical principles, both effective in about the same frequency range. One is the utilization of wave propagation through hollow waveguides. The other is the utilization of transit time in electron streams.

The present frequency range of microwaves is roughly 500 to 100,000 megacycles, which does not sound very "specialized." Waveguide sizes range from 15 inches to 0.1 inch in width. The largest are formed of sheet aluminum, the smallest are drawn of solid silver. The most concentrated activity has been in the so-called "*X*-band" around 10,000 megacycles. In this band, electron-tube voltages range from 300 volts for low power of .03 watt, up to 100,000 volts for pulse power of one megawatt. A few further examples will give some idea of the diversified knowledge and experience that is acquired and utilized in this field.

We borrow from the techniques of sound waves in air, and we go much deeper in refinement. In size, they are comparable with microwaves. Sound waves and microwaves are carried through pipes and are radiated from horns. They are resonated in hollow cavities. However, microwaves are propagated in the medium of free space, which is perfectly stable. Their velocity is a million times as great, so their frequencies are a million times as great.

Also we borrow from the techniques of light waves, which are much smaller waves in the same medium, free space. Optical focusing by reflectors and lenses is approximated in microwave beam antennas. The best reflector in optics is a polished silver surface; the reflection of microwaves by the same surface is even closer to perfection.

While microwaves are finding a wide variety of applications, the most spectacular are in the many kinds of radar for war and peace. The military radar was first intended to perform functions previously allocated to sound detectors and searchlights.

But microwaves in radar have succeeded where both sound and light failed, in the all-weather detection of enemy aircraft. Radar operates over ranges of hundreds of miles. It accomplishes not only detection, but instantaneous display in distance and direction, and finally automatic tracking. This last especially is needed for guiding a missile to a target. The same principles are applied to friendly craft in air navigation and blind flying for all-weather transportation. The smaller microwaves are reflected in some degree by clouds and rainfall, so they are put to work scanning the weather for miles around.

The most remarkable generator of microwaves is the magnetron developed during World War II. It is analogous to a power alternator. A typical magnetron for *X*-band has a "stator" or anode with 16 poles that resonate with the intervening slots. The "shaft" is a hot cathode making available many amperes of electrons. An external permanent magnet provides a stationary field parallel to the cathode. When a high-voltage pulse is applied between cathode and anode, the electrons are

* Wheeler Laboratories, Great Neck, N. Y.

pulled into cycloidal orbits which quickly assume an orderly form like an 8-pole "rotor," turning about the shaft at a billion revolutions per second. After a thousand turns, the applied pulse is over, and the rotor collapses. This entire operation lasts only one microsecond, and may be repeated a thousand times a second. During the pulse, the power output is $\frac{1}{4}$ megawatt.

For detection of microwaves, the obsolete crystal rectifier was reborn in a stable form. The crystal diode now has become a common tool; the research in its materials and behavior led the way to the "transistor," which is one of the wonders of this generation.

An iron surface has no particular use in microwaves. But powdered iron, developed for reducing eddy-current losses at lower frequencies, finds application as a material used for absorbing microwaves. The latest form of iron, ferrites, exhibits a most remarkable property toward microwaves: when subjected to a superimposed constant magnetic field, it has a gyromagnetic behavior that causes a phase shift of waves passing through. This has enabled the design of a waveguide that passes microwaves in one direction only.

Air and other gases determine the insulation strength in microwave components. Increasing the air pressure increases the pulse power capacity. Conversely, gases at reduced pressure are used in some components to provide an automatic switch that closes at the instant when sparking or arcing is caused by the transmitter pulse.

In propagation through the air, molecular resonance causes absorption of the shorter microwaves. This same principle enables gas analysis in waveguides by observing the absorption at certain frequencies. Also it has been used in the molecular clock based on the resonance of the ammonia molecule.

The high frequencies of microwaves make available many wide-band channels, each useful for the communication of one television signal or hundreds of voice signals. Low-power focused beams of microwaves are now relaying such channels all over the United States, especially for television networks. Much progress has been made toward enclosing these microwave paths in metal pipes, protected from the weather and interfering waves.

In radio astronomy, the largest light telescope (Palomar, 200-inch) has been dwarfed by the 600-inch radio telescope at the Naval Research Laboratory, and much larger ones are under construction. In the past few years, microwave telescopes have observed large regions of space which are obscured to light waves by intervening clouds; also they have discovered "radio stars" which radiate microwaves but no visible light.

In nuclear science, microwaves perform many functions. One of the most spectacular is the motive force for the linear accelerator at Stanford University, which ejects electrons having nearly a billion electron-volts of energy.

The future of microwaves will see techniques and applications which are beyond today's imagination. Like many other branches of science and engineering, the field of microwaves offers endless opportunity.

To the college graduate, we of the microwave group offer one field of activity with a great variety of problems to be solved and a great need for imagination in perceiving and attacking the problems. If he is fascinated with the field, as we are, he is welcome to join us. He is welcome to call it specalization or diversification, whichever he prefers, and to pursue either as his objective.

Report of Advances in Microwave Theory and Techniques—1955

D. D. KING†

THE THEORY and techniques we wish to review comprise the transmission, control, measurement, and generation of microwaves. Excluded are antenna and propagation problems, as well as the specifically electronic aspects of microwave amplifiers and generators. To order the subjects being considered we have established the following broad headings: I. Waveguides; II. Gyromagnetic Media; III. Measurements; IV. Detection; V. Sources. Within each of these, more specific subdivisions help to classify the large number of papers which have appeared.

The large quantity of papers, and the attendant number of subdivisions needed to order them, are proof of the broad activity in the microwave field. However, what was once considered a small area has thereby been subdivided into even smaller parts. In this review, we have provided many subcategories in order to show more clearly the different directions of effort in the microwave field. We hope this does not lend support to the superspecialist, interested only in say TE_{01n} mode reaction wavemeter design in the *p*-band. To the reader with such limited interests we must address a warning: our discussion is not cross-referenced, and waveguide measurements on gyromagnetic media might be listed under I, II, or III depending on relative emphasis.

I. Waveguides

The term "waveguide" is gradually being freed from its early identification with hollow metal pipes. The literal definition—anything that guides an electromagnetic wave—properly includes the variety of structures now coming into use. Some of these guides bear little resemblance to the rectangular pipes that first bore the name waveguide. However, the structure enjoying the most rapid development harks back to the period when only the principal (TEM) mode was known to transmission engineers. The terms stripline, microstrip, planar transmission line, and other similar names are applied to various modifications of a structure supporting only TEM waves between flat metal strips.

Striplines

The characteristic impedance of a line consisting of one or two long thin strips placed between two relatively broad conducting planes has been successfully calculated. The attenuation of several such structures has also been evaluated. The calculations involve suitable transformations in the complex plane of the line cross-section.

[1] D. Park, "Planar transmission lines," Trans. IRE, vol. MTT-3, pp. 8–12; April, 1955.
[2] D. Park, "Planar transmission lines—II," Trans. IRE, vol. MTT-3, pp. 7–11; October, 1955.
[3] J. M. C. Dukes, "Characteristic impedance of air-spaced strip transmission line," Proc. IRE, vol. 43, p. 876; July, 1955. (Correspondence)
[4] B. A. Dahlman, "A double-ground-plane strip-line system for microwaves," *Jour. IEE*, vol. 102, part B, pp. 488—492; July, 1955. Also Trans. IRE, vol. MTT-3, pp. 52–57; October, 1955.
[5] W. H. Hayt, Jr., "Potential solution of a homogeneous strip-line of finite width," Trans. IRE, vol. PGMTT-3, pp. 16–18; July, 1955.
[6] E. Burshtein and L. Solov'ev, "Propagation of a fundamental wave between parallel surfaces," *C. R. Acad. Sci. (URSS)*, vol. 101, pp. 465–468; March 21, 1955. (In Russian).

The development of circuit components in striplines is proceeding rapidly. The simple structure and ease of manufacture of striplines is perhaps even more evident in the component field. Filters and directional couplers with excellent performance are very simply fabricated in strip form.

[7] M. Arditi and J. Elefant, "Microstrip applied to band-pass microwave filters," *Elec. Commun.*, vol. 32, pp. 52–61; March, 1955.
[8] S. B. Cohn, "Shielded coupled-strip transmission line," Trans. IRE, vol. MTT-3, pp. 29–38; October, 1955.

By replacing the closely confined TEM mode with the loosely bound HE_{11} or dipole mode of a dielectric rod, a millimeter-wave version of strip lines is obtained. Here, half of a dielectric rod is placed on a metal image surface. Some success at circuit components in this system is also being achieved.

[9] D. D. King, "Circuit components in dielectric image lines," Trans. IRE, vol. MTT-3, pp. 35–39; December, 1955.

Surface Waves

The wave of the image surface of the dielectric line mentioned above is a type of surface wave. The study of surface waves in general is important both for waveguide applications and for antennas. The surfaces being studied include dielectric rods and tubes, dielectric coated wires, as well as metal sheets and cylinders.

[10] P. Mallach, "Investigations on dielectric waveguides in rod or tube form," *Fernmeldetech. Z.*, vol. 8, pp. 8–13; January, 1955.
[11] G. Piefke, "Theory of the harms-goubau wire waveguide at metre wavelengths," *Arch. elekt. Übertragung*, vol. 9, pp. 81–93; February, 1955.
[12] H. E. M. Barlow and A. E. Karbowiak, "An experimental investigation of axial cylindrical surface waves supported by capactive surfaces," *Jour. IEE*, vol. 102, part B, pp. 313–322; May, 1955.
[13] G. J. Rich, "The launching of a plane surface wave," *Jour. IEE*, vol. 102, part B, pp. 237–246; March, 1955.
[14] R. S. Elliott, "Azimuthal surface waves on circular cylinders," *J. Appl. Phys.*, vol. 26, pp. 368–376; April, 1955.
[15] A. E. Karbowiak, "On the surface impedance of a corrugated waveguide," *Jour. IEE*, vol. 102, part B, pp. 501–502; July, 1955.

† Radiation Lab., Johns Hopkins University, Baltimore 18, Md.

The experimental investigations by Barlow and Karbowiak have produced particularly interesting results. These authors have succeeded in launching on a dielectric rod a surface wave with phase velocity greater than the velocity of light. This result tends to support the conclusion that a Zenneck wave can exist over the earth's surface. Experimental evidence for this wave has been lacking, although theoretical arguments on it date back to Zenneck's early work in 1907.

Artificial Dielectrics

The control of microwaves by artificial dielectrics brings us close to the border between radiation and guided waves. The applications of artificial dielectrics are probably largely in the design of horns, lenses and other antennas. However, we include references to microwave work in periodic structures.

[16] J. Brown and W. Jackson, "The properties of artificial dielectrics at centimetre wavelengths," *Jour. IEE*, vol. 102, part B, pp. 11–16; January, 1955.
[17] M. M. Z. El-Kharadly, "Some experiments on artificial dielectrics at centimetre wavelengths," *Jour. IEE*, vol. 102, part B, pp. 17–23; January, 1955.
[18] R. I. Primich, "A general experimental method to determine the properties of artificial media at centimetre wavelengths, applied to an array of parallel metallic plates," *Jour. IEE*, vol. 102, part B, pp. 26–36; January, 1955.
[19] J. Brown and W. Jackson, "The relative permittivity of tetragonal arrays of perfectly conducting thin discs," *Jour. IEE* vol. 102, part B, pp. 37–42; January, 1955.

Periodic Structures

The artificial dielectrics mentioned above are periodic structures in three dimensions. One dimensional periodicity along a waveguide also produces a new set of properties. The resulting slow waves are particularly important in electron beam devices. However, the basic theory of the isolated guide is receiving considerable attention.

[20] S. Sensiper, "Electromagnetic wave propagation on helical structures (A review and survey of recent progress)," Proc. IRE, vol. 43, pp. 149–161; February, 1955.
[21] M. Müller, "Application of recurrent-network equivalent circuit in determining the attenuation of helical transmission lines loaded by resistive coatings," *Fernmeldetech. Z.*, vol. 8, pp. 29–34; January, 1955.
[22] C. C. Grosjean and V. J. Vanhuyse, "Experimental verification of a frequency equation for corrugated waveguides," *Nuovo Cim.*, vol. 1, pp. 193–200; January 1, 1955.
[23] C. C. Grosjean, "On the theory of circularly symmetric TM waves in infinite iris-loaded guides," *Nuovo Cim.*, vol. 1, pp. 427–438; March 1, 1955. (In English).
[24] V. J. Vanhuyse, "On the (β_0, k) diagrams for circularly symmetric TM waves in infinite iris-loaded waveguides," *Nuovo Cim.*, vol. 1, pp. 447–452; March 1, 1955. (In English).
[25] V. J. Vanhuyse, "On the proper frequencies of terminated corrugated waveguides," *Physica*, vol. 21, pp. 269–280; April, 1955; *ibid.*, vol. 32, p. 603; July, 1955.
[26] A. J. Simmons, "Phase shift by periodic loading of waveguide and its application to a broadband circular polarization," Trans. IRE, vol. MTT-3, pp. 18–21; December, 1955.

Hollow Waveguides

Extensions and refinements of the theory of hollow waveguides continue to appear in large numbers. Among the most welcome refinements is an exact treatment of hollow waveguides with finite wall conductivity.

[27] A. E. Karbowiak, "Theory of imperfect waveguides: The effect of wall impedance," *Jour. IEE*, vol. 102, part B, pp. 698–708; September, 1955.

Here the fields in the guide are matched to the surface impedance of the metal at the guide wall. In addition to confirming the standard approximate results, this theory provides valuable information on mode purity in an imperfect guide. Thus, in the rectangular case, only TE_{0n} and TE_{m0} modes can propagate down a uniform imperfect guide without change in form, *i.e.*, without conversion to other modes. In circular guides the purity of both TE_{0n} and TM_{0m} is unimpaired by wall losses.

An interesting analog for the cutoff parameters of hollow guides with arbitrary cross-section has been described.

[28] P. R. Clement and W. C. Johnson, "A distributed electrical analog for waveguides of arbitrary cross section," Proc. IRE, vol. 43, pp. 89–92; January, 1955.

Here a thin parallel-plate resonator is constructed whose end plates have the shape of the guide cross section. The resonant frequency of the resonator is simply related to the cutoff frequency of the guide. Either TE and TM modes are handled by open or short circuiting the edges of the closely spaced plates.

Perturbations in the uniformity of hollow guides lead to a variety of analytical complications. A fair share of these are listed in the following references:

[29] L. Lewin, "Propagation in curved and twisted waveguides of rectangular cross-section," *Jour. IEE*, vol. 102, part B, pp. 75–80; January, 1955.
[30] M. Jouguet, "Problems of propagation in cylindrical systems," *Câbles B. Trans.*, vol. 9, pp. 3–39; January, 1955.
[31] J. Kornfeld, "Stability of the H_{01} mode in circular waveguides, and the occurrence of harmonic modes on deformation to an elliptical cylinder," *Arch. elekt. Übertragung*, vol. 9, pp. 29–38; January, 1955.
[32] P. I. Sandsmark, "Effect of ellipticity on dominant-mode axial ratio in nominally circular waveguides," Trans. IRE, vol. MTT-3, pp. 15–20; October, 1955.

Dielectric filling and end-effects are also treated in several papers.

[33] S. K. Chatterjee, "Propagation of microwave through an imperfectly conducting cylindircal guide filled with an imperfect dielectric," *Jour. Indian Inst. Sci.*, Section B, vol. 37, pp. 1–9; January, 1955.
[34] J. W. Carr, "Transverse electric Resonances in a coaxial line containing two cylinders of different dielectric constant," Trans. IRE, vol. MTT-3, pp. 41–44; July, 1955.
[35] V. Pfirrmann, "The Behavior of the Open End of a Coaxial Line," *Arch. elekt. Übertragung*, vol. 9, pp. 8–12; January, 1955.

Ridges and Steps

An important variant of rectangular guide is ridge guide. More precise calculations of its parameters and continued favor in practical applications are shown by the references below.

[36] H. G. Unger, "Calculations for ridge waveguides," *Arch. elekt. Übertragung*, vol. 9, pp. 157–161; April, 1955.
[37] S. Hopfer, "The design of ridged waveguides," Trans. IRE, vol. MTT-3, pp. 20–29; October, 1955.
[38] T. G. Mihran, "Impedance of open- and closed-ridge waveguide," Proc. IRE, vol. 43, p. 1014; August, 1955. (Correspondence.)
[39] T. N. Anderson, "Double-ridge waveguide for commercial airlines weather radar installation," Trans. IRE, vol. MTT-3, pp. 2–9; July, 1955.

Proceeding from a ridge along the guide axis to transverse steps, we encounter two papers which fill a long standing need.

[40] R. E. Collin, "Theory and design of wide-band multisection quarter-wave transformers," PROC. IRE, vol. 43, pp. 179–185; February, 1955.
[41] S. B. Cohn, "Optimum design of stepped transmission-line transformers," TRANS. IRE, vol. MTT-3, pp. 16–21; April, 1955.

The authors here independently arrive at an optimum design for quarter-wave transformers. As might be suspected, Tchebycheff distributions appear in the result instead of the previously accepted binomial steps.

However, the binomial rule is still useful. Thus, a skillful application of modified binomial stepping to twists has resulted in tremendous savings in space and bandwidth for this waveguide component.

[42] H. A. Wheeler and H. Schwiebert, "Step-twist waveguide components," TRANS. IRE, vol. MTT-3, pp. 44–52; October, 1955.

Directional Couplers, Junctions, and Other Circuit Elements in Waveguide

Significant advances are being made in the methods of coupling two guides. By tapering the phase velocity in the coupled guides, efficient directional couplers have been built covering three or more octaves. A more general method of coupling involves periodically varying both the velocities and the coupling. If such a coupler can be many wavelengths long, it can be made completely insensitive to frequency.

[43] J. S. Cook, "Tapered velocity couplers," *Bell Sys. Tech. Jour.*, vol. 7, pp. 807–822; July, 1955.
[44] A. G. Fox, "Wave coupling by warped normal modes," *Bell Sys. Tech. Jour.*, pp. 823–852; July, 1955.
[45] W. H. Louisell, "Analysis of the singe tapered mode coupler," *Bell. Sys. Tech. Jour.*, pp. 853–870; July, 1955.

Another type of broadband coupler has been devised for dominant mode waveguides. Here the field is gradually concentrated on ridges or fins in the guide, and then transferred to the coupled guide.

[46] S. D. Robertson, "The ultra-bandwidth fineline coupler," PROC. IRE, vol. 43, pp. 739–741; June. 1955.

Analysis of more conventional couplers has also proceeded apace.

[47] G. D. Monteath, "Coupled transmission lines as symmetrical directional couplers," *Jour. IEE*, vol. 102, part B, pp. 383–392; May, 1955.
[48] R. C. Knechtli, "Further analysis of transmission-line directional couplers," PROC. IRE, vol. 43, pp. 867–869; July, 1955.
[49] P. Andrews, "A simple waveguide directional coupler," *Jour. Brit. IRE*, vol. 15, pp. 112–116; February, 1955.

Directional couplers are a special class of junctions. Some work on other junction types in hollow waveguide has also been published.

[50] W. K. Kahn, "*E*-plane forked hybrid-T junction," TRANS. IRE, vol. MTT-3, pp. 52–58; December, 1955.
[51] M. A. Meyer and H. B. Goldberg, "Applications of the turnstile junction," TRANS. IRE, vol. MTT-3, pp. 40–45, December, 1955.
[52] A. F. Harvey, "Standard waveguides and couplings for microwave equipment," *Jour. IEE*, vol. 102, part B, pp. 493–500; July, 1955.

The need for more complex junctions is one aspect of the trend toward higher modes and multiple modes of polarizations in hollow guides. More convenient application of microwave filter design is another evidence of this trend.

[53] H. N. Dawirs, "Graphical filter analysis," TRANS. IRE, vol. MTT-3, pp. 15–21; January, 1955.
[54] H. N. Dawirs, "A chart for analyzing transmission-line filters from input impedance characteristics," PROC. IRE, vol. 43, part I, pp. 436–443; April, 1955.

Resonant cavities are an important element both in microwave circuits and oscillators. A more complete analysis of radial and reentrant resonators has taken place during the year.

[55] J. R. Whinnery and D. C. Stinson, "Radial Line discontinuities," PROC. IRE, vol. 43, pp. 46–51; January, 1955.
[56] D. C. Stinson, "Resonant frequencies of higher-order modes in radial resonators," TRANS. IRE, vol. MTT-3, pp. 18–23; July, 1955.
[57] E. L. Ginzton and E. J. Nalos, "Shunt impedance of klystron cavities," TRANS. IRE, vol. MTT-3, pp. 4–7; October, 1955.

A basic mathematical point in the theory of cavity resonators has also been clarified. This concerns the completeness of the set of modes used to describe the field in a resonator. The need for including the dc (irrotational) field is often overlooked. Only under special conditions is this permissible.

[58] S. A. Schelkunoff, "On representation of electromagnetic fields in cavities in terms of natural modes of oscillation," *J. Appl. Phys.*, vol. 26, pp. 1231–1234; October, 1955.

The analysis of microwave circuits often proceeds most conveniently by matrix methods. A particularly effective example of this appeared in the study of circular polarization in a cavity.

[59] M. Tinkham and M. W. P. Standberg, "The excitation of circular polarization in microwave cavities," PROC. IRE, vol. 43, pp. 734–738; June, 1955.
[60] E. W. Matthews, Jr., "The use of scattering matrices in microwave circuits," TRANS. IRE, vol. MTT-3, pp. 21–26; April, 1955.
[61] B. Beghlin, "The matrix equation of loss-free exponential lines," *Compt. Rend. Acad. Sci.* (Paris), vol. 240, pp. 168–170; January 10, 1955.

II. GYROMAGNETIC MEDIA

The introduction of gyromagnetic media has produced a revolution in microwave circuits. A new class of components has become possible, based on the usual equivalent circuit elements plus a new one, the gyrator. The nonreciprocal components based on the gyrator are, perhaps, the most spectacular. However, a new class of both reciprocal and nonreciprocal circuit elements is emerging. In addition to performing hitherto impossible functions, these devices are often susceptible to convenient electrical control through the applied magnetic field.

The central problem in the field of gyromagnetic microwave circuits is the behavior of a waveguide containing gyromagnetic material. The analysis of this problem, usually in terms of a ferrite, is proceeding actively.

[62] M. A. Gintsburg, "The anisotropic waveguide," *Zh. Tekh, Fiz.*, vol. 25, pp. 358–363; February, 1955.
[63] A. Chevalier, T. Kahan, and E. Polacco, "Propagation of electromagnetic waves in an anisotropic gyromagnetic medium in a rectangular waveguide," *Compt. Rend. Acad. Sci.* (Paris), vol. 240, pp. 1323–1324; March 21, 1955.
[64] L. M. Vallese, "Understanding the gyrator," PROC. IRE, vol. 43, part I, p. 483; April, 1955. (Correspondence.)
[65] N. G. Sakiotis, H. N. Chait, and M. L. Kales, "Nonlinearity of propagation in ferrite media," PROC. IRE, vol. 43, p. 1011; August, 1955. (Correspondence.)

[66] B. Laux and K. J. Button, "Theory of new ferrite modes in rectangular wave guide," *J. Appl. Phys.*, vol. 26, pp. 1184–1185; September, 1955. (Correspondence.)
[67] B. Lax and K. J. Button, "New ferrite mode configurations and their applications," *J. Appl. Phys.*, vol. 26, pp. 1186–1187; September, 1955. (Correspondence.)
[68] A. D. Berk and B. A. Lengyel, "Magnetic fields in small ferrite bodies with applications to microwave cavities containing such bodies," PROC. IRE, vol. 43, pp. 1587–1591; November, 1955.

Some of the practical results of the ferrite revolution in circuit elements are described in the papers listed below. These include circulators, isolators, attenuators, couplers, and switches.

[69] C. Stewart, "Some applications and characteristics of ferrite at wavelengths of 0.87 cm and 1.9 cms," TRANS. IRE, vol. MTT-3, pp. 27–31; April, 1955.
[70] J. A. Rich and S. E. Webber, "Ferrite atttenuators in helixes," PROC. IRE, vol. 43, pp. 100–101; January, 1955. (Correspondence.)
[71] J. B. Gunn and C. A. Hogarth, "A novel microwave attenuator using germanium," *J. Appl. Phys.*, vol. 26, pp. 353–354; March, 1955.
[72] R. W. Damon, "Magnetically controlled microwave directional coupler," *J. Appl. Phys.*, pp. 1282–1283; October, 1955. (Correspondence.)
[73] R. F. Sullivan and R. C. LeCraw, "New type ferrite microwave switch," *J. Appl. Phys.*, pp. 1282–1283; October, 1955. (Correspondence.)

Basic to the success of these devices are the properties of the ferrite material itself. New data on the characteristics of various ferrites as a function of frequency has been gathered by several observers.

[74] A. Nishioka and H. Okamoto, "Measurement of the complex permeability of carbonyl iron powders at 4,000 mc/s," *J. Phys. Soc. Japan*, vol. 10, p. 79; January, 1955.
[75] H. Suhl, "Ferromagnetic resonance in nickel ferrite between one and two kilomegacycles (per second)," *Phys. Rev.*, vol. 97, pp. 555–557; January 15, 1955.
[76] H. Suhl, L. G. Van Uitert, and J. L. Davis, "Ferromagnetic resonance in magneisum-manganese aluminum ferrite between 160 and 1,900 mc," *J. Appl. Phys.*, vol. 26, pp. 1180–1182; September, 1955. (Correspondence.)
[77] B. Lax, "Figure of merit for microwave ferrites at low and high frequencies," *J. Appl. Phys.*, vol. 26, p. 919; July, 1955. (Correspondence.)

The losses observed in ferromagnetic resonance are particularly important, both theoretically and in applications. The absorption losses and domain motion have been studied and a theory developed to account for the observed effects.

[78] A. M. Cloyston, "Relaxation phenomena in ferrites," *Bell Sys. Tech. Jour.*, pp. 739–760; July, 1955.
[79] F. Brown and C. L. Gravel, "Direct observation of domain rotation in ferrites," *Phys. Rev.*, vol. 98, pp. 442–448; April 15, 1955.
[80] J. Smit and H. G. Beljers, "Ferromagnetic resonance absorption in $BaFe_{12}O_{19}$ a highly anisotropic crystal," *Phillips Res. Rep.*, vol. 10, pp. 113–130; April, 1955.

Specific properties such as temperature dependence and saturation have direct application to component design. These, of course, are also being studied.

[81] B. J. Duncan and L. Swern, "Temperature dependence of the microwave properties of ferrites in waveguide," PROC. IRE, vol. 43, pp. 623–624; May, 1955. (Correspondence.)
[82] L. G. Van Uitert, "Low magnetic saturation ferrites for microwave applications," *J. Appl. Phys.*, vol. 26, pp. 1289–1290; November, 1955.

III. MEASUREMENTS

The number of quantities which can be measured to advantage in the microwave region has not increased in the past year. However, the techniques for performing the measurements continue to advance and multiply. In all of the classes of measurements we shall consider, we are potentially better instrumented than ever before.

Impedance Measurement

Point-by-point impedance data is inadequate for most broad-band components and systems. Perhaps the most desirable display of data for the engineer is a locus plotted on the reflection-coefficient plane or Smith chart. A very elegant solution of this problem was described during 1955. The waveguide equipment makes use of square-law product detectors to multiply unknown and reference signals. Output voltages are placed on the deflection plates of an oscilloscope to trace the desired locus of z in the ρ-plane. The compact system utilizes five hybrid junctions in standard waveguide form. The 12 per cent band of the X-band guide is covered without need for adjustment.

[83] Henry L. Bachman, "A waveguided impedance meter for the automatic display of complex reflection coefficient," TRANS. IRE, vol. MTT-3, pp. 22–30; January, 1955.

Two rather comprehensive surveys of special impedance measuring methods also appeared during the year.

[84] A. Lebrun, "Techniques for the measurement of impedances at Metre and decimetre wavelengths and their use for studying the dielectric properties of solids and liquids," *Ann. Phys.* (Paris), vol. 10, pp. 16–70; January/February, 1955.
[85] H. Severin, "The squeeze section, a simple and universal measurement apparatus for centimetre wavelengths," *Tech. Mitt. schweiz Telegn-Teleph. Verw*, vol. 33, pp. 130–135; March 1, 1955. (In German.)

Power Measurement

Bolometers and thermistors are the principal means for measuring microwave power. Improvements in their calibration and performance continue to be recorded.

[86] M. Sucher and H. J. Carlin, "The operation of bolometers under pulsed power conditions," TRANS. IRE, vol. MTT-3, pp. 45–52; July, 1955.
[87] J. A. Lane, "The measurement of power at a wavelength of 3 cm by thermistors and bolometers," PROC. IRE, part B, vol. 102, pp. 819–824; November, 1955.

A new self-balancing bridge for these elements is also reported.

[88] Glenn F. Engen, "A Self-Balancing D-C Bolometer Bridge," presented at URSI meeting, Washington, D. C., May 4, 1955.

A different approach to power measurement in the milliwatt region relies on a differential air thermometer coupled to the standard and unknown power absorbers. Glass cells containing carbon strips serve to dissipate the power. These are joined through a capillary containing a liquid pellet. The position of the pellet registers differential pressure and hence differential power.

[89] A. C. Gordon-Smith, "A milliwattmeter for centimetre wavelengths," *Jour. IRE*, vol. 102, part B, pp. 685–686; September, 1955.

For high power measurements, a calorimeter is required. A new load for this service has been developed.

[90] W. Hersch, "A very wide-band dummy load for measuring power at very-high and ultra-high frequencies," *Jour. IEE*, vol. 102, part B, pp. 96–98; January, 1955.

Amplitude and Phase Measurements

Although often combined in impedance data, the amplitude and phase of a signal are often sought separately. The near field of a radiator or the field within a resonator are examples of a situation where such data is desirable. Probe methods as well as indirect scattering techniques have been described for this problem.

[91] J. H. Richmond and T. E. Tice, "Probes for microwave near-field measurements," TRANS. IRE, vol. MTT-3, pp. 32–34; April, 1955.
[92] J. S. Ajioka, "A microwave phase contour plotter," PROC. IRE, vol. 43, pp. 1088–1090; September, 1955.
[93] J. H. Richmond, "A modulated scattering technique for measurement of field distributions," TRANS. IRE, vol. MTT-3, pp. 13–15; July, 1955.
[94] J. G. Linhart and T. H. B. Baker, "A method of measuring the intensity distributions of radio-frequency electric and magnetic fields in resonant cavities," *Brit. J. Appl. Phys.*, vol. 6, pp. 100–103; March, 1955.
[95] S. W. Kitchen and A. D. Schelberg, "Resonant-cavity field measurements," *J. Appl. Phys.*, vol. 26, pp. 618–621; May, 1955.

Another application of phase and amplitude methods is in permittivity measurements.

[96] T. J. Buchanan and E. H. Grant, "Phase and amplitude balance methods for permittivity measurements between 4 and 50 cm," *Brit. J. Appl. Phys.*, vol. 6, pp. 64–66; February, 1955.

A single rotating probe can combine the amplitude and phase measurements to yield standing-wave data.

[97] F. J. Tischer, "Rotatable inductive probe in waveguides," PROC. IRE, vol. 43, pp. 974–980; August, 1955.

Direct determination of amplitude and phase by coherent detection in a hybrid junction is also conveniently accomplished.

[98] J. H. Richmond, "Measurement of time-quadrature components of microwave signals," TRANS. IRE, vol. MTT-3, pp. 13–15; April, 1955.

Four-Pole Measurements

The four-pole is the basic element for transmission networks. Direct measurement of four-pole parameters is therefore of the greatest importance. The treatment of loss in a four-pole has been the subject of several papers. In one of these, the general dissipative four-pole is represented by a new equivalent circuit consisting of a lossy section of transmission line with ideal transformers at each end. This representation is particularly well adapted to precise analysis by the methods of Weissfloch (tangent method) and Deschamps.

[99] H. M. Altschuler, "A method of measuring dissipative four-poles based on a modified Wheeler network," TRANS. IRE, vol. MTT-3 pp. 30–36; January, 1955.

The preceding method is well adapted to networks having considerable loss. Where very small losses are encountered, the measuring procedure can be modified to advantage by the inclusion of a lossy shunt element. This reduces the standing waves to more convenient values for measurement. Proper analysis of the data permits extraction of the original low-loss parameters.

[100] H. M. Altschuler and A. A. Oliner, "A shunt technique for microwave measurements," TRANS. IRE, vol. MTT-3, pp. 24-30; July, 1955.

Four-pole techniques are also well adapted to measuring insertion loss, the location of discontinuities, and dielectric constants.

[101] K. Tomiyasu, "Intrinsic insertion loss of a mismatched microwave network," TRANS. IRE, vol. MTT-3, pp. 40–44; January, 1955.
[102] O. T. Neau, "A practical method of locating waveguide discontinuities," TRANS. IRE, vol. MTT-3, pp. 45–46; January, 1955. (Correspondence.)
[103] A. A. Oliner and H. M. Altschuler, "Methods of measuring dielectric constants based upon a microwave network viewpoint," *J. Appl. Phys.*, vol. 26, pp. 214–219; February, 1955.

A new class of four-poles, the nonreciprocal, has also made its appearance in circuit components. Preliminary work shows that extension of present methods to this type of four-pole should proceed without difficulty.

[104] A. C. Macpherson, "Measurement of microwave nonreciprocal four-poles," PROC. IRE, vol. 43, p. 1017; August, 1955.

Cavity Techniques

Resonant cavities have long been used with success in measuring magnetic properties. Refinements in this technique are continuing.

[105] E. G. Spencer and R. C. LeCraw, "Wall effects on microwave measurements of ferrite spheres," *J. Appl. Phys.*, vol. 2, p. 250; February, 1955. (Correspondence.)
[106] J. Uebersfeld, "Various ways of using cavity resonators in paramagnetic resonance," *J. Phys. Rad.*, vol. 16, pp. 78–79; January, 1955.

Sending an electron beam through a cavity alters its electrical properties. Although this effect is fairly obvious, the magnitude of the tuning range obtainable with adequate Q has probably been unsuspected. An analysis of the problem and extensive supporting data have been presented in a paper.

[107] F. R. Arams and H. K. Jenny, "Wide-range electronic tuning of microwave cavities," PROC. IRE, vol. 43, pp. 1102–1110; September, 1955.

Special Techniques

The use of higher modes or of several polarizations of one mode in the same guide is becoming increasingly common. At the terminals of such a guide the proper separation of modes must then be accomplished. Several papers have appeared which describe successful attacks on this problem. From the present trend it appears that we shall be able to overcome most of the problems which have so far prevented exploitation of the full capacity of a hollow waveguide.

[108] A. C. Beck, "Measurement techniques for multimode waveguides," TRANS. IRE, vol. MTT-3, pp. 35–41; April, 1955.
[109] H. P. Raabe, "A rotary joint for two microwave transmission channels of the same frequency band," TRANS. IRE, vol. MTT-3, pp. 30–41; July, 1955.
[110] P. A. Crandell, "A turnstile polarizer for rain cancellation," TRANS. IRE, vol. MTT-3, pp. 10–15; January, 1955.

Circular polarization in a round guide induced by helices has been used to provide a convenient high-speed phase shifter. Here, the phase shift is proportional to the angular position of the helices.

[111] W. Sichak and D. J. Levine, "Microwave high-speed continuous phase shifter," PROC. IRE, vol. 43, pp. 1661–1663; November, 1955.

Millimeter wave techniques are also steadily advancing. Papers on this subject and the related problem of surface roughness in metal guides are listed below.

[112] W. E. Willshaw, H. R. L. Lamont, and E. M. Hickin, "Experimental equipment and techniques for a study of millimetre-wave propagation," *Jour. IEE*, vol. 102, part B, pp. 99–111; January, 1955.
[113] W. W. Balwanz, "A method of wavelength measurement for the microwave and millimeter wave regions," presented at URSI meeting, Washington, D. C., May 4, 1955.
[114] A. F. Harvey, "The electroforming of components and instruments for millimetre wavelengths," *Jour. IEE*, vol. 102, part B, pp. 223–230; March, 1955.
[115] A. F. Harvey, "A surface-texture comparator for microwave structures," *Jour. IEE*, vol. 102, part B, pp. 219–222; March, 1955.
[116] J. Allison and F. A. Benson, "Surface roughness and attenuation of precision-drawn, chemically polished, electropolished, electroplated, and electroformed waveguides," *Jour. IEE*, vol. 102, part B, pp. 251–252; March, 1955.

IV. Detection and Noise Sources

The principal microwave detector is the crystal diode. Improved schemes for measuring its noise temperature and optimizing mixer performance have been advanced during the year.

[117] R. E. Davis and R. C. Dearle, "A method for the accurate measurement of the noise temperature ratio of microwave mixer crystals," Trans. IRE, vol. MTT-3, pp. 27–35; December, 1955.
[118] W. L. Pritchard, "Notes on a crystal mixer performance," Trans, IRE, vol. MTT-3, pp. 37–39; January, 1955.

The thermionic diode serving as a microwave detector has been analyzed in a new manner. Here it is shown that the space-charge limited diode can be considered as a velocity modulated detector when operated at microwaves.

[119] P. A. Redhead, "Microwave detection in a thermionic diode," Proc. IRE, vol. 43, pp. 995–1000; August, 1955.

The noise figures of radiometer circuits have been analyzed. Here, it appears that the use of two separate receivers with cross-correlated outputs provides somewhat better sensitivity than the original Dicke system.

[120] S. J. Goldstein, "A comparison of two radiometer circuits," Proc. IRE, vol. 43, pp. 1663–1666; November, 1955.

Noise sources are used principally to measure the noise figure of receivers. Of course, the physics of gas discharges is an interesting and important subject in itself. However, the papers on this subject listed below are largely concerned with the practical problem of obtaining an accurately known and useful noise output from a discharge.

[121] M. I. Skolnik and H. R. Puckett, Jr., "Relaxation oscillations and noise from low-current arc discharges," *J. Appl. Phys.*, vol. 26, pp. 74–79; January, 1955.
[122] W. H. Bostick and M. A. Levine, "Experiments on the behavior of an ionized gas in a magnetic field," *Phys. Rev.*, vol. 97, pp. 13–21; January 1, 1955.
[123] L. W. Davies and E. Cowcher, "Microwave and metro-wave radiation from the positive column of a gas discharge," *Aust. J. Phys.*, vol. 8, pp. 108–128; March, 1955.
[124] W. W. Mumford and R. L. Schafersman, "Data on the temperature dependence of X-band fluorescent lamp noise sources," Trans. IRE, vol. MTT-3, pp. 12–17; December, 1955.
[125] E. Maxwell and B. J. Leon, "Noise measurements in the UHF range," Trans. IRE, vol. MTT-3, p. 62; December, 1955.

V. Generators

Oscillators and amplifiers of the future will cover broad bands. This is evident from the research now underway. The newer electron beam devices show the greatest promise in this respect, and are receiving a proportionate share of the total effort.

Electron Beam Devices

The interaction of an electron beam with a periodic structure is being studied from several points of view. Specific structures have been analyzed and built to provide oscillators and amplifiers. Most important among these at present is the backward wave oscillator or carcinotron. The crossed-field or M-type carcinotron is capable of powers in the hundreds of watts, electronically tunable over wide bands. The conventional backward-wave oscillator or O-type carcinotron exhibits excellent local oscillator characteristics over the same tuning range.

[126] R. R. Warnecke, P. Guenard, O. Doehler, and B. Epsztein, "The 'M'-type carcinotron tube," Proc. IRE, vol. 43, part I, pp. 413–424; April, 1955.
[127] H. R. Johnson, "Backward-wave oscillators," Proc. IRE, vol. 43, pp. 684–697; June, 1955.
[128] R. W. Grow and D. A. Watkins, "Backward-wave oscillator efficiency," Proc. IRE, vol. 43, pp. 848–856; July, 1955.
[129] W. V. Christensen and D. A. Watkins, "Helix millimeter-wave tube," Proc. IRE, vol. 43, pp. 93–96; January, 1955.

Traveling-wave amplifiers with minimum noise figure are also the object of numerous investigations.

[130] H. A. Haus and F. N. H. Robinson, "A minimum noise figure of microwave beam amplifiers," Proc. IRE, vol. 43, pp. 981–991; August, 1955.
[131] S. W. Harrison, "On the minimum noise figure of traveling-wave tubes," Proc. IRE, vol. 43, p. 227; February, 1955. (Correspondence.)
[132] T. E. Everhart, "Concerning the noise figure of a backward-wave amplifier," Proc. IRE, vol. 43, part I, pp. 444–449; April, 1955.

The use of dispersive backward-wave amplifiers for narrow-band service has been described. By cascading several dispersive amplifiers a high gain, narrow band, voltage tuned amplifier can be obtained. Recirculation schemes for higher gain have also been used successfully with broad band amplifiers.

[133] M. R. Currie and J. R. Whinnery, "The cascade backward-wave amplifier: A high-gain voltage-tuned filter for microwaves," Proc. IRE, vol. 43, pp. 1617–1631; November, 1955.
[134] F. R. Arams, "Traveling-wave tube system having multiplied gain," Proc. IRE, vol. 43, p. 102; January, 1955. (Correspondence.)

More general studies of the interaction between microwave circuits and electron beams include helical, hairpin, and other circuit designs.

[135] M. Chodorow and E. L. Chu, "Cross-wound twin helices for traveling-wave tubes," *J. Appl. Phys.*, vol. 26, pp. 33–43; January, 1955.
[136] A. Karp, "Traveling-wave tube experiments at millimeter wavelengths with a new, easily built, space harmonic circuit," Proc. IRE, vol. 43, pp. 41–46; January, 1955.
[137] J. R. Pierce, "Interaction of moving charges with wave circuits." *J. Appl. Phys.*, vol. 26, pp. 627–638; May, 1955.
[138] H. Heffner, "A coupled mode description of beam-type amplifiers," Proc. IRE, vol. 43, pp. 210–217; February, 1955.
[139] W. H. Louisell and J. R. Pierce, "Power flow in electron beam devices," Proc. IRE, vol. 43, part I, pp. 444–449; April, 1955.

New and sometimes radically different schemes for electron beam devices are being advanced. Two of these are listed below.

[140] Walter R. Beam, "On the possibility of amplification in space-charge-potential-depressed electron streams," PROC. IRE, vol. 43, pp. 454–462; April, 1955.
[141] H. Heffner, "The practicality of E-type traveling-wave devices," PROC. IRE, vol. 43, pp. 1007–1008; August, 1955.

Many of the new schemes are most promising for millimeter wave generation. The potential activity in this portion of the spectrum is very great; the precursors of this development are appearing in increasing numbers. Unfortunately, the efficiency of many of the proposed schemes is notoriously low.

[142] J. L. Farrands, "The generation of millimetre waves," *Jour. IEE*, vol. 102, part B, p. 264; March, 1955.
[143] H. Motz and K. B. Mallory, "Generation of submillimeter waves," *J. Appl. Phys.*, vol. 26, p. 1384; November, 1955. (Correspondence.)
[144] P. D. Coleman and M. D. Sirkis, "Harmodotron—A beam harmonic, higher-order mode device for producing millimeter and submillimeter waves," *J. Appl. Phys.*, vol. 26, pp. 1385–1386; November, 1955. (Correspondence.)
[145] J. G. Linhart, "Čerenkov radiation of electrons moving parallel to a dielectric boundary," *J. Appl. Phys.*, vol. 26, pp. 527–533; May, 1955.

In the related field of short-millimicrosecond-pulses, traveling tubes have been very successfully exploited. Earlier regenerative systems using traveling-wave tubes have been supplemented by a much simpler generator in which the proper transients are applied directly to the helix and focusing electrode of the traveling wave tube.

[146] A. C. Beck and G. D. Mandeville, "Microwave traveling-wave tube millimicrosecond pulse generators," TRANS. IRE, vol. MTT-3, pp. 48–51; December, 1955.

The regenerative scheme is, however, being developed further for repeater purposes. A method for regenerating binary pulses directly at microwave frequencies is being tried with considerable success.

[147] O. E. DeLange, "The regeneration of binary microwave pulses," TRANS. IRE, vol. MTT-3, p. 62; December, 1955.

Magnetrons, Klystrons, and Triodes

In the rivalry of broad band electronically tunable oscillators, the interdigital magnetron is a strong competitor. A voltage tunable magnetron covering the 1.5–3.5 kmc band has been developed. In local oscillator service, this tube exhibits only a 3 db higher noise figure than the reflex klystron. Its structure is extremely simple and compact when compared with backward wave oscillators.

[148] J. A. Boyd, "The Mitron—an interdigital voltage-tunable magnetron," PROC. IRE, vol. 43, pp. 332–338; March, 1955.
[149] A. Singh, "Modes and operating voltages of interdigital magnetrons," PROC. IRE, vol. 43, pp. 470–476; April, 1955.

An outstanding reflex klystron oscillator for the 50–60 kmc band has also been developed. Although quite straightforward in design, the performance of this tube far exceeds previous achievements.

[150] E. D. Reed, "A tunable, low voltage reflex klystron for operation in the 50 to 60-kmc band," *Bell. Sys. Tech. Jour.*, pp. 563–600; May, 1955.

Full exploitation of planar electrode structures has also produced relatively conventional triodes capable of oscillator service up to 10 kmc. At 1.2 kmc a noise figure of 7 db is quoted.

[151] J. E. Beggs and N. T. Lavoo, "A triode useful to 10,000 mc," PROC. IRE, vol. 43, pp. 15–19; January, 1955.

The output spectra attainable with conventional oscillators have received considerable attention. Most noteworthy is the development of a system for phase stabilization of microwave oscillators. The phase locking of a microwave oscillator to the harmonic of a crystal has been accomplished. This reduces the spectrum width of the stabilized oscillator to the width of the reference signal. When used in reverse, a system of this type can function as a frequency divider in the microwave region, where no other kind is presently available.

[152] M. Peter and M. W. P. Standberg, "Phase stabilization of microwave oscillators," PROC. IRE, vol. 43, pp. 869–873; July, 1955.

Other reports on stabilization and studies of output spectra are given below.

[153] L. Jampierre, "Study of the relative frequency fluctuations of two reflex klystrons stabilized by different methods," *Ann. Telecommun.*, vol. 10, pp. 65–78, 87–99; March/April, 1955.
[154] R. E. Wall, Jr. and A. E. Harrison, "A method of forming a broad-band microwave frequency spectrum," TRANS. IRE, vol. MTT-3, pp. 4–10; January, 1955.
[155] T. Moreno and R. L. Jepsen, "Hysteresis in klystron oscillators," PROC. IRE, vol. 43, p. 344; March, 1955. (Correspondence.)
[156] P. D. Strum, "Klystron noise," TRANS. IRE, vol. MTT-3, p. 45; January, 1955. (Correspondence.)

CONCLUSION

The summary of microwave progress just given is fragmentary in two senses. First, it is incomplete, particularly with regard to some of the less accessible foreign periodicals. Second, it does not hang together as well as might be hoped. Both of these features have a significance beyond simply proving the inadequacy of the author. Thus, we are much in need of closer contacts with other workers who publish in foreign journals and languages. We are also being drawn into many new and diverse areas of science and its application. The first of these can be remedied by a special effort to look at foreign progress. The second, our growing diversification, is a sign of natural growth and vigor. We can take satisfaction from the expansion of microwave theory and techniques during 1955 and in preceding years, even though this may tax our learning capacity in new fields.

Coupled-Strip-Transmission-Line Filters and Directional Couplers

E. M. T. JONES† AND J. T. BOLLJAHN†

Summary—**This paper describes the theory of operation of coupled strip line filters and directional couplers, and presents information from which these components may be easily designed. Low-pass, band-pass, all-pass, and all-stop filter characteristics are obtained from these coupled lines either by placing open or short circuits at two of the four available terminal pairs, or by interconnecting two of the terminal pairs. Directional couplers having perfect directivity and constant input impedance at all frequencies, and for all degrees of coupling, are obtained by placing equal resistive loads at each of the four terminal pairs.**

Introduction

THE ELECTROMAGNETIC COUPLING that exists between parallel transmission lines has been used to advantage by a number of investigators to construct filters and directional couplers from coupled open-wire transmission lines, and coupled coaxial lines.[1–5] This natural coupling can be used equally well in the construction of shielded strip transmission line filters and directional couplers. This paper derives formulas from which these coupled-strip-line filters and coupled-strip-line directional couplers may be designed.

Coupled Transmission-Line Impedance and Admittance Matrices

The general physical configuration of coupled strip lines to be considered here is illustrated in Fig. 1. A convenient way to describe the behavior of these coupled strip transmission lines is by means of the impedance matrix which will now be derived. Consider the shielded coupled transmission lines shown in Fig. 1, where the two transmission lines are supported midway between the two ground planes and are driven by a set of five constant-current generators at each end. The four current generators $i_1/2$ energize the even or unbalanced mode on the structure producing voltages on the two conductors of the form

$$v_{a_1}(z) = v_{b_1}(z) = -jZ_{oe}i_1\frac{\cos k(l-z)}{\sin kl}, \tag{1}$$

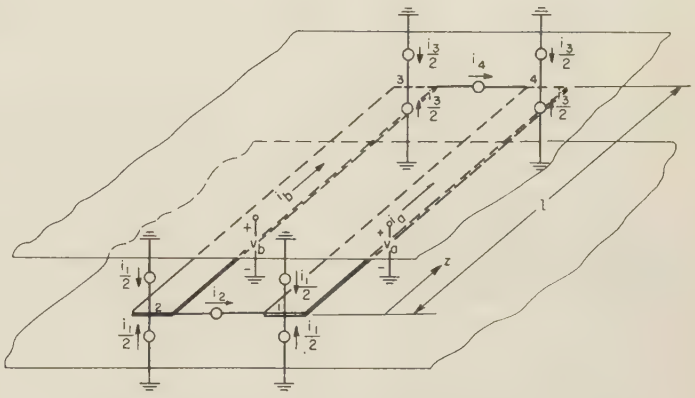

Fig. 1.—Notation used in deriving the impedance matrix of coupled transmission lines.

where

Z_{oe} = characteristic impedance of one wire to ground with equal currents in the same direction.

Likewise, the current generators $i_3/2$ produce voltages on the two conductors

$$v_{a_3}(z) = v_{b_3}(z) = -jZ_{oe}i_3\frac{\cos kz}{\sin kl}. \tag{2}$$

The current generators i_2 and i_4 produce odd or balanced voltages on the lines of the form

$$v_{a_2}(z) = -v_{b_2}(z) = -jZ_{oo}i_2\frac{\cos k(l-z)}{\sin kl}, \tag{3}$$

and

$$v_{a_4}(z) = -v_{b_4}(z) = -jZ_{oo}i_4\frac{\cos kz}{\sin kl}, \tag{4}$$

where

Z_{oo} = characteristic impedance of one wire to ground with equal currents in opposite directions.

The total current and voltage at each of the terminals (1, 2, 3, and 4) are easily related to the currents and voltages of the even- and odd-mode excitation. Assume that the positive current in each case is into a terminal; then the terminal currents are

$$\begin{aligned} I_1 &= i_1 + i_2 \\ I_2 &= i_1 - i_2 \\ I_3 &= i_3 - i_4 \\ I_4 &= i_3 + i_4. \end{aligned} \tag{5}$$

† Stanford Research Institute Menlo Park, Calif.

[1] A. Alford, "Coupled networks in radio-frequency circuits," PROC. IRE, vol. 29, pp. 55–70; February, 1941.

[2] J. J. Karakash and D. E. Mode, "A coupled coaxial transmission-line band-pass filter," PROC. IRE, vol 38, pp. 48–52; January, 1950.

[3] W. L. Firestone, "Analysis of transmission line directional couplers," PROC. IRE, vol. 42, pp. 1529–1538; October, 1954.

[4] B. M. Oliver, "Directional electromagnetic couplers," PROC. IRE, vol. 42, pp. 1686–1692; November, 1954.

[5] R. C. Knechtli, "Further analysis of transmission-line directional couplers," PROC. IRE, vol. 43, pp. 867–869; July, 1955.

FILTER	Z_I	α, β and θ_c
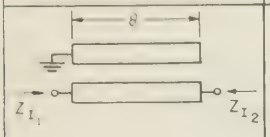 1- LOW PASS	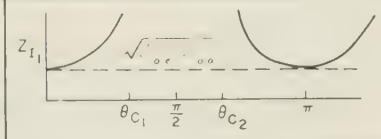 $Z_{I_1} = \dfrac{2Z_{oe}Z_{oo}\cos\theta}{[-(Z_{oe}-Z_{oo})^2+(Z_{oe}+Z_{oo})^2\cos^2\theta]^{1/2}}$ $Z_{I_2} = \dfrac{Z_{oe}Z_{oo}}{Z_{I_1}}$	$\cosh(\alpha+j\beta) = \dfrac{[-(Z_{oe}+Z_{oo})^2\cos^2\theta+(Z_{oe}-Z_{oo})^2]^{1/2}}{2\sqrt{Z_{oe}Z_{oo}}}$ $\cos\theta_{c_1} = -\cos\theta_{c_2} = \left[\dfrac{\frac{Z_{oe}}{Z_{oo}}-1}{\frac{Z_{oe}}{Z_{oo}}+1}\right]$
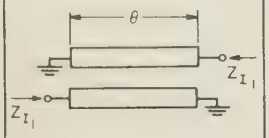 2-BAND PASS	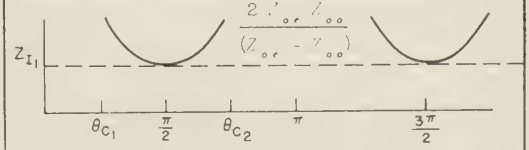 $Z_{I_1} = \dfrac{2Z_{oe}Z_{oo}\sin\theta}{[(Z_{oe}-Z_{oo})^2-(Z_{oe}+Z_{oo})^2\cos^2\theta]^{1/2}}$	$\cosh(\alpha+j\beta) = \left[\dfrac{\frac{Z_{oe}}{Z_{oo}}+1}{\frac{Z_{oe}}{Z_{oo}}-1}\right]\cos\theta$ $\cos\theta_{c_1} = -\cos\theta_{c_2} = \left[\dfrac{\frac{Z_{oe}}{Z_{oo}}-1}{\frac{Z_{oe}}{Z_{oo}}+1}\right]$
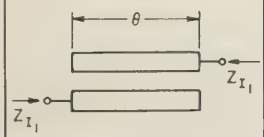 3-BAND PASS	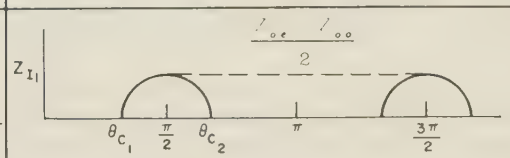 $Z_{I_1} = \dfrac{[(Z_{oe}-Z_{oo})^2+(Z_{oe}+Z_{oo})^2\cos^2\theta]^{1/2}}{2\sin\theta}$	$\cos\theta_{c_1} = -\cos\theta_{c_2} = \left[\dfrac{\frac{Z_{oe}}{Z_{oo}}-1}{\frac{Z_{oe}}{Z_{oo}}+1}\right]$ $\cosh(\alpha+j\beta) = \left[\dfrac{\frac{Z_{oe}}{Z_{oo}}+1}{\frac{Z_{oe}}{Z_{oo}}-1}\right]\cos\theta$

Fig. 2(a)

CASE	Z_I	α, β and θ_c
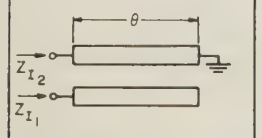 4-BAND PASS	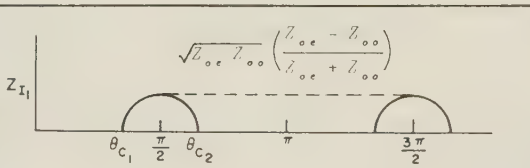 $Z_{I_1} = \dfrac{\sqrt{Z_{oe}Z_{oo}}\,[(Z_{oe}-Z_{oo})^2-(Z_{oe}+Z_{oo})^2\cos^2\theta]^{1/2}}{\sin\theta\,(Z_{oe}+Z_{oo})}$ $Z_{I_2} = \dfrac{Z_{oe}Z_{oo}}{Z_{I_1}}$	$\cosh(\alpha+j\beta) = \dfrac{1}{\sin\theta}\left[1-\left(\dfrac{Z_{oe}+Z_{oo}}{Z_{oe}-Z_{oo}}\right)^2\cos^2\theta\right]^{1/2}$ $\cos\theta_{c_1} = -\cos\theta_{c_2} = \left[\dfrac{\frac{Z_{oe}}{Z_{oo}}-1}{\frac{Z_{oe}}{Z_{oo}}+1}\right]$
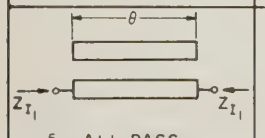 5- ALL PASS	$Z_{I_1} = \dfrac{Z_{oe}+Z_{oo}}{2}$	$\beta = \theta$
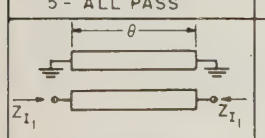 6- ALL PASS	$Z_{I_1} = \dfrac{2Z_{oe}Z_{oo}}{Z_{oe}+Z_{oo}}$	$\beta = \theta$
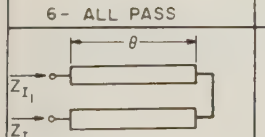 7- ALL PASS	$Z_{I_1} = \sqrt{Z_{oe}Z_{oo}}$	$\cos\beta = \dfrac{\frac{Z_{oe}}{Z_{oo}}-\tan^2\theta}{\frac{Z_{oe}}{Z_{oo}}+\tan^2\theta}$

Fig. 2(b)

CASE	Z_I	α, β, Z_c
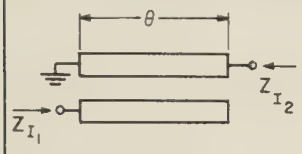 8-ALL STOP	$Z_{I_1} = -j\dfrac{2Z_{oo}Z_{oe}}{Z_{oo}+Z_{oe}}\cot\theta$ $Z_{I_2} = \dfrac{Z_{oe}Z_{oo}}{Z_{I_1}}$	$\alpha = \omega$
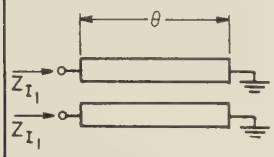 9-ALL STOP	$Z_{I_1} = j\sqrt{Z_{oe}Z_{oo}}\tan\theta$	$\cosh\alpha = \dfrac{Z_{oe}+Z_{oo}}{Z_{oe}-Z_{oo}}$
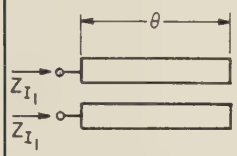 10-ALL STOP	$Z_{I_1} = -j\sqrt{Z_{oe}Z_{oo}}\cot\theta$	$\cosh\alpha = \dfrac{Z_{oe}+Z_{oo}}{Z_{oe}-Z_{oo}}$

Fig. 2(c).—Image parameters for coupled transmission line filters.

When these equations are solved for the mode currents in terms of the terminal currents, it is found that

$$\begin{aligned} i_1 &= \tfrac{1}{2}(I_1 + I_2) \\ i_2 &= \tfrac{1}{2}(I_1 - I_2) \\ i_3 &= \tfrac{1}{2}(I_4 + I_3) \\ i_4 &= \tfrac{1}{2}(I_4 - I_3). \end{aligned} \tag{6}$$

Since constant-current generators having infinite internal impedance are used in this derivation, each terminal voltage is the sum of all the mode voltages at that terminal. Thus

$$\begin{aligned} V_1 &= (v_{a_1} + v_{a_2} + v_{a_3} + v_{a_4})\big|_{z=o} \\ V_2 &= (v_{b_1} + v_{b_2} + v_{b_3} + v_{b_4})\big|_{z=o} \\ V_3 &= (v_{b_1} + v_{b_2} + v_{b_3} + v_{b_4})\big|_{z=l} \\ V_4 &= (v_{a_1} + v_{a_2} + v_{a_3} + v_{a_4})\big|_{z=l}. \end{aligned} \tag{7}$$

When (1)–(4) and (6) are substituted in (7), the coefficients of I_1, I_2, I_3, and I_4 are easily identified as the elements of the impedance matrix. Performing this operation, it is found that the matrix elements are

$$\begin{aligned} Z_{11} = Z_{22} = Z_{33} = Z_{44} &= -j(Z_{oe}+Z_{oo})\frac{\cot\theta}{2} \\ Z_{12} = Z_{21} = Z_{34} = Z_{43} &= -j(Z_{oe}-Z_{oo})\frac{\cot\theta}{2} \\ Z_{13} = Z_{31} = Z_{24} = Z_{42} &= -j(Z_{oe}-Z_{oo})\frac{\csc\theta}{2} \\ Z_{14} = Z_{41} = Z_{23} = Z_{32} &= -j(Z_{oe}+Z_{oo})\frac{\csc\theta}{2} \end{aligned} \tag{8}$$

where θ is the electrical length of the coupled wires.

The admittance matrix may also be derived by substituting a double-T configuration of voltage generators at each end for the double-π configuration of constant current generators used above. The results of this analysis show that the elements of the admittance matrix are

$$\begin{aligned} Y_{11} = Y_{22} = Y_{33} = Y_{44} &= -j(Y_{oo}+Y_{oe})\frac{\cot\theta}{2} \\ Y_{12} = Y_{21} = Y_{34} = Y_{43} &= -j(Y_{oo}-Y_{oe})\frac{\cot\theta}{2} \\ Y_{13} = Y_{31} = Y_{24} = Y_{42} &= -j(Y_{oo}-Y_{oe})\frac{\csc\theta}{2} \\ Y_{14} = Y_{41} = Y_{23} = Y_{32} &= -j(Y_{oo}+Y_{oe})\frac{\csc\theta}{2}. \end{aligned} \tag{9}$$

Coupled Transmission-Line Filters

There are ten filters that can be obtained from a pair of coupled strip lines by placing open or short circuits on various terminal pairs, or by connecting ends of the lines together. Fig 2(a), (b), and (c), on this page and the previous page, show single sections of the ten possible coupled transmission-line filters together with their image parameters. In the schematic diagrams of the coupled line filters, the input and output terminal pairs are designated by small open circles. The image impedance, or admittance, seen looking into each of

these terminal pairs is also shown near the terminal pair. Open-circuited terminal pairs of the coupled lines are shown with no connection in the filter schematic diagram, while short-circuited terminal pairs are designated with the standard grounding symbol.

Reference to Fig. 2 shows that it is possible to obtain low-pass, band-pass, and all-stop filters from a pair of coupled transmission lines. The low-pass filter 1 has an infinite number of pass bands centered about multiples of π, while the band-pass filters 2, 3, and 4 have an infinite number of pass bands centered about odd multiples of $\pi/2$. It is interesting to note that the bandwidth of the three band-pass filters is the same, while the bandwidth of the low-pass filter is just half that of the band-pass filters. Inspection of Fig. 2 also shows that there are close relationships among the image impedances of these filters. In particular, the product of the image impedances Z_{I_1} and Z_{I_2} of the unsymmetrical filters 1, 4, and 8 are each equal to $Z_{oo}Z_{oe}$. Furthermore, the product of the image impedances of the dual symmetrical filters 2 and 3, 5 and 6, and 9 and 10 are also equal to $Z_{oe}Z_{oo}$. Finally, the square of the image impedance of the symmetrical all-pass filter 7 is equal to $Z_{oe}Z_{oo}$.

Filter 8 does not have much practical utility; however, it does have interesting property of possessing an infinite image attenuation at all frequencies. Filters 9 and 10 are not very useful by themselves, but they can be made into band-pass filters by adding suitable reactive elements to their terminals. For example, the equivalent circuit of filter 9 is a symmetrical π composed of inductances. The susceptance of the inductances in each of the shunt arms is $-Y_{oe}\cot\theta$, while the susceptance of the series arm is

$$\frac{-(Y_{oo}-Y_{oe})\cot\theta}{2}.$$

The addition of series capacitances converts filter 9 into a well-known type of band-pass filter. The equivalent circuit of filter 10 is a symmetrical T network of capacitances. Each of the series capacitances has a reactance of $-Z_{oo}\cot\theta$, while the shunt capacitance has a reactance of

$$\frac{-(Z_{oe}-Z_{oo})\cot\theta}{2}.$$

In this case, series inductances must be added to this filter to convert it into a band-pass filter.

The image-parameter design equations presented in Fig. 2 are obtained in the following manner. First, the four-element impedance or admittance matrix of the filters is obtained from the four network equations

$$[V] = [Z][I] \tag{10}$$

or

$$[I] = [Y][V] \tag{11}$$

by applying the appropriate boundary conditions. Here $[V]$ and $[I]$ are four-element column matrices, while $[Z]$ and $[Y]$ are sixteen-element square matrices. For example, in filter 7 if it is assumed that terminal 3 and 4 are connected, the boundary conditions are $V_3 = V_4$ and $I_3 = -I_4$. In all the other filters the boundary conditions are $V=0$ or $I=0$ at terminals that are short-circuited or open-circuited, respectively. Second, the image impedance, Z_I, or image admittance, Y_I, and image transfer constant $(\alpha+j\beta)$ are calculated from the elements of the resulting four-element impedance matrix Z' or admittance matrix Y' by the following relations

$$Z_{I_1} = \left(Z_{11}'^2 - \frac{Z_{11}'Z_{12}'^2}{Z_{22}'}\right)^{1/2}, \quad Z_{I_2} = \left(Z_{22}'^2 - \frac{Z_{22}'Z_{12}'^2}{Z_{11}'}\right)^{1/2},$$

$$\cosh(\alpha+j\beta) = \frac{(Z_{11}'Z_{22}')^{1/2}}{Z_{12}'} \tag{12}$$

or

$$Y_{I_1} = \left(Y_{11}'^2 - \frac{Y_{11}'Y_{12}'^2}{Y_{22}'}\right)^{1/2}, \quad Y_{I_2} = \left(Y_{22}'^2 - \frac{Y_{22}'Y_{12}'^2}{Y_{11}'}\right)^{1/2},$$

$$\cosh(\alpha+j\beta) = \frac{Y(_{11}'Y_{22}')^{1/2}}{Y_{12}'}. \tag{13}$$

Physical Layout of Coupled-Strip-Line Filters

In most applications it is necessary to cascade several of the basic filter sections shown in Fig. 2 in order to achieve the desired performance from the filter. Fig. 3 illustrates the way these basic filter sections might be cascaded using strip line techniques. It is seen that where the input and output of basic sections occur at opposite ends of the strips (*i.e.*, as in filters 1, 2, 3, 5, 6, and 8) any number of sections may be cascaded. However, when the input and output of a single section occur at the same end, (*i.e.*, as in filters 4, 7, and 10) only two sections may be cascaded.

The image impedance of the coupled strip line filters is either higher or lower than the characteristic impedance of an isolated strip. Therefore, it is necessary to connect the filters to strips having different widths than the coupled strips, in order to reduce the mismatch loss at the terminals. For example, when the image impedance of the filter is less than the characteristic impedance of an isolated strip, the connecting strip is made wider than the coupled strips and, when the image impedance of the filter is greater than the characteristic impedance of an isolated strip, the connecting line is made narrower. The proper width of the connecting lines is illustrated for the filters in Fig. 3. At the bottom of Fig. 3 is shown the way in which the all-stop filters 9 and 10 may be converted to band-pass filters by adding series capacitors and series inductors, respectively.

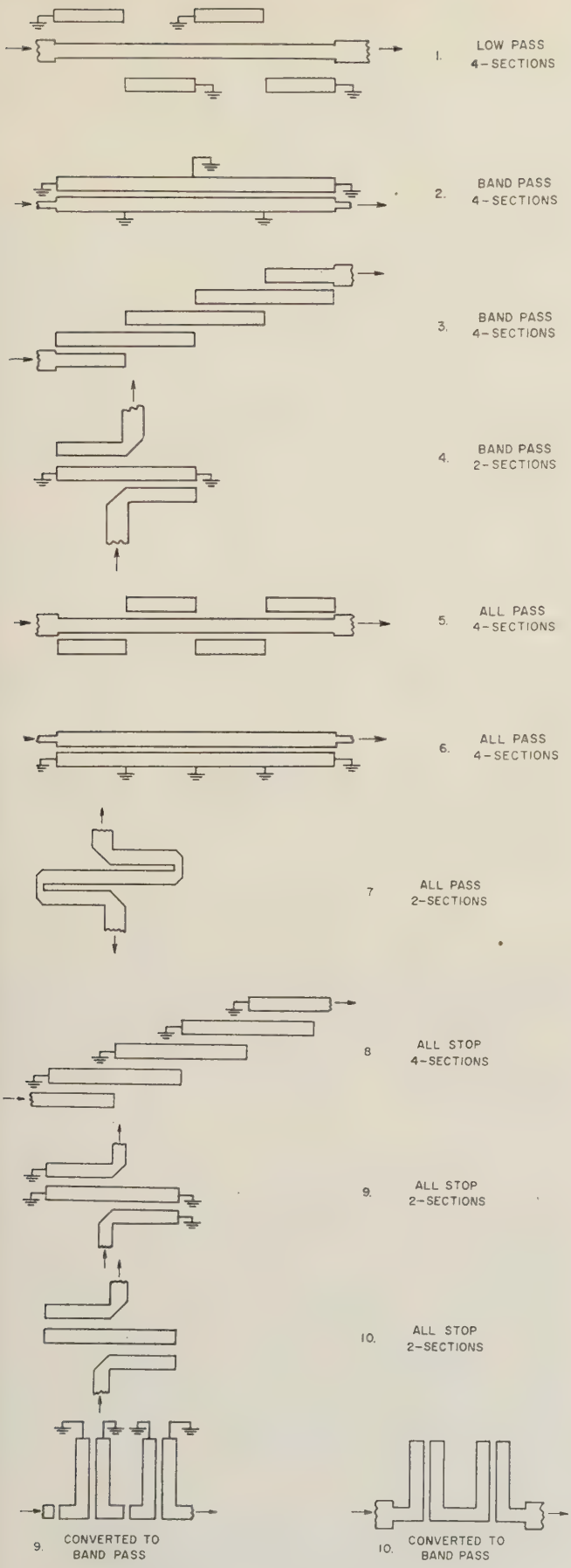

Fig. 3.—Physical layout of coupled strip line filters.

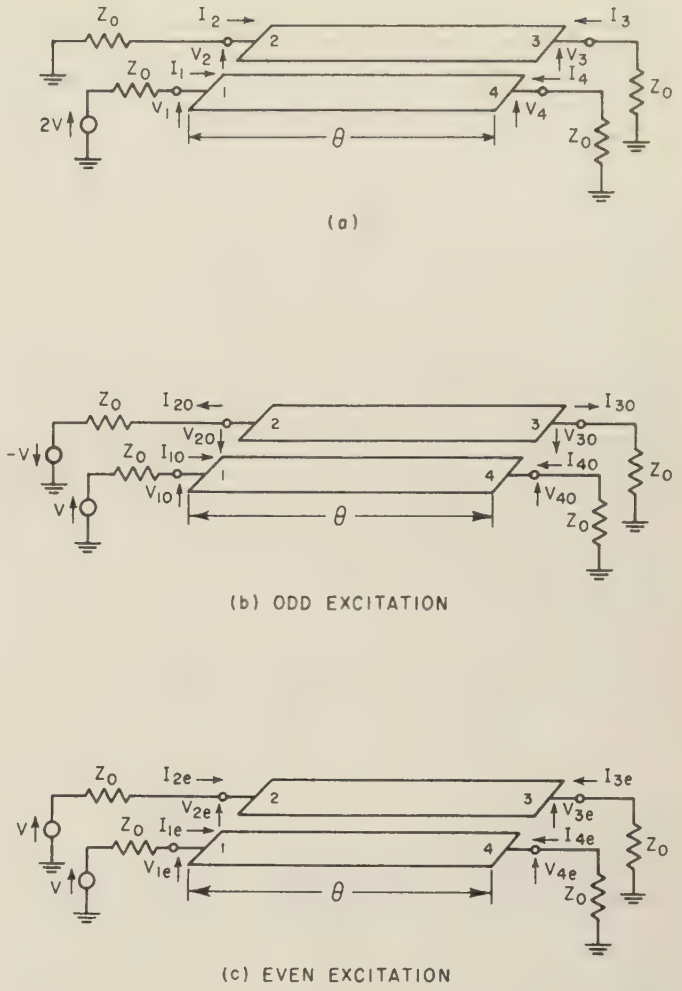

Fig. 4.—Strip line directional coupler with even and odd excitation.

Coupled-Strip-Line Directional Couplers

When the four terminal pairs of the coupled strip transmission lines illustrated in Fig. 1 are terminated in the proper constant resistance, the device behaves as a directional coupler with constant input impedance and infinite directivity at all frequencies, and for all degrees of coupling.[6] In this coupler energy is coupled backward instead of forward. Hence, if a signal is fed into one terminal pair, the coupled signal emerges from the adjacent terminal pair and no signal emerges from the diagonally opposite terminal pair.

The characteristics of this directional coupler can be determined rigorously from the impedance matrix. However, its behavior will be derived here from certain symmetry arguments, because it is believed that such a presentation gives the best physical picture of the directional coupler operation.

A simplified schematic diagram of the directional coupler is shown at the top of Fig. 4 with resistance terminations Z_o at each terminal. The coupler is ex-

[6] Oliver and Knechtli, *loci cit.*, have also recently analyzed coupled transmission-line directional couplers and shown that they can be designed to have infinite directivity and constant input impedance for all degrees of coupling.

cited with a voltage $2V$ in series with terminal 1. At the bottom of Fig. 2, the same directional coupler is shown in two different states of excitation. In the odd excitation, out-of-phase voltages are applied in series with terminals 1 and 2, while the even excitation applies in-phase voltages in series with these terminals. Through the principle of superposition it may be seen that the behavior of the directional coupler with voltage $2V$ applied in series with terminal 1 can be obtained from its behavior with even and odd voltage excitations.

It is seen that the characteristic impedance of one of these strips to ground in the odd excitation is Z_{oo}, while the characteristic impedance of a strip to ground in the even excitation is Z_{oe}. In order for the directional coupler to have a perfect match at all frequencies it is necessary that the input impedance Z_{in} be equal to Z_o. Applying the principal of superposition, it is seen that the input impedance of the directional coupler terminated in Z_o can be written as

$$Z_{\text{in}} = \frac{V_{1o} + V_{1e}}{I_{1o} + I_{1e}} = \frac{\dfrac{Z_{1o}}{Z_o + Z_{1o}} + \dfrac{Z_{1e}}{Z_o + Z_{1e}}}{\dfrac{1}{Z_o + Z_{1o}} + \dfrac{1}{Z_o + Z_{1e}}}, \tag{14}$$

where

$$Z_{1o} = Z_{oo}\frac{(Z_o + jZ_{oo}\tan\theta)}{Z_{oo} + jZ_o\tan\theta} \tag{15}$$

and

$$Z_{1e} = Z_{oe}\frac{(Z_o + jZ_{oe}\tan\theta)}{Z_{oe} + jZ_o\tan\theta}. \tag{16}$$

When (15) and (16) are substituted in (14), it is found that $Z_{1n} = Z_o$ when

$$Z_o = (Z_{oo}Z_{oe})^{1/2}. \tag{17}$$

This characteristic impedance of the coupler, $(Z_{oe}Z_{oo})^{1/2}$, is always less than the characteristic impedance of a single strip line of the same width. Therefore, the width of the lines connecting to the coupler is required to be slightly wider than the coupled strips. Although for couplings weaker than -15 db, the change in width is negligible.

Under the condition that $Z_o = (Z_{oe}Z_{oo})^{1/2}$, the voltage appearing at terminal 1 of the coupler is $V_1 = V$. The voltages $V_{2e} = V_{1e}$ and $V_{3e} = V_{4e}$ may be determined from the straightforward analysis of a transmission line of length θ, and characteristic impedance Z_{oe} terminated at either end by an impedance $(Z_{oe}Z_{oo})^{1/2}$ and fed by a voltage V. Likewise the voltages $V_{2o} = -V_{1o}$ and $V_{3o} = -V_{4o}$ may be determined from a similar analysis of a transmission line of length θ and characteristic impedance Z_{oo} terminated by $(Z_{oe}Z_{oo})^{1/2}$. The results of this analysis show that

$$V_2 = V_{2e} - V_{2o}$$

$$= j\frac{V\sin\theta\left[\sqrt{\dfrac{Z_{oe}}{Z_{oo}}} - \sqrt{\dfrac{Z_{oo}}{Z_{oe}}}\right]}{2\cos\theta + j\sin\theta\left[\sqrt{\dfrac{Z_{oe}}{Z_{oo}}} + \sqrt{\dfrac{Z_{oo}}{Z_{oe}}}\right]}, \tag{18}$$

$$V_3 = V_{3e} - V_{3o} = 0 \tag{19}$$

$$V_4 = V_{4e} - V_{4o}$$

$$= \frac{2V}{2\cos\theta + j\sin\theta\left[\sqrt{\dfrac{Z_{oe}}{Z_{oo}}} - \sqrt{\dfrac{Z_{oo}}{Z_{oe}}}\right]}. \tag{20}$$

The maximum coupled voltage, V_2, occurs when the coupler is a quarter wavelength long (*i.e.*, $\theta = 90°$). Therefore, from (18) a maximum coupling coefficient k may be defined as

$$\left|\frac{V_2}{V}\right| = k = \frac{\dfrac{Z_{oe}}{Z_{oo}} - 1}{\dfrac{Z_{oe}}{Z_{oo}} + 1}. \tag{21}$$

With this substitution, the voltage at terminal 2 can be written as

$$V_2 = V\frac{jk\sin\theta}{\sqrt{1 - k^2\cos\theta} + j\sin\theta} \tag{22}$$

while the voltage at terminal 4 becomes

$$V_4 = \frac{V\sqrt{1 - k^2}}{\sqrt{1 - k^2\cos\theta} + j\sin\theta}. \tag{23}$$

Eqs. (22) and (23) are the same as those obtained by Oliver.[4] Reference to his Fig. 6 or to (22) above shows that for small values of k the coupler will operate over a 3 to 1 frequency band between 3 db points, while for stronger couplings even wider bandwidths of operation are obtained.

Coupled Transmission Line Impedances Z_{oe} and Z_{oo}

The characteristic impedances Z_{oe} and Z_{oo} of infinitesimally thin coupled strip lines have been calculated rigorously by Cohn[7] who presents the information in the form of a nomogram. The reader is also referred to Cohn's paper for approximate values of Z_{oe} and Z_{oo} for thick strips and strips printed on dielectric sheets.

In applications where these components must be operated at high rf potentials, the possibility of breakdown is minimized by using round conductors instead of strips. Approximate formulas for Z_{oe} and Z_{oo} for the round conductors have been derived by Honey.[8]

[7] S. B. Cohn, "Shielded coupled-strip line," Trans. IRE, vol. MTT-3, pp. 29–38; October, 1955.

[8] R. C. Honey, Stanford Research Institute, private communications.

He finds that

$$Z_{oe} - Z_{oo} = \frac{120}{\sqrt{\epsilon_r}} ln \coth \frac{\pi s}{2b} \tag{24}$$

$$Z_{oe} + Z_{oo} = \frac{120}{\sqrt{\epsilon_r}} ln \coth \frac{\pi d}{4b} \tag{25}$$

where s = center to center spacing of the wires, d = wire diameter, b = ground plane spacing, and ϵ_r = relative dielectric constant of medium surrounding the wires.

For configurations of coupled lines that are not amenable to analysis it is always possible to determine Z_{oo} and Z_{oe} from measurements of the static capacity of the strips. Thus

$$Z_{oo} = \frac{100\sqrt{\epsilon_r}}{3C_{oo}} = \frac{100\sqrt{\epsilon_r}}{3[C_{22} - C_{23}]} \tag{26}$$

while

$$Z_{oe} = \frac{100\sqrt{\epsilon_r}}{3C_{oe}} = \frac{100\sqrt{\epsilon_r}}{3[C_{22} + C_{23}]} \tag{27}$$

where

C_{oo} = one half the capacity between the two center conductors ($\mu\mu$f/cm),

C_{oe} = one half the capacity between the parallel combination of the two center conductors and ground ($\mu\mu$f/cm),

C_{22} = coefficient self capacity ($\mu\mu$f/cm) of either of the center conductors,

C_{22} = coefficient of induction ($\mu\mu$f/cm) between the two center conductors (a negative quantity).

The capacity C_{22} is easily measured as the capacity between either strip and ground when the other strip is grounded, while the capacity $C_{22} - C_{23}$ is just one half the capacity between the parallel combination of the two center conductors and ground.

ACKNOWLEDGEMENT

The work reported in this paper was conducted under Contract No. AF 33(038)-7850 sponsored by the Air Force Cambridge Research Center, and Contract No. DA 36-039-sc-63232 and DA 36-039-sc-64625 sponsored by the Signal Corps Engineering Laboratories.

Absolute Measurement of Receiver Noise Figures at UHF*

E. MAXWELL† AND B. J. LEON†

Summary—**Absolute measurements of noise-figures in the UHF range are described, using hot and cold thermal sources as standards. It was found that the noise temperature of the T-5 6 watt fluorescent tube is 16.1 ±0.6 db above $kT\Delta\nu$. Noise diodes were found to be in error at these frequencies by approximately 1 db.**

INTRODUCTION

THE noise figure of a receiver is conventionally defined as

$$F = \frac{\text{Noise power output of receiver}}{\text{Receiver gain} \times \text{available noise power from source}}.$$

It is measured either by comparing the noise power produced by the receiver with a signal from a calibrated signal generator, or with an external source of noise power of known intensity. The signal generator technique is straightforward but difficult to do precisely and requires that the "noise bandwidth" of the receiver be determined.[1] The second technique, which uses a calibrated noise generator, is simpler to apply and is usually capable of greater precision provided that a reliable standard of noise is available. Two types of noise generators which are primary standards, and hence self-calibrating, are the thermal source and the noise diode. The thermal source is simply a resistor at some temperature, T, which is capable of delivering noise power $kT\Delta\nu$ to some external device. Although simple in principle it is obviously restricted to laboratory use and has relatively low noise output. The diode noise source is a temperature limited diode. It can be shown[2] that the diode current contains a shot noise component whose means square value is

$$\bar{i}^2 = 2eI\Delta\nu$$

in the frequency interval $\Delta\nu$. e is the electronic charge and I the dc diode current. If the diode is shunted by a resistance R the combination is a noise generator with available power $2eIR\Delta\nu$. At frequencies high enough, so that the transit time of the electrons may not be neg-

* The research in this document was supported jointly by the Army, Navy, and Air Force under contract with the M.I.T. This paper was presented at the URSI-IRE symposium held in Washington, D. C.; May 2–5; 1956.

† Massachusetts Institute of Technology, Cambridge, Mass.

[1] G. E. Valley and H. Wallman, "Vacuum Tube Amplifiers," McGraw-Hill Book Co., New York, p. 695; 1948.

[2] *Ibid.*, p. 701.

lected, a suitable reduction factor $\psi(\nu)$ must be applied. Johnson[3] has calculated this correction factor for the coaxial type of noise diode subject to some simplifying assumptions, and this correction is generally applied when using this type of noise diode in the UHF spectrum. Commercial diode noise generators for this frequency range make use of the Bendix TT-1 coaxial noise diode shunted by a lumped resistor equal to the line impedance. Such devices are relatively broadband in impedance match. However, the fractional error in available noise power output will be equal to the voltage standing wave ratio, so that a mismatch of 1.25 is equivalent to 1 db uncertainty in output. Careful adjustment of the terminating impedance should reduce or eliminate this error.

Gas discharge devices have also been used as a convenient source of noise at microwave frequencies.[4,5] In its usual form this device consists of a gas discharge tube, usually a commercial fluorescent lamp, electrically matched into a waveguide. The discharge acts substantially like a black body radiator whose temperature is the electron temperature of the discharge. Approximate agreement was reported by Easely and Mumford between electron temperatures found from probe measurements and the equivalent temperatures deduced from noise measurements.[6] (The method of calibrating the noise measuring equipment was not stated but presumably a signal generator was used.) However, at the present time the gas discharge tube must be regarded as a secondary reference whose noise output is to be determined by direct comparison with a primary noise standard.

We have used diode noise generators for some time in measuring the noise figure of UHF receivers in the vicinity of 400 mcps. The terminating impedances were trimmed up so that errors due to impedance mismatch were negligible at the operating frequency. Nevertheless we observed a discrepancy between these measurements and those made with a fluorescent tube source (using the previously accepted figure[6] of 15.84 db excess noise at 40°C). The noise figures measured with the diode noise source seemed to be one or two db higher than those observed with the gas discharge source. Accordingly it was decided to build some thermal noise sources for independently checking these observations.

To measure the noise figure with a thermal source one first observes the noise power output of the receiver when fed from a source impedance at room temperature, T_0, and again when the source impedance is at some other temperature T. If the noise power outputs in these two cases are N_0 and N respectively, then the noise figure is given by

$$F_{T_0} = \frac{\frac{T}{T_0} - 1}{\frac{N}{N_0} - 1}.$$

It is customary to refer all measurements to a room temperature of 290°K so that F becomes:

$$F = \frac{\frac{T}{290} - 1}{\frac{N}{N_{290}} - 1}.$$

If the measurements are made at an ambient temperature, T_0, other than room temperature the noise figure is given by

$$F = \frac{\frac{T}{290} - 1 - \frac{N}{N_0}\left[\frac{T_0}{290} - 1\right]}{\frac{N}{N_0} - 1},$$

where N_0 is the noise power output when the source impedance is at temperature T_0.

In order to obtain reasonable precision N/N_0 should not be too close to 1. If we assume typical noise figures of the order of 5 db (3.2 arithmetically) and $T \sim$ 1,000°K, N/N is approximately 1.6 and F can be determined to within 0.1 db. Temperatures of the order of 1,000°K are convenient to work with so this technique is seen to be entirely practical for reasonably low noise-figures.

Instead of making T large compared to T_0, we can make it small. For the limiting case of $T=0$, and $F=3.2$, $N/N_0=0.69$. F can be determined to within about 0.25 db. Temperatures of the order of 4°K may be obtained with liquid helium and are low enough for this purpose. In our work both high temperature and low temperature thermal sources were employed and reasonable agreement was observed between measurements.

High Temperature Source

The high temperature source used was a long lossy helical line constructed by winding a helix of 42 turns of no. 27 Karma wire on a ceramic form $1\frac{1}{2}$ inches in diameter. Details of construction are shown in Fig. 1. The form was constructed of commercial "Lava"[7] which was first turned down to size and threaded and subsequently fired. The helix pitch is 20 turns per inch. The ceramic form is encased in a snugly fitting steel tube, the spacing between wire and shield being 0.016 inch. The helix is directly coupled to a stainless steel 50 ohm line. It was designed for a nominal impedance of 50 ohms and the input voltage standing wave ratio, when

[3] H. Johnson, "A Co-axial line noise diode source for UHF," *RCA Rev.*, vol. 8, p. 169; March, 1947.

[4] W. W. Mumford, "A broad band microwave noise source," *B. S. T. J.*, vol. 28, p. 608; October, 1949.

[5] H. Johnson and K. R. DeRemer, "Gaseous discharge superhigh frequency noise source," Proc. IRE, vol. 39, p. 908; August, 1951.

[6] M. A. Easley and W. W. Mumford, "Electron temperature vs noise temperature in low pressure mercury-argon discharges," *J. Appl. Phys.*, vol. 22, p. 846; September, 1951.

[7] This is a talc-like material sold by the American Lava Company.

hot, is 1.5. An electric furnace was built around the helical line after assembly. In practice the source is continuously maintained at a temperature of about 1,000°K. The temperature is monitored by three thermocouples situated along the length of the furnace. The temperature differential along the length of the furnace is less than 9°.

Since the noise-figure of a receiver depends on the effective source impedance this must be the same for the thermal and the room temperature sources. The admittance of the thermal source was measured with a General Radio Type 1602B Admittance Meter. Thermal sources were equipped with *GR* type 874 connectors so the admittance meter could be connected directly to the source output terminals and the admittance, referred to those terminals, measured directly without the use of any connecting cable. The room temperature source is then used together with an impedance transformer, also equipped with *GR*-874 connectors, and the transformer adjusted so that the impedance of the room temperature source is identically equal to that of the thermal source. The physical arrangement is shown in Fig. 2. The noise figure of the receiver is then determined for the case where the source impedance is equal to that of the thermal source. For other values of source impedance an appropriate impedance transformer could have been inserted between the thermal source and receiver. In practice, however, the thermal sources are not used for routine noise-figure measurements but rather as standards for calibrating noise-diodes and fluorescent tube sources. For this purpose it is more convenient to transform all other impedances to be identical with that of the thermal source. After the equivalent noise temperature of the secondary source has been determined it is, of course, used without any impedance transforming device. Any attenuation in the impedance transformer must be allowed for. In our case this correction was 0.1 db.

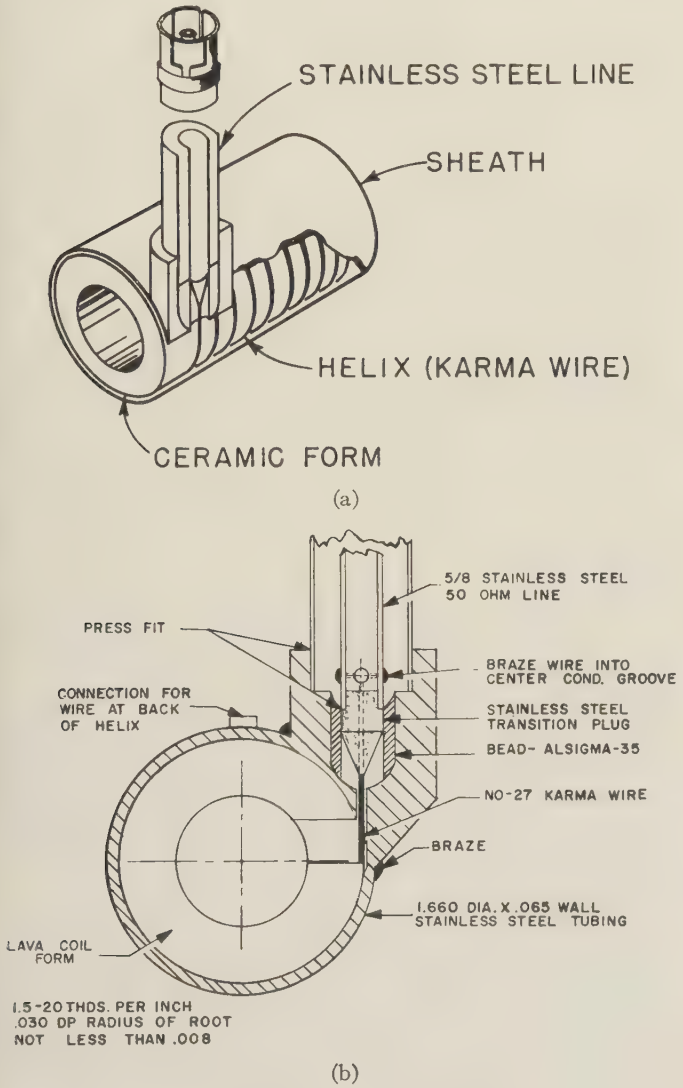

Fig. 1—High temperature thermal noise source.

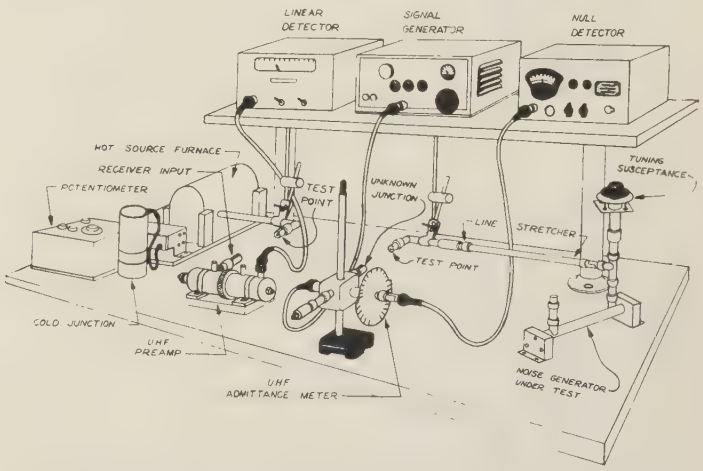

Fig. 2—Physical arrangement of equipment for measuring noise temperatures with thermal source.

Low Temperature Source

The low temperature source is illustrated in Fig. 3. It consists simply of a small 50 ohm plantinized glass resistor which terminates a 50 ohm transmission line. The resistor is immersed in liquid helium so that its temperature is therefore 4.2°K. The transmission line is made of stainless steel, chosen for low heat conductivity, which is silver plated to reduce the electrical attenuation. In using this device a reasonable amount of care must be used to cool it down slowly and to allow it to warm up slowly after use, otherwise the thermal shock may break the fragile resistor. A platinized glass resistor which is 50 ohms at room temperature falls to about 35 ohms at 4.2°K. (The small temperature coefficient is due to the fact that most of the resistance is caused by boundary scattering.) This source is much simpler to construct than the hot source but of course requires a supply of liquid helium.

Stem Corrections

Since the thermal sources must be connected to the receiver by transmission lines along which the temperature varies continuously from source to receiver.

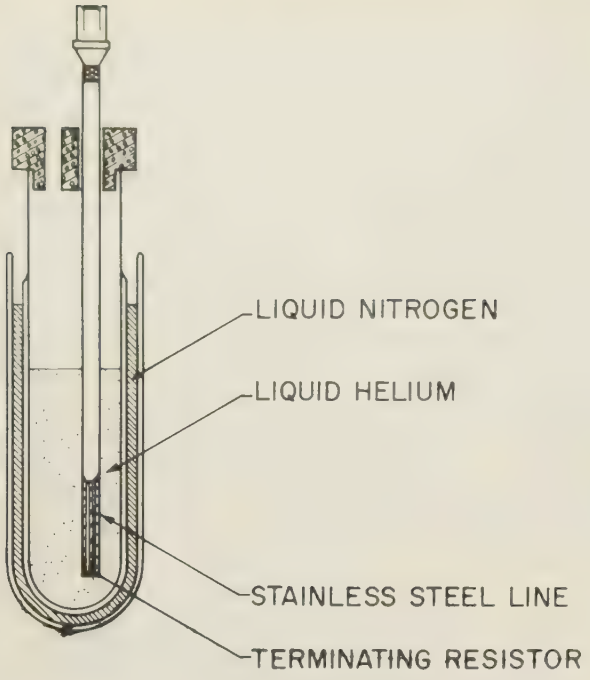

Fig. 3—Low temperature source.

it is important to know the magnitude of the appropriate stem correction. If we have a noise source, at temperature T, which is connected to a receiver through a four terminal network which is at temperature T_2, and has a gain G, the power delivered is given by[8]

$$P = GkT\Delta\nu + (1 - G)\, kT_2\Delta\nu.$$

If the network is a transmission line whose gain (attenuation) and temperature are both a function of position, then it may be shown that the noise power delivered is

$$kT\Delta\nu \exp\left(-\int_0^l \alpha(x)dx\right) + k\Delta\nu \int_0^l T(x)\alpha(x) \exp\left(-\int_x^l \alpha(\xi)d\xi,\right)dx$$

where (x) the attenuation constant at point x, $T(x)$ the temperature at point x, and l = the total length of the line. The effect of the correction is to lower the apparent temperature of the hot source and raise the apparent temperature of the cold source. If $T(x)$ and $\alpha(x)$ are given as empirical data the correction may be calculated by numerical integration. However, it is sometimes more useful to calculate outside limits to the correction which may be done somewhat more simply. If for the case of the hot source, it is assumed that the connecting line is all at room temperature but that the attenuation of the line is that corresponding to the high temperature, then the corresponding correction will certainly be larger than the true correction. This upper limit was calculated to be 9° for a source temperature of 965°K and hence the correction is less than 0.05 db. In the case of the cold source the corresponding upper limit to the correction is of the order of 0.025 db and therefore also negligible.

Results of Measurements with Thermal Sources

Although the thermal noise sources may be used directly to measure the noise figure of a receiver, it is usually more convenient to use them as primary standards for calibrating working standards. The hot source is preferable for day-to-day work. The chief utility of the cold source is to provide a cross-check.

We have used two types of working standards. These are the Bendix TT-1 diode noise generator (in a modified commercial instrument) and the fluorescent-tube gas-discharge noise generator. The diode source was compared with both hot and cold sources at a frequency of 425 mcps. For noise figures of the order of 5 db it was found that measurements made with the diode noise generator were on the average 1.14 db higher than with the hot source and 1.28 db higher than with the cold source. The transit time correction calculated by Johnson[8] is only 0.3 db at this frequency. It must be concluded that this correction is too small by 0.7–1.0 db or that there is some other source of error inherent in the diode. In our work with the diode generator we have applied a correction of −1.2 db at this frequency.

The fluorescent tube sources use a standard 6 watt, T5, cool white fluorescent lamp. Coupling to the discharge was effected by a helical line wound directly on the glass envelope of the tube. Some details of the design are given in Fig. 4. The design used was evolved from an earlier version due to Hill Montague of the Naval Research Laboratory.[9] The helix dimensions were chosen to match into a 50 ohm line. Pertinent data on the input impedance and attenuation through the discharge areas follows.

Input Admittance*

Frequency	Hot	Cold	Attenuation
200	21.7—j 1.0	22.6—j 2.2	13 db
400	20.6—j 0.7	25.0—j 3.75	26 db
600	20.7—j 0.8	36 —j 1.6	32 db
900	22.9—j 7.8	16.5—j 9.0	50 db

* Referred to input terminals in 20 millimho line.

The hot admittance is that seen at the input terminals when the helical line is tightly coupled to the gas discharge. The cold impedance is that of the termina-

[8] A. van der Ziel, "Noise," Prentice-Hall, Inc., New York, p. 16; 1954.

[9] Since this paper was written a description of his work has appeared in NRL Report 4560.

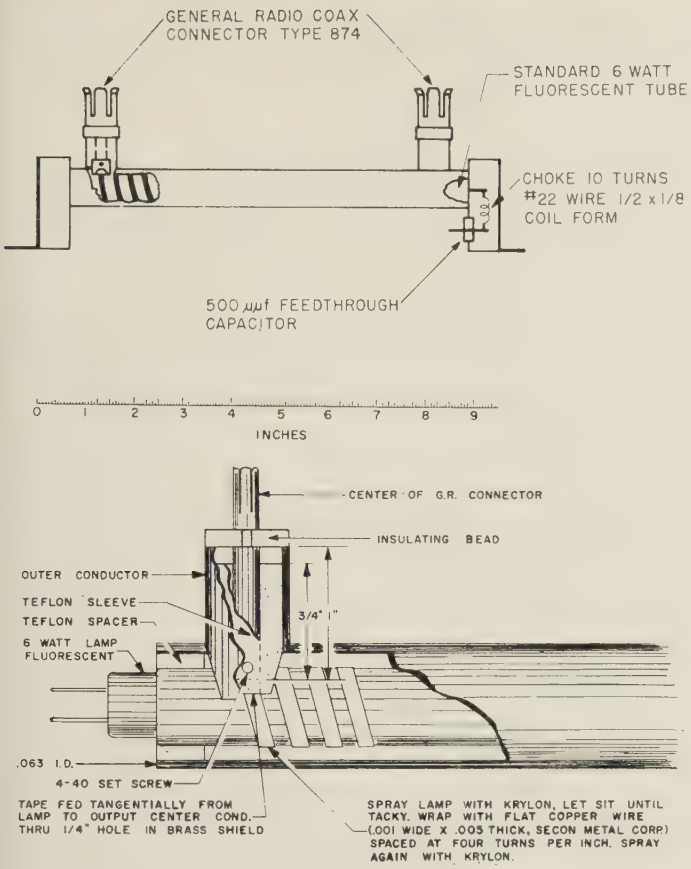

Fig. 4—Fluorescent tube noise source.

tion transformed back to the input terminals when the discharge is turned off. The helical line parameters were adjusted to secure a near optimum match into the line when loaded with the discharge. The characteristic impedance of the line is complex under this condition and consequently the cold impedance appears somewhat mismatched. For very precise measurements the room temperature measurement should be made using a separate matched load and not the cold impedance of the fluorescent tube source.

The fluorescent lamp was operated with a discharge current of 100 ma. DC and the output end was always in the positive column end of the discharge. The average excess noise output for 9 tubes was 16.1 db above $kT\Delta\nu$ with a spread of 15.85 to 16.31 db among the group. This is for a bulb temperature of 40°C. Mumford[4,6] has given the temperature coefficient of the excess noise for these tubes.

In some tubes there was a decided asymmetry of the following sort. If the polarity of the discharge were reversed and the same time output and termination ends switched so that the output end was always adjacent to the anode then variations in noise output of as much as 0.4 db were observed in some tubes. It was suspected that this might have been due to structural asymmetries in the lamp construction. Several special sources were therefore constructed using longer tubes, both 8 watt and 13 watt types, while keeping the helix length the same. This kept the ends of the discharge well out of the field of the helix. The average excess noise for five tubes was 16.4 db or 0.3 db higher than for the 6 watt tubes. For each of these tubes measurements were made using all four permutations of discharge polarity and output position. The maximum spreads in excess noise for the five tubes were 0.4 db, 0.3 db, 0.2 db, 0.1 db, and 0.1 db. Since the maximum spread was the same as that observed with the shorter tubes, these occasional departures from the mean cannot be definitely assigned to structural asymmetry. Furthermore the difference in noise output of the 6 watt and the 8 and 13 watt tubes emphasizes the fact that the commercial fluorescent tube, although cheap and convenient, is not an invariable noise standard. Discharge tubes using pure argon, neon, or helium are undoubtedly to be preferred except for cost.

Acknowledgement

The authors are indebted to A. E. Wennstrom, who participated in some of the early phases of the work, to Hill Montague of the Naval Research Laboratory for information on his fluorescent-tube noise-source design, and to L. D. Smullin of the Lincoln Laboratory for support and encouragement of this program.

Note

Further measurements of the noise output of standard 6-watt fluorescent lamps have shown that the apparent excess noise may vary by as much as −0.6 db over the course of a day. This effect seems to be correlated with fluctuations in the mercury vapor pressure but does not depend in any consistent fashion upon the bulb temperature. Some special lamps were obtained from Sylvania in which no mercury had been deliberately added. These provided a noise output of 16.3 db constant to within about 0.1 db or less. These tubes contain a small residual mercury vapor pressure which is cleaned up by the fluorescent coating after 20 to 30 hours of operation. After clean-up the tubes require a higher starting voltage.

Design and Development of Strip-Line Filters

E. H. BRADLEY†

Summary—Strip transmission lines offer an alternate medium in which microwave filters can be realized. Since bandpass filters designed in waveguide or coaxial lines would necessarily be large at ultra-high frequencies, strip lines provide a practical means of realizing filters which are simply fabricated and which represent an appreciable saving in size and weight.

Design techniques which were formerly employed in the realization of waveguide and coaxial filters have been applied in the synthesis of strip-line filters having "maximally-flat" and Tchebycheff response characteristics. In this paper, these techniques as well as those for realizing the required circuit parameters in strip line will be described. Using engraving techniques instead of the more commonly employed photo-etching techniques, strip-line filters can be fabricated with such precision that tuning screws are generally not required to align the filters to a desired center frequency. Bandpass filters having a 10 per cent bandwidth at S-band have been developed with a mid-band insertion loss of less than 1 db and a rejection of greater than 50 db at frequencies 9 per cent from the center frequency. The effect of temperature variations on the filter performance has been evaluated and will be discussed. Techniques will also be presented for eliminating spurious responses in filters required to operate over a frequency range of several octaves.

The application of strip-line techniques in the development of multiplexers and other microwave components, such as detector mounts, attenuators, and loads, will be discussed.

Introduction

SINCE World War II, technological advances in the utilization of ultra-high frequencies in the fields of communications, navigation, air surveillance and television have promoted an increasing interest in the development of rf filters designed to provide frequency discrimination and signal selection in both airborne and ground based equipment. Since such components designed in waveguide and coaxial lines would be large in the uhf spectrum, a relatively new distributed line structure, namely, strip-line, is particularly well suited for the realization of filters which are simply fabricated, are readily reproduced, and, in most cases, represent an appreciable saving in size and weight.

The purpose of this paper is, in general, to acquaint the engineer with some of the advantages afforded in the realization of rf components in a strip-line structure at ultra-high frequencies, and, more specifically, to present a general design procedure which can be employed in strip-line for the development of bandpass filters having a prescribed bandwidth, skirt selectivity, and pass-band ripple tolerance. In a previous paper,[1] design techniques for waveguide and coaxial filters,[2–4] were applied in the synthesis of strip-line filters having a "maximally-flat" selectivity. In this paper, a more general procedure is presented from which strip-line filters can be designed having either "maximally-flat" or Tchebycheff characteristics. However, as a result of the mathematical simplicity of the design equations in the former paper, the formulas presented here are recommended primarily for the use in the design of bandpass filters having a prescribed ripple tolerance or Tchebycheff response.

Experimental strip-line filters having 10 per cent bandwidths at S-band have been developed with less than 1 db mid-band insertion loss and with greater than 50 db rejection at frequencies 9 per cent from the center frequency. Using engraving techniques instead of the more commonly employed photo-etching techniques[5,6] strip-line filters can be fabricated with such precision that tuning screws are generally not required to align the filters to a desired center frequency. The design techniques discussed in this paper are general and, therefore, not restricted to the realization of the above filter characteristics. The application of strip-line techniques in the development of other microwave components such as detector mounts, attenuators and loads will also be discussed.

Filter Design Procedure

Bandpass filters to be realized in a strip-line structure can be synthesized in a manner similar to that employed in the design of lumped parameter filters at much lower frequencies.[7,8] This close correlation between lumped and distributed parameter circuits is not always recognized. For that reason, it is hoped that the following design procedure will be both enlightening and helpful to those engineers who are interested in the development of bandpass filters in a strip-line structure.

The first step in the design of filters is the selection of an appropriate power loss ratio, P_0/P_L, or transmission coefficient, $|t(j\omega)|^2$, corresponding to a network having the desired rejection-band characteristics. One type of commonly used transmission coefficient, which results in what is called a "maximally-flat" selectivity, is that derived from the Butterworth function:

$$|t(j\omega)|^2 = \frac{1}{1+\omega^{2n}}, \tag{1}$$

† Melpar, Inc., Falls Church, Va.

[1] E. H. Bradley and D. R. White, "Band-pass filters using strip-line techniques," *Electronics*, vol. 25, pp. 152–155; May, 1955.

[2] W. W. Mumford, "Maximally-flat filters in waveguide," *Bell. Sys. Tech. Jour.*, vol. 27, pp. 684–713; October, 1948.

[3] G. C. Southworth, "Principles and application of waveguide transmission," D. Van Nostrand Co., Inc., New York, N. Y., p. 297; 1950.

[4] G. L. Ragan, "Microwave transmission circuits," Rad. Lab. Ser., McGraw-Hill Book Co., New York, N. Y. pp. 645–673; 1948.

[5] R. M. Barrett, "Etched sheets serve as microwave components," *Electronics*, vol. 25, pp. 114–118; June, 1952.

[6] K. S. Packard, "Machine methods make strip transmission line," *Electronics*, vol. 27, pp. 148–150; September, 1954.

[7] E. A. Guillemin, "Modern methods of network synthesis," *Advances in Electronics*, vol. III, Academic Press, Inc., New York, N. Y. pp. 261–303; 1951.

[8] J. R. Whinnery, "Design of microwave filters," *Proc. Sym. Mod. Network Synth.*, New York, pp. 296–311; April, 1952.

where n designates the number of frequency sensitive elements in the low-pass prototype shown in Fig. 1 and ω is the normalized frequency variable in radians. Still another type of transmission coefficient, which is based on the Tchebycheff polynomial $T_n(j\omega)$ and causes an oscillatory behavior in the pass-band, is expressed in (2):

$$|I(j\omega)|^2 = \frac{1}{1 + \epsilon^2 T_n^2(\omega)}, \tag{2}$$

where ϵ specifies the ripple tolerance in the pass-band. The Butterworth function, whose poles are uniformly distributed on a semicircle centered at the origin of the complex frequency plane, is classified as a special case of the Tchebycheff function, in which the poles lie on the periphery of a semi-ellipse centered at the origin. For given band-rejection characteristics or skirt selectivity, fewer elements are required when the synthesis is based on a Tchebycheff distribution.

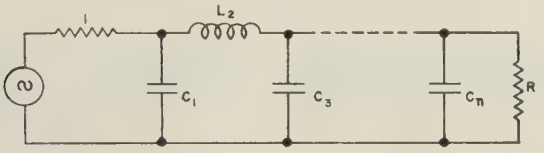

Fig. 1—Low-pass filter prototype.

In the design of filters requiring extremely sharp skirt selectivity, the Jacobian elliptic function is often used to approximate the desired response function. However, for most practical applications, the use of either the Butterworth or Tchebycheff approximation will suffice.

Following the selection of an appropriate transmission coefficient, which for the purpose of this paper is assumed to be either the Butterworth or Tchebycheff response function, the corresponding low-pass prototype can be synthesized from (1) or (2) using a procedure outlined in Appendix A. From this low-pass prototype, a bandpass filter [*c.f.* Fig. 2(a)] can be readily obtained with a low-pass-to-bandpass transformation which is equivalent to replacing each series inductance of the prototype with a series LC circuit resonant at the desired center frequency and each shunt capacitance with a parallel resonant tank. As will be seen later, this configuration is not as easily realized in strip-line as is the circuit shown in Fig. 2(b).

It should be noted that the transmission coefficient of the former network has an equal zero distribution at zero and infinite frequencies in the complex frequency plane, whereas the filter shown in Fig. 2(b) has an unequal distribution with $2n-1$ zeros at zero frequency and 1 at infinite frequencies (n is here defined as the number of resonant elements). For this reason, there exists no one-to-one relationship between the response characteristics of these two circuits. However, if the driving-point impedances of the two networks are equated and if the circuit components of one network is expressed in terms of the other, the pole distribution of each network will be identical. Although the zero distribution of the filters differ, the response characteristics are essentially identical in the neighborhood of the passband for small filter bandwidths. For large bandwidths, the frequency response characteristic of the filter having an unequal zero distribution will be asymmetrical.

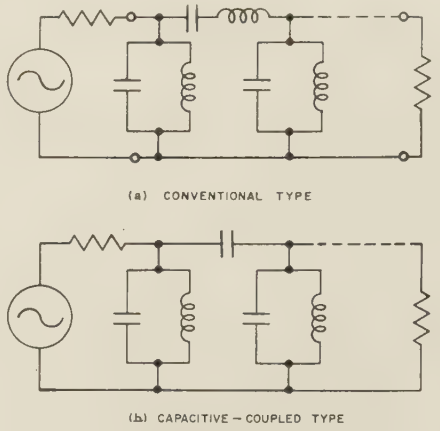

Fig. 2—Lumped element bandpass filters.

By equating the driving-point impedances for the band-pass equivalent of the low-pass prototype [*c.f.* Fig. 2(a)] and the capacitive-coupled filter shown in Fig. 2(b), the circuit parameters of the latter network can be expressed in terms of those of the prototype.[9] In order to design an equivalent filter in strip-line, an analogy can be made between the capacitive-coupled filter and the direct-coupled cavity-type filter of Fig. 3.

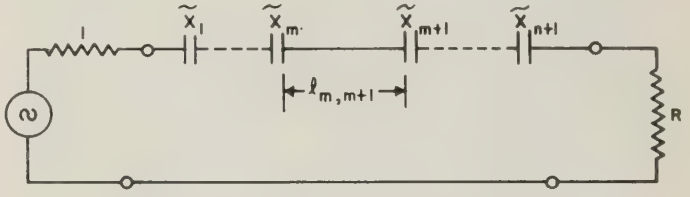

Fig. 3—Direct-coupled cavity-type filter.

Considering the first resonant circuit as an asymmetrically loaded cavity, the normalized coupling reactance at the input, $\tilde{X}_1$, can be expressed in terms of the prototype as follows:

$$|\tilde{X}_1| \simeq \sqrt{\frac{2}{\pi} C_1 \frac{f_0}{\Delta f}}, \tag{3}$$

where C_1 is derivable from the prototype (*c.f.* Fig. 1)

f_0 = center frequency of the bandpass filter
Δf = filter bandwidth.

In the design of filters having bandwidths in excess of 10 per cent, the accuracy of (3) is questionable.

[9] Ragan, *op. cit.*, pp. 661–666.

The normalized reactance of the end discontinuity is

$$|\tilde{X}_{n+1}| = |\tilde{X}_1| \sqrt{\frac{\overline{Ln}}{RC_1}} \quad \text{for } n \text{ even} \qquad (4)$$

and

$$|\tilde{X}_{n+1}| = |\tilde{X}_1| \sqrt{\frac{\overline{RC_n}}{C_1}} \quad \text{for } n \text{ odd}, \qquad (5)$$

and the normalized reactances of all other discontinuities are

$$|\tilde{X}_m| = |\tilde{X}_1|^2 \frac{\sqrt{L_{m-1}C_m}}{C_1} \quad \text{for } m \text{ odd but } > 1, \qquad (6)$$

and

$$|\tilde{X}_m| = |\tilde{X}_1|^2 \frac{\sqrt{L_m C_{m-1}}}{C_1} \quad \text{for } m \text{ even}, \qquad (7)$$

where

m = serial number of the discontinuity = 1, 2, 3, $\cdots \leqq \eta$

R, L_m, C_m = prototype parameters designated in Fig. 1.

The separation of the reactance elements is

$$l_{m,m+1} = \frac{\lambda\alpha}{2\pi\sqrt{\epsilon}} \cdot \left[k\pi - \frac{1}{2}\left(\tan^{-1}\frac{2}{|\tilde{X}_m|} + \tan^{-1}\frac{2}{|\tilde{X}_{m+1}|} \right) \right], \qquad (8)$$

where

$\lambda\alpha$ = electrical wavelength in air

k = a positive integer

ϵ = dielectric constant of the transmission medium.

Physical Realization

Following the design of the bandpass filter, there remains the difficult problem of physically realizing the required circuit components in a strip-line structure. In order to achieve this objective, it is necessary to 1) choose the type of line structure, 2) select the most appropriate dielectric material for the particular application, 3) compile a reference library of normalized capacitive reactances vs gap spacing, and 4) fabricate the multi-stage filter using photo-etching and/or engraving techniques.

There are several different type strip transmission line structures,[10,11] the better known of which are illustrated in Fig. 4. In the development of rf components where line discontinuities are required, Melpar has employed the "sandwich" structure in order to reduce those problems introduced by line radiation and to facilitate the packaging of components. The choice of an air-dielectric or solid-dielectric structure is predicated largely upon the system requirements regarding space and weight as well as upon the allowable midband insertion loss.

In general, strip-line filters designed to operate at high frequencies (*i.e.*, $f_0 > 3{,}000$ mc) should be designed in an air-dielectric structure such as shown in Fig. 4(d). At lower frequencies where the consideration of space is often important, similar components can be designed in a solid-dielectric structure whose over-all size is reduced by the square root of the dielectric constant; in so doing, however, the weight of the units is appreciably increased. In the development of narrow bandwidth filters (*e.g.*, bandwidth less than 1 per cent), the presence of a solid-dielectric material between the strip and the associated ground planes generally increases the midband insertion loss of the assembly to an extent dependent upon the frequency of operation. When a solid-dielectric structure is desired, the line shown in Fig. 4(c) is particularly advantageous. Although the single-line structure [*c.f.*, Fig. 4(b)] can be fabricated more readily, the use of a double-strip structure greatly simplifies the fabrication of other strip-line components, such as attenuators, loads, detector mounts, and tunable filters. Although certain general recommendations can be made, the choice of an air or solid-dielectric structure must be consistent with the specific electrical and physical specification of the component. In order to facilitate the development and interconnection of strip-line components, the line structure shown in Figs. 4(c) and 4(d) have been standardized at Melpar.

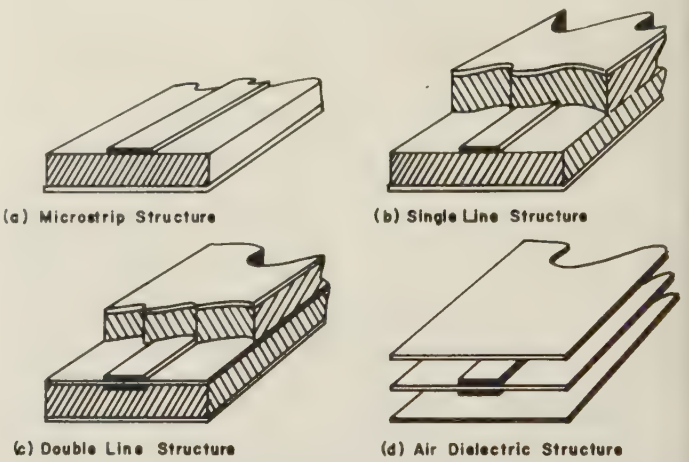

Fig. 4—Strip transmission line structures.

The choice of a dielectrical material for use in the strip-line structure is particularly important for several reasons:

1) Variations in the wavelength will drastically effect the electrical performance of the filter.
2) A lossy dielectric material will appreciably increase the midband insertion loss and limit the maximum loaded Q which can be realized.

For these reasons, only those materials having a low loss-tangent, a satisfactory degree of homogeneity, suitability for copper cladding and good environmental

[10] E. G. Fubini, W. E. Fromm, and H. S. Keen, "New techniques for high-Q strip components," Convention Record of the IRE, Part 8, p. 91; 1954.

[11] D. D. Greig and H. F. Englemann, "Microstrip—A new transmission technique for the kilomegacycle range," Proc. IRE, vol. 40, pp. 1644–1650; December, 1952.

characteristics can be considered. Following an extensive investigation of various copper-clad dielectric materials (*viz.*, Mycalex, pure teflon, epoxy, ceramic, and teflon fiberglass), teflon fiberglass has been selected for use at Melpar.

The final preparatory step in the realization of the capacitive-coupled strip-line filters is the compilation of normalized reactance data. A series capacitance is easily realized in a strip transmission line by making a gap in the center conductor [*c.f.*, Fig. 5(a)]. A reference library of normalized capacitive reactances as a function of gap spacing can be compiled experimentally in either of two ways:

1) Test one-stage strip-line filters having different gap spacings at a specified frequency.
2) Make impedance measurements on a single gap using slotted-line techniques.

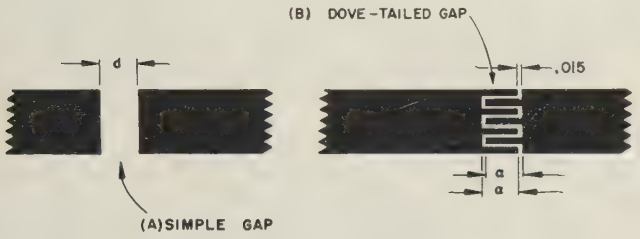

Fig. 5—Series capacitance realization in strip line.

The former approach has been employed at Melpar since the capacitive reactance of a gap spacing can be readily computed from (9) following the measurement of the loaded Q of a one-stage filter:

$$|\tilde{X}_g| = \sqrt{\frac{4}{\pi}\frac{f_0}{\Delta_f}}. \qquad (9)$$

In order to realize the higher capacitances required at the lower frequencies without making the gap spacings unrealistically small (less than 0.010 inches), a dove-tailed gap shown in Fig. 5(b) is employed. Typical reference libraries of standard and dove-tailed gaps compiled at 2,000 mc in an air-filled line are shown in Fig. 6.

In an effort to maintain closer tolerances in the fabrication of strip-line filters, an engraving technique has been developed to replace the less accurate photo-etching methods still used on less precise work. An experimental evaluation of the reproducibility of strip-line filters using both fabrication techniques has verified that improved tolerances can be realized with engraving. Using photo-etching techniques, the widths of the smallest capacitive gaps employed (viz., 0.010 inch) were found to vary from −35 per cent to +5 per cent, while the variation in similar engraved gaps can be maintained within micrometer tolerances. Although the bandwidth on the photoetched cavities ($Q_L = 40$) centered at 3,000 mc varied as much as 19 per cent, the bandwidth of the engraved cavities varied less than 6 per cent.

Experimental Results

Using the formulas and reference data discussed above, bandpass filters having either Tchebycheff or "maximally-flat" response characteristics can be designed and fabricated. The choice of a particular filter selectivity is dependent upon the desired application.

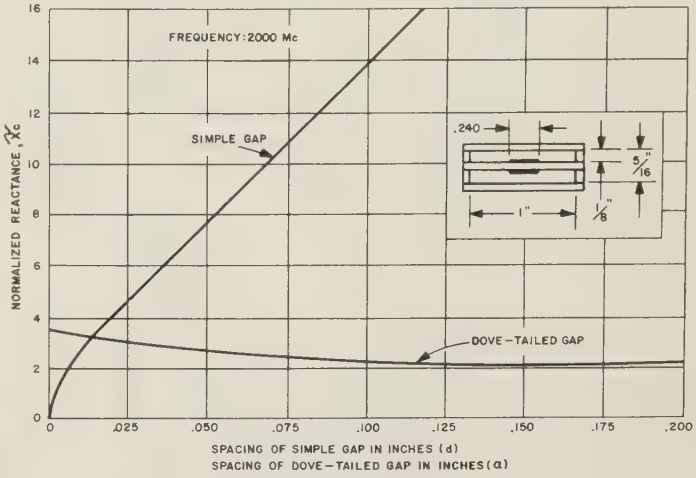

Fig. 6—Design data for strip-line filters.

Five-stage bandpass filters having a Tchebycheff response function and a 3-db ripple tolerance have been developed in an air-dielectric structure at 2,150 mc with a 10 per cent bandwidth. A typical unit shown in Fig. 7 has a minimum insertion loss of less than 1 db,

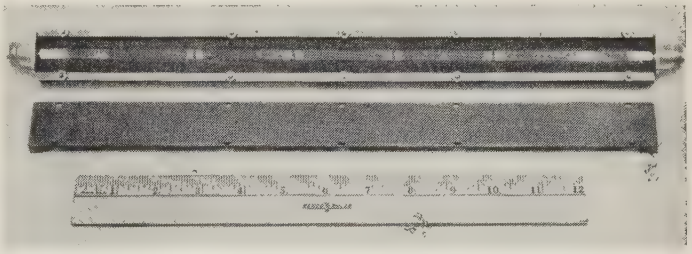

Fig. 7—Five-stage filter having Tchebycheff response.

and a rejection of greater than 50 db at frequencies 9 per cent from the center frequency; the theoretical and experimental response functions are plotted in Fig. 8.

For those applications where ripples in the filter pass-band must be kept to a minimum, strip-line filters can be designed to have a "maximally-flat" selectivity using the same design equations. Six-stage "maximally-flat" filters having a 10 per cent bandwidth and 40 db rejection at frequencies 12 per cent from the center frequency have been developed at 1,435 mc. Typical theoretical and experimental response functions for such a solid-dielectric filter are shown in Fig. 9.

It is of interest to note that the performance of strip-line filters under extreme environmental operating conditions is particularly good. In temperature cycling a six-stage filter with an air-dielectric structure from

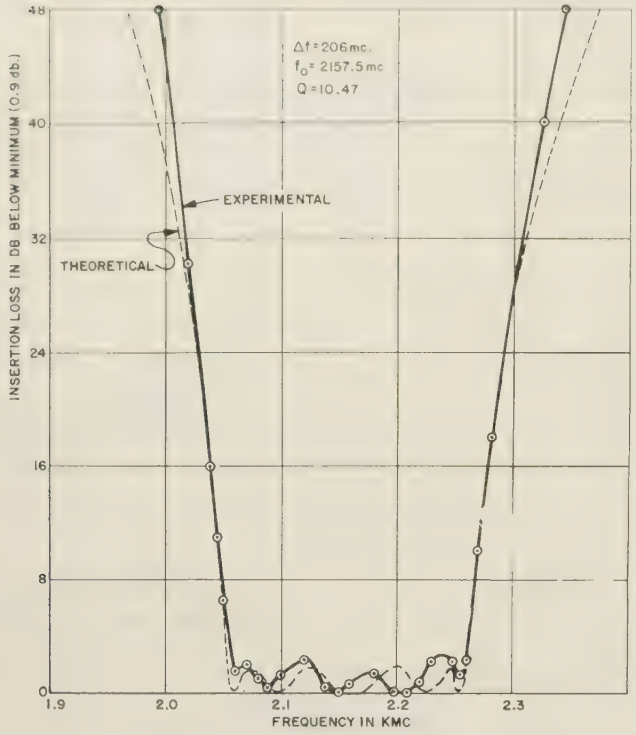

Fig. 8—Tchebycheff response characteristics of five-stage strip-line filter.

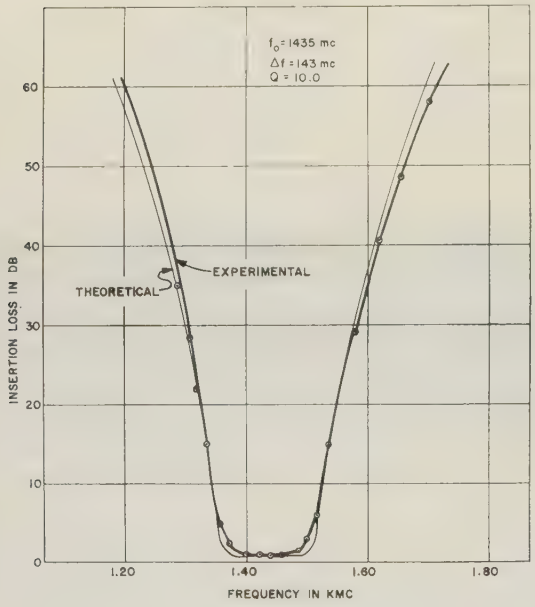

Fig. 9—Maximally-flat response characteristics of six-stage strip-line filter.

+25°C to +125°C, the center frequency decreased only 0.03 per cent at 125°C corresponding to a 0.3 db change in the insertion loss at the 8 db points on the filter skirts.

Bandpass filters having both Tchebycheff and "maximally-flat" response functions are currently being developed for use in the frequency range from 400 to 6,000 mc. In order to shorten those filters designed at the lower frequencies, the strip-line can be fabricated in a "snake-like" configuration with reactance gaps or the equivalent lumped capacitors located in the linear portion of the line. The effect of reflections from the impedance discontinuities at the bends has been found to be negligible.

In many applications, filters must have a large insertion loss over a wide frequency spectrum outside of their fundamental pass-bands. However, distributed parameter networks, similar to those discussed here, are subject to spurious responses at approximately integer multiples of the fundamental. Spurious responses of this type can be removed with a low-pass filter having a cutoff frequency somewhat less than that of the first spurious response; this type of filter can be readily developed in a strip-line structure.[12]

Associated Strip-Line Components

Strip-line is not only well-suited for the realization of bandpass filters but also for the fabrication of numerous other associated rf components,[13] such as tunable detector mounts, pad attenuators, rf loads, and multiplexers.

For example, tunable detector mounts having bandwidths greater than 10 per cent have been designed to tune over a frequency range from 400 mc to greater than 6,000 mc. A typical unit, shown in Fig. 10, has a sensitivity of greater than −48 dbm over the designed frequency range when operated in conjunction with a conventional video amplifier. These mounts have been developed in both solid and air-dielectric structures.

Fixed attenuators having insertion losses of 3 to 10 db have been developed with vswr's of less than 1.3 over a 2 to 1 frequency range centered at S-band using 50-ohm resistive cards placed symmetrically between the strip and the adjacent ground planes. Using similar techniques, strip-line loads have been developed for use over a comparable frequency range.

Since most laboratory test equipment is designed for use with either waveguide or coax structures, the development of both coax-to-strip-line and waveguide-to-strip-line adaptors was required. Broadband transitions for both waveguide and coax have been developed and are show in Fig. 11; the vswr of each of these units is less than 1.3 over its operation frequency range. Flange connectors are utilized to facilitate the interconnection of strip-line components without requiring the use of intermediate adaptors. In order to facilitate the evaluation of these components, a strip-line slotted section operating in a standard Hewlett Packard carriage has been designed to operate over a frequency range from 2,000 to 6,000 mc; this unit is shown in Fig. 12.

[12] H. C. Hyams, "Design of a flat strip or printed circuit microwave low-pass filter," *Melpar Tech. Rep.*

[13] N. R. Wild, "Photoetched microwave transmission lines," *Symposium on Microwave Strip Circuits*, Tufts College; October 1954.

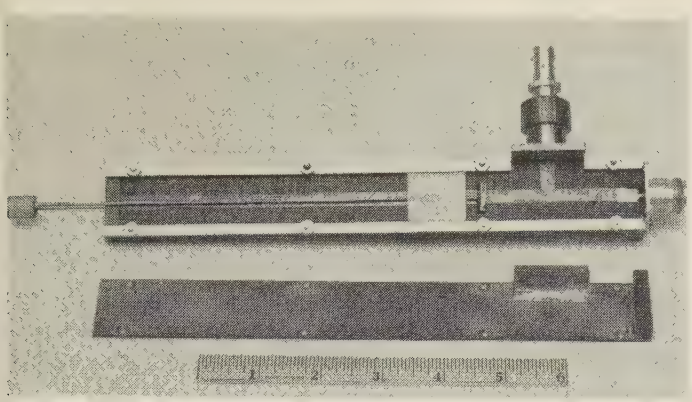

Fig. 10—Tunable strip-line detector mounts.

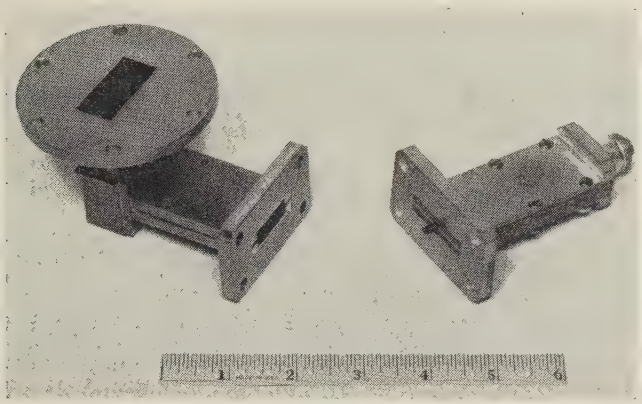

Fig. 11—Strip-line transitions to waveguide and coaxial line.

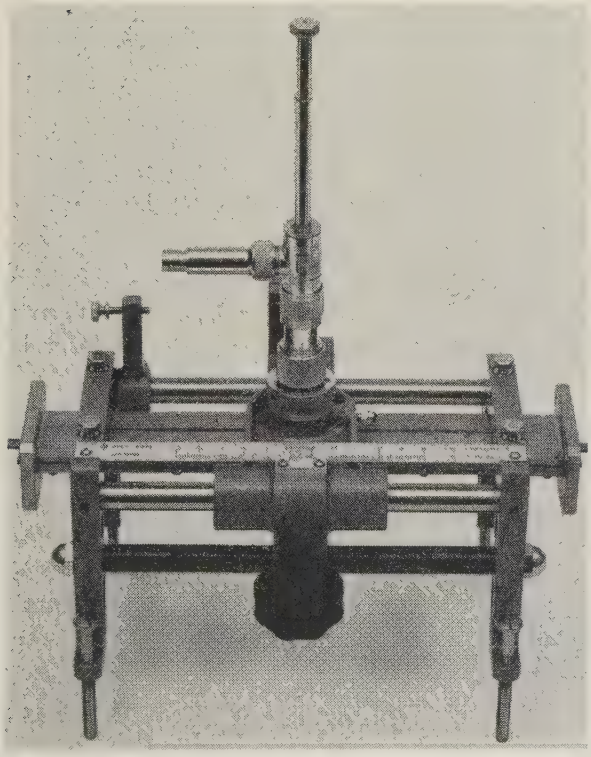

Fig. 12—Strip-line slotted section.

Conclusion

The design formulas and the realization techniques presented here provide the engineer with a formalized design procedure for the development of bandpass filters having a prescribed bandwidth, skirt selectivity and passband ripple tolerance in a strip-line structure. Rf components developed in strip line have certain advantages over their waveguide and coaxial line counterparts in the uhf spectrum. For that reason, it is anticipated that strip-line techniques will be found increasingly applicable in this frequency range for the future development of rf components, such as bandpass filters.

Appendix A

Synthesis of Two-Terminal-Pair Networks Terminated at Both Ends[14]

The power-loss ratio, P_0/P_L, or the transmission coefficient, $|t(j\omega)|^2$, is used to specify the insertion loss characteristics of a two-terminal-pair network terminated at both ends. Mathematically, this rational function or ratio of two polynomials can take any one of many different forms depending upon the desired frequency response. The Butterworth function (sometimes called the "maximally-flat" function), the Tchebycheff functions of the first and second kind, and the Jacobian elliptic function are commonly used in the design of amplifiers, receivers and filters.

A low-pass prototype having resistive terminations at both terminal pairs can be synthesized[15] such that its response function approximates the Tchebycheff polynomial of the first kind having a ripple tolerance ϵ, or

$$|t(j\omega)|^2 = \frac{1}{1+\epsilon^2 T_n^2(\omega)}. \tag{10}$$

where

$t(j\omega)$ = ratio of the voltage of the transmitted wave to the voltage of the incident wave.

ϵ = ripple tolerance[16]

$T_n(\omega)$ = Tchebycheff polynomial of the first kind.[17]

Furthermore,

$$|t(j\omega)|^2 = 1 - |\rho(j\omega)|^2 \tag{11}$$

[14] The following appendix is not intended to give a rigorous development of a synthesis technique, but rather to formulate a workable procedure which can be readily applied by the engineer.

[15] E. A. Guillemin, unpublished class-room notes.

[16] The ripple tolerance in db is $-10 \log (1+\epsilon^2)$.

[17] The Tchebycheff polynomial, $T_n(\omega)$, can be expanded as follows:

$$T_1(\omega) = \omega$$
$$T_2(\omega) = 2\omega^2 - 1$$
$$T_{n+1}(\omega) = 2\omega T_n(\omega) - T_{n-1}(\omega).$$

or

$$|\rho(j\omega)|^2 = \rho(j\omega)\rho(-j\omega) = \frac{\epsilon^2 T_n^2(\omega)}{1+\epsilon^2 T_n^2(\omega)}, \qquad (12)$$

where

$\rho(j\omega)$ = reflection coefficient.

To insure physical realizability, the poles of the function expressed in (12) must be in the left half of the complex frequency plane (*i.e.*, $\sigma_n \leqq 0$ where the complex variable, s, is defined as $s_n = \sigma_n + j\omega_n$). The zeros of the function are not so restricted; however, in order to maximize the gain-bandwidth product for a given associated shunt capacitance, the zeros must lie in the left half-plane.

For the purpose of this discussion, a minimum phase function (*i.e.*, zeros in the left half-plane) will be formulated. Using the following equations, the poles and zeros can be immediately identified:

$$s_{pk} = -\sin\frac{k\pi}{2n}\sinh\phi_2 + j\cos\frac{k\pi}{2n}\cosh\phi_2, \qquad (13)$$

where

S_{pk} = location of the pole in the complex plane.
$k = 1, 3, 5, \cdots 2n-1$.
n = order of the polynomial (*i.e.*, number of frequency sensitive elements in the low-pass structure).

$$\sinh\phi_2 = \frac{(\alpha+\beta)^{1/n} - (\alpha-\beta)^{1/n}}{2} \qquad (14)$$

$$\cosh\phi_2 = \frac{(\alpha+\beta)^{1/n} + (\alpha-\beta)^{1/n}}{2} \qquad (15)$$

$$\alpha = \sqrt{1+\frac{1}{\epsilon^2}} \qquad (16)$$

$$\beta = \frac{1}{\epsilon} \qquad (17)$$

and

$$s_{0m} = -j\cos\frac{m\pi}{2n} \qquad (18)$$

where

S_{0m} = location of m^{th} zero in the complex plane
$m = 1, 3, 5, \cdots 2n-1$.

With the left half-plane poles and zeros specified in (13) and (18), respectively, the reflection coefficient, $\rho(j\omega)$, can be formulated.

$$\rho(j\omega) = \frac{\prod_{m=1,3,5}^{2n-1}(s - s_{0m})}{\prod_{k=1,3,5}^{2n-1}(s - s_{pk})}. \qquad (19)$$

The driving point impedance, $Z_{11}(j\omega)$, can then be expressed in terms of the reflection coefficient, or

$$Z_{11}(j\omega) = \frac{1-\rho(j\omega)}{1+\rho(j\omega)}. \qquad (20)$$

A two-terminal-pair ladder network terminated at both ends can be synthesized from the driving-point impedance. The method of attack is dependent upon the desired circuit configuration. If the network is to have a shunt capacitor across the input terminals, a pole of the driving-point *admittance*, $Y_{11}(j\omega)$, must be removed at $s = \infty$. If a series inductance is desired at the input, a pole at $s = \infty$ must be removed from the driving-point *impedance*, $Z_{11}(j\omega)$. The expansion then continues until all of the components in the desired ladder network have been specified.

In a similar manner, a low-pass prototype can be synthesized such that its response function provides a "maximally-flat" (Butterworth) selectivity, or

$$|t(j\omega)|^2 = \frac{1}{1+\omega^{2n}}. \qquad (21)$$

Using (22), the left half-plane poles of the Butterworth function can be specified

$$s'_{pk} = -\sin\frac{k\pi}{2n} + j\cos\frac{k\pi}{2n}, \qquad (22)$$

where

s'_{pk} = location of the k^{th} pole in the complex plane,
$k = 1, 3, 5, \cdots 2n-1$,
n = order of the polynomial.

It should be noted that, in this case, the n zeros of $\rho(j\omega)$ all occur at $s = 0$, or

$$s_{0m}' = 0, \qquad (23)$$

where

S'_{0m} = location of the $m_0'^{th}$ zeros in the complex plane,
$m = 1, 3, 5, \cdots 2n-1$.

With the left half-plane poles and zeros specified in (22) and (23), respectively, the reflection coefficient for the Butterworth approximation can also be formulated using (19).

Example

The design procedure which has been outlined in the previous paragraphs can best be illustrated with an example. In order to simplify the mathematics, it will be assumed that a three-stage network having resistive terminations at both ends and a 3 db ripple in the pass-band (*i.e.*, $\epsilon = 1$) is required.

With

$$\alpha = \sqrt{2} \quad \text{from (16)}$$

$$\beta = 1 \quad \text{from (17)}$$

$$\sinh\phi_2 = 0.298 \quad \text{from (14)}$$

$$\cosh\phi_2 = 1.043 \quad \text{from (15)}$$

the poles of the network can be computed from (13),

$$s_{p1} = -0.149 + j0.903$$

$$s_{p3} = -0.298 + j0.$$

$$s_{p5} = -0.149 - j0.903.$$

From (18), the zeros are found to be

$$s_{01} = -j0.866$$

$$s_{03} = -j0$$

$$s_{05} = +j0.866.$$

Substituting the poles and zeros in (19),

$$\rho(j\omega) = \frac{s(s^2 + 0.750)}{s^3 + 0.596s^2 + 0.927s + 0.250}.$$

From (20),

$$Z_{11}(j\omega) = \frac{0.596s^2 + 0.177s + 0.250}{2s^3 + 0.596s^2 + 1.677s + 0.250}.$$

Since a shunt capacitance is desired at each terminal pair, the continued fraction will be formulated such that a pole is initially removed from the driving-point admittance, $1/Z_{11}(j\omega)$, at $s = \infty$.

$$\begin{array}{r|l} & 3.36s \\ \hline .596s^2 + .177s + .250 & 2s^3 + .596s^2 + 1.677s + .250 \\ & 2s^3 + .596s^2 + .838s \\ \hline & .839s + .250 \end{array}$$

$$\begin{array}{r|l} & .71s \\ \hline .839s + .250 & .596s^2 + .177s + .250 \\ & .596s^2 + .177s \\ \hline & .250 \end{array}$$

$$\begin{array}{r|l} & 3.36s \\ \hline .250 & .839s + .250 \\ & .839s \\ \hline & .250 \\ & 1.0 \\ \hline .250 & .250 \end{array}$$

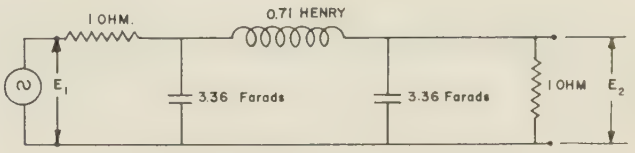

FIG. 13—Low-pass prototype ($\eta = 3$) having Tchebycheff response ($\epsilon = 1$).

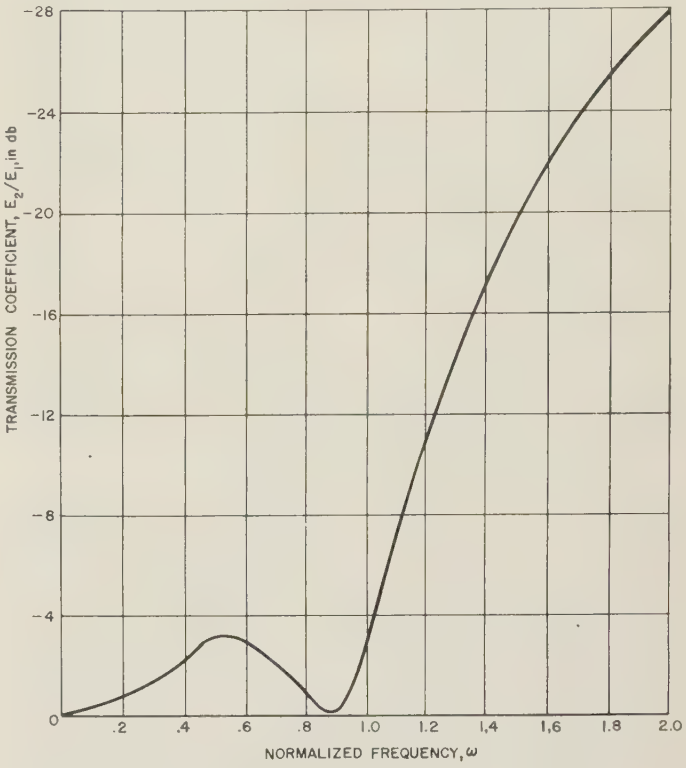

Fig. 14—Tchebycheff response ($\epsilon = 1$) characteristics for low-pass prototype ($\eta = 3$).

The resulting network and its selectivity are shown in Figs. 13 and 14, respectively.

ACKNOWLEDGMENT

The author wishes to acknowledge the helpful assistance of Messrs. D. J. Alstadter, P. Rock and H. C. Turnage in the compilation of the data presented in this report, and Messrs. E. A. Beck and C. P. Andrikian for their technical contributions in the development of the associated strip-line components.

Measurement of Crystal Impedances at Low Levels*

H. N. DAWIRS† AND E. K. DAMON†

Summary—It is very important to know the impedances of crystal diodes when constructing circuits such as mixers and detectors in which the crystals are used. It is always difficult to measure these impedances due to the nonlinear characteristics of the crystals but it is most difficult to make the measurements at minimum levels at which the crystals operate, since with such methods as the slotted line, the detector must operate at a still lower level to obtain the required probe decoupling. Thus, since the load whose impedance is being measured is itself a crystal operating at its minimum level, it is practically impossible to obtain a detector with sufficient sensitivity to make the measurement.

Crystal impedances at these minimum levels are of utmost importance as it is here that optimum matching is essential for maximum sensitivity.

This paper describes practical techniques which use only standard equipment to measure crystal impedances at low levels. The detector used is a crystal of the same type as that being measured. The method is capable of precise results and good measurements can be obtained at low levels with little more effort than is normally required in making careful impedance measurements.

THE proper design of detectors and mixers using crystals requires a knowledge of the impedance characteristics of these crystals. Such knowledge is particularly important at low levels where only crystals are sensitive enough to serve as detectors or mixers and maximum sensitivity is required. It is difficult, however, to measure or even to define the impedance of a crystal due to its nonlinearity.

Consider the measurement of crystal impedances by the usual slotted line method in which the crystal whose impedance is to be measured is mounted in a suitable holder on the end of the line as a load (see Fig. 1).

Since the crystal is nonlinear its power level must be maintained constant throughout a measurement. The relative power level at which the crystal is operating can be determined by measuring its dc or modulation output, as shown in Fig. 1.

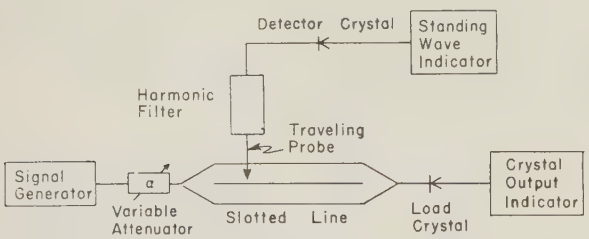

Fig. 1—Measurement of crystal impedances using modified slotted-line method.

Also when the measuring signal is applied to the crystal, harmonics are generated and fed back into the line, interfering with the measurements. The effect of these harmonics may be eliminated by a low-pass filter in the probe circuit to prevent them from reaching the detector, so that the measurements are made essentially at the fundamental frequency. The results are strictly valid only when the crystal is operating under conditions identical to those under which the measurements were made, but are useful as long as the output circuits are duplicated and low impedance return circuits are provided for the dc and modulation signals which are generated by the crystal.

Since it is desired to measure crystal impedance at the lowest levels at which they will operate, it is necessary to use a similar crystal as a detector, or as the mixer in a superheterodyne receiver. Thus the minimum level at which measurements can be made is determined by the detector crystal, which operates at a much lower level than the load crystal because of the necessary probe decoupling. Thus it is impossible to measure the impedances of crystals operating at very low levels by conventional slotted line methods.

Elimination of the difference in operating levels of the load and detector crystals resulting from the probe decoupling may be accomplished by interchanging the generator and detector as shown in Fig. 2. It can be

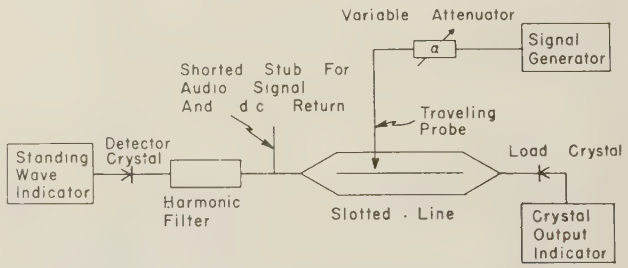

Fig. 2—Slotted-line measuring circuit obtained by interchanging generator and detector.

shown, (see Appendix I) that for loads on the ends of the slotted line, with a signal fed into the line through the probe, the current in one load as a function of probe position is proportional to the voltage existing in the line at the probe. The restrictions are the same as for the conventional slotted line method (*i.e.*, very loose coupling of the probe to the line, etc.).

It can be shown that if the two loads have the same standing wave ratio, there is a spacing for which the standing waves for the two loads will coincide, and the currents in the two loads will be identical at all times. Thus if the current in the load crystal is maintained at a fixed level, the current in the detector crystal will also remain constant. The voltage standing wave ratio will be determined from the variation in attenuation required to maintain the level constant. Thus the system is linear and, with an accurately calibrated at-

* The research reported in this paper was sponsored by the Air Res. and Dev. Command, Wright Air Dev. Center, Wright-Patterson AFB, Ohio.

† Antenna Lab., Dept. Elec. Engrg., Ohio State Univ., Columbus, Ohio.

tenuator, crystal impedances can be precisely measured at low levels.

The two standing waves in the line can be made to coincide quite closely, by means of a triple-stub tuner in the detector circuit as shown in Fig. 3. This tuner also serves as a dc and modulation signal return for both crystals. The fact that, in practice, the two standing waves in the line are not likely to coincide exactly means that there is some variation in the detector crystal output. This variation must be added to the attenuator variation to obtain the voltage standing-wave ratio induced in the line by the load crystal. With careful tuning this variation can be kept small so that the nonlinear characteristics of the detector crystal do not affect the system appreciably.

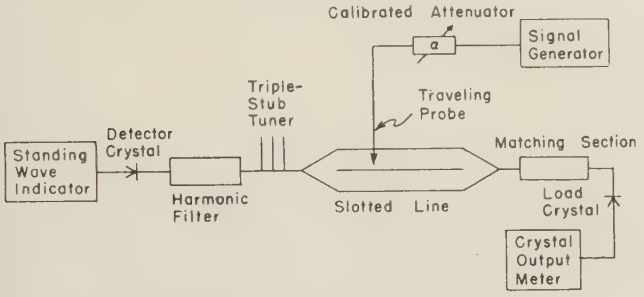

Fig. 3—Circuit for measuring crystal impedances at low levels.

At low levels the impedance of the load crystal is so high that the effective impedance at a high-voltage point in the line is comparable to the transfer impedance between the probe and the line. When this occurs the probe is no longer loosely coupled to the line and consequently the measurements are no longer valid.

However, a matching section may be used to transform the high impedance of the crystal to a value more nearly equal to the characteristic impedance of the line, thus reducing the standing waves in the line. This method requires an accurately constructed matching section and involves considerable computation to determine the impedance of the crystal itself. The matching section may introduce considerable loss which can interfere with the measurement of the crystal. However, the crystal most certainly will be used with a matching section in practice, in which case the losses in the matching section should logically be included in the measurements.

The high crystal impedances may also be determined without a matching section by making all measurements in the vicinity of a voltage minimum[1] (see Appendix II). Such measurements require very precise positioning of the probe for accuracy.

Curve 1 in Fig. 4 shows the voltage standing-wave ratio of a crystal alone with respect to a 50 ohm line. The measurements were made with a matching network as shown in Fig. 3, and then the impedance of the crystal itself was calculated from these measurements.

[1] Montgomery, "Technique of microwave measurements," McGraw-Hill Book Company, New York, p. 505, 1947.

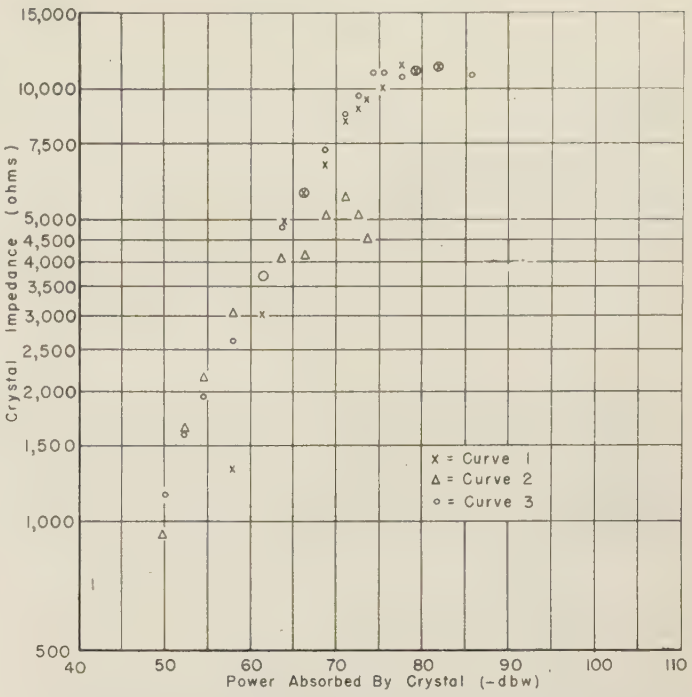

Fig. 4—Comparison of voltage standing-wave ratios determined by three different measurement techniques.

Curve 2 shows the measurements made on the same crystal with no matching section.

Curve 3 is obtained without the matching section but with all measurements made in the vicinity of a voltage minimum.

The Curves in Fig. 5 show the voltage standing-wave ratios of a number of 1N21B crystals with respect to 50 ohms, as determined by measurements made in the vicinity of a voltage minimum.

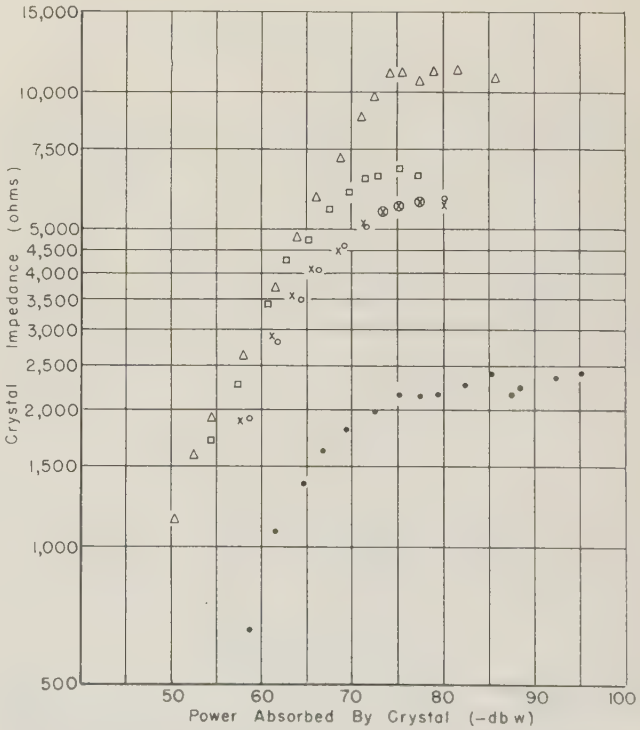

Fig. 5—Voltage standing-wave ratios with respect to fifty ohms measured on five different 1N21B crystals.

Conclusion

Curves 1 and 3 in Fig. 4 inspire considerable confidence in the two methods of measuring crystal impedances at low levels.

The techniques described should be valuable in obtaining crystal impedance data as the basis for the design of crystal mixers and detectors, for further studying the characteristics of crystals, and, as suggested by Fig. 5, for selecting crystals with similar characteristics.

Appendix I

Consider a slotted line with a load on each end which is fed through a loosely coupled probe as shown in the diagram of Fig. 6(a). Figure 6(b) is the equivalent circuit diagram. It is desired to know the currents in the impedances as a function of probe position.

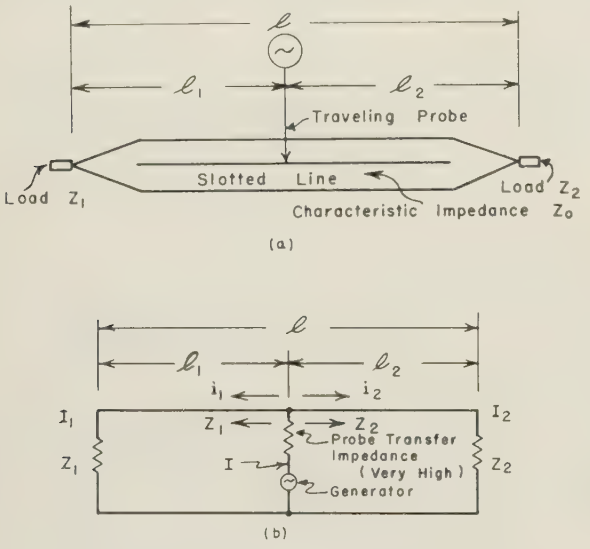

Fig. 6—(a) Diagram of the slotted-line setup. (b) Equivalent circuit diagram.

All impedances are normalized to the characteristic impedance Z_0 of the slotted line. Since the probe is loosely coupled to the line the transfer impedance is very high and the probe current I is considered to be constant.

i_1 and z_1 respectively are the current and the impedance seen by the probe looking toward Z_1. Similarly i_2 and z_2 are the current and impedance respectively, seen by the probe looking toward Z_2. Now by conventional transmission line theory:

$$i_1 = I_1(\cos \beta l_1 + Z_1 \sin \beta l_1)$$

$$i_2 = I_2(\cos \beta l_2 + jZ_2 \sin \beta l_2)$$

$$z_1 = \frac{Z_1 \cos \beta l_1 + j \sin \beta l_1}{\cos \beta l_1 + jZ_1 \sin \beta l_1}$$

$$z_2 = \frac{Z_2 \cos \beta l_2 + j \sin \beta l_2}{\cos \beta l_2 + jZ_2 \sin \beta l_2}.$$

At the probe the voltages across the two branches are equal, *i.e.*:

$$i_1 z_1 = i_2 z_2.$$

Solving for I_2,

$$I_2 = I_1 \frac{Z_1 \cos \beta l_1 + j \sin \beta l_1}{Z_2 \cos \beta l_2 + j \sin \beta l_2}.$$

The total probe current I will be the sum of the two branch currents, *i.e.*,

$$I = i_1 + i_2.$$

Solving these equations for I_1:

$$I_1 = \frac{I}{(Z_1+Z_2)\cos \beta l + j(1+Z_1Z_2)\sin \beta l}(Z_2 \cos \beta l_2 + j \sin \beta l_2)$$

$$= i(Z_2 \cos \beta l_2 + j \sin \beta l_2)$$

where

$$i = \frac{I}{(Z_1 + Z_2)\cos \beta l + j(1 + Z_1Z_2)\sin \beta l}$$

is a constant since I is assumed to be constant and Z_1, Z_2, and l are fixed. Hence

$$I_1 = \alpha(Z_2 \cos \beta l + j \sin \beta l),$$

which is precisely the same variation as is experienced by the voltage in a line of characteristic impedance Z_0 when it is terminated in an impedance of Z_2. Thus the voltage wave in the slotted line due to the load Z_2 may be determined by the current in Z_1. Similarly the voltage wave in the line due to the load Z_1 may be measured by the current in Z_2.

Appendix II

It is to be noted that if the two standing waves in the line do not coincide exactly it will be inconvenient to apply the so-called "twice-minimum" technique, since two values, the detector variation and the attenuator variation, are involved. However, measurements at two arbitrary points near the minimum give the same results. The following formula is convenient for determining the resulting voltage standing-wave ratio:

$$\text{vswr} \cong \frac{\sqrt{R_1 - 1} + \sqrt{R_2 - 1}}{2\pi d_\lambda} \text{ for } d_\lambda \text{ small}$$

where

$$R_1 = \left|\frac{E_1}{E_m}\right|^2 \quad \text{and} \quad R_2 = \left|\frac{E_2}{E_m}\right|^2.$$

E_1, E_2, and E_m are voltages measured at points l_1, l_2, and the minimum respectively, and d_0 is the distance in wavelengths between the points l_1 and l_2.

Long-Line Effect and Pulsed Magnetrons*

W. L. PRITCHARD†

Summary—A simplified theory of long-line effect is developed leading to expressions for maximum tolerable line length and vswr. The theory is verified experimentally and photographic evidence of the deleterious effect of long-line behavior is presented. The prevention of long-line effect by various methods, including decoupling the magnetron, attenuation, phase shifter, and ferrite isolators, is discussed.

I. Introduction

"LONG-LINE Effect" can be defined as the group of phenomena happening when an oscillator is coupled to a long, mismatched transmission line. Its theory is a special case of the more general theory of oscillator operation with reactive loading. It is a serious problem in communications and radar systems at microwave frequencies because most of the available transmitting oscillators must be coupled directly to the antenna system (power amplifiers are still not generally available), and long lengths of transmission line are frequently needed in the installation. Its deleterious effects are erratic AFC operation (in systems using AFC), effective loss in receiver sensitivity and serious distortion in fm systems among others.

The purpose of this paper is to present an elementary theory of the effect, experimental confirmation, and some remedial technique. Pulsed magnetron oscillators will be considered primarily, but most of the theory is general enough to be applied to any oscillator.

II. Simplified Theory

1. *Assumptions and the Magnetron Equivalent Circuit*

We assume here that the magnetron is representable by a shunt resonant circuit and that the resonant frequency is that at which the net susceptance of the magnetron and load is zero. It is possible to develop a more refined theory which considers the effects of magnetron and load conductance, but it is complex and adds very little to the understanding of the problem or its solutions.

Fig. 1 represents the magnetron coupled to a long transmission line by the simple equivalent circuit. We assume a resistive mismatch producing a vswr of ρ at the end of a line of electrical length, θ. If B is the input susceptance of the transmission line, then at the angular frequency of oscillation ω we have

$$B_m + B/n^2 = 0. \tag{1}$$

Since the magnetron has been represented as a shunt resonant circuit, its susceptance is given by

$$B_m = \omega_0 C(\omega/\omega_0 - \omega_0/\omega) \cong 2(\omega - \omega_0)C, \tag{2}$$

where ω_0 is the natural resonant angular frequency of the magnetron. Substituting (2) in (1) yields

$$\omega - \omega_0 = -B/2n^2C. \tag{3}$$

From the standard theory of cavities[1] represented as resonant circuits, we have the relation

$$\omega_0 C = Q_E/n^2. \tag{4}$$

Q_E is defined as the "external Q" of the circuit when the transmission line is terminated in a matched load ($R_0 = 1$). It is the Q resulting from external losses only while Q_0, the "unloaded Q," is defined as the Q resulting from internal losses in the conductance, G, only. Eq. (3) can now be written as

$$\omega - \omega_0 = -B\omega_0/2Q_E. \tag{5}$$

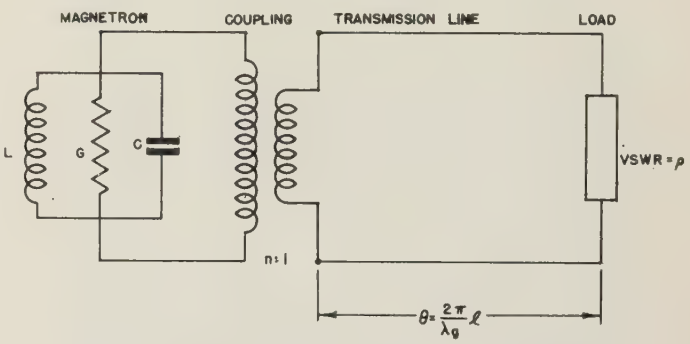

Fig. 1—Equivalent circuit of magnetron coupled to a long mismatched line.

2. *Pulling Figure*

We now define pulling figure, P, as the total excursion of the frequency, f, when the standing wave ratio on the line is equal to 1.5 and is varied through all possible phases. Under these conditions, B, which is the input susceptance of the line, will vary and its total change can be calculated, from the formula for the input admittance of a transmission line, as equal to $\pm .417$ enabling us to eliminate Q_E from (5) by considering f_1 and f_2 as the extreme changes in frequency as B is varied. We can write

$$f_1 = f_0 - .417\ f_0/2Q_E,$$
$$f_2 = f_0 + .417\ f_0/2Q_E.$$

Then

$$P = f_2 - f_1 = .417\ f_0/Q_E, \tag{6}$$

and from (5)

$$\omega_0 = \omega + B\pi P/.417. \tag{7}$$

* This paper was originally presented at the Electron Devices Symposium of the IRE in 1951.

† Raytheon Manufacturing Co., Microwave and Transmitter Branch, Wayland, Mass.

[1] Montgomery, Dickey, Purcell, "Principles of Microwave Circuits," Rad. Lab. Ser., vol. 8, McGraw-Hill Book Company, Inc., New York, N. Y. 1948, pp. 207–239.

Eq. (7), when combined with the expression for B as a function of ω to be derived from conventional line theory, is basic to the whole problem of long-line effect. We would like to relate further the pulling figure of the magnetron to its circuit efficiency. This efficiency, η_e, is defined as the ratio of the power delivered to an external load to the total power available in the resonant circuit. It can be shown that it is related to the unloaded and external Q's of the magnetron by the relation

$$\eta_e = \frac{1}{1 + Q_E/Q_0} = \frac{1}{1 + 1/\beta}, \tag{8}$$

where $\beta = Q_0/Q_E$.

Combining (6) and (8) yields

$$\eta_e = \frac{1}{1 + .417\, f_0/PQ_0} = \frac{\beta}{1 + \beta} \cdot \tag{9}$$

$$P = .417\, f_0\beta/Q_0.$$

Fig. 2 is a curve of η_e vs β. Since pulling figure is linearly related to β, the coupling factor, Fig. 2 also represents efficiency as a function of pulling figure. It is important to note that at high efficiencies a small change in efficiency produces a very large change in P. This will be elaborated when methods of overcoming the long-line effect are discussed.

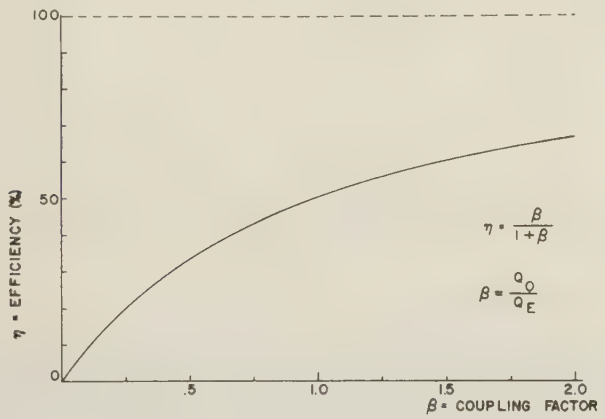

Fig. 2—Efficiency vs coupling factor.

3. *The Susceptance of a Mismatched Transmission Line*

The input admittance of a lossless line is given by

$$Y = \frac{Y_l + j \tan\theta}{1 + jY_l \tan\theta} \cdot \tag{10}$$

Also necessary for the derivation of B are the following standard relations:

$$\Gamma = \frac{1 - Y_l}{1 + Y_l}, \quad \Gamma = |\Gamma| e^{j\phi}, \quad |\Gamma| = \frac{\rho - 1}{\rho + 1} \cdot \tag{11}$$

Using the relations (11) and separating the imaginary part of (10), we can write, after routine manipulating,

$$B = \frac{-\sin\psi}{\dfrac{\rho^2 + 1}{\rho^2 - 1} + \cos\psi}, \tag{12}$$

where

$$\psi = \phi - 2\theta.$$

Eq. (12) is important. It is the necessary relation between the input susceptance of a transmission line and its length and standing wave ratio and, in combination with (7), will enable us to derive the critical conditions for long-line instability. It is plotted in Fig. 3 for various values of ρ.

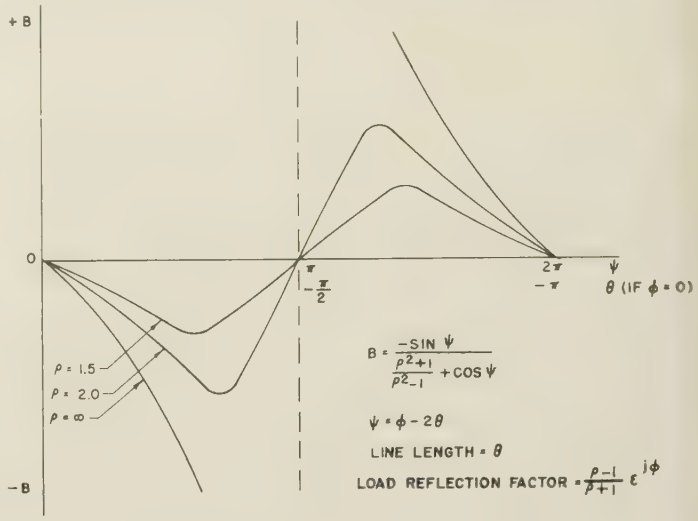

Fig. 3—Line susceptance vs line length.

4. *Magnetron Instability and "Skip Length"*

By substituting the value of B just determined in (7), we have

$$\omega_0 = \omega - \frac{(\pi P/.417)\sin\psi}{\dfrac{\rho^2 + 1}{\rho^2 - 1} + \cos\psi}, \tag{13}$$

where

$$\psi = \phi - 2\theta = \phi - (2\omega/c)(\lambda/\lambda_g)l. \tag{14}$$

The second term of the right side of (13) is a function of ω by virtue of the expression (14) relating ψ to the electrical length of the line. The factor λ/λ_g will be unity on a coaxial line, but for a waveguide will be of the order of magnitude of $\sqrt{2}/2$. Strictly speaking, it is also a function of frequency, since a waveguide is dispersive, but for this discussion it will be assumed constant. Eq. (13) can be plotted vs ω and is shown in Fig. 4. Note that $\omega_0 = \omega$ periodically and this period can be determined by differentiation of (14). $\Delta\omega$, the change in ω between alternate points where $\omega_0 = \omega$ is then found to be

$$\Delta\omega = \frac{\pi}{l}\frac{\lambda}{\lambda_g} c. \tag{15}$$

This equation is extremely important in considering curative measures for instability and will be discussed further. We note here that in a waveguide the period $\Delta\omega$ approaches zero as we come nearer the cutoff frequency and λ_g approaches infinity.

Fig. 4 is plotted for two different values of standing wave ratio. Note that for the higher value of ρ there is the possibility of magnetron oscillation at two frequencies in certain regions of ω_0. These are the regions of instability and are controlled by the phase angle ϕ of the load. If the spectrum of the transmitter signal is narrower than the frequency spread between unstable points, then this phase can be adjusted so as to maintain stable operation. However, this quasi-stable operating condition may not be ideal since the nonlinearity of the curve can cause distortion and alteration of the spectrum width even if there are no actual "jumps" in frequency.

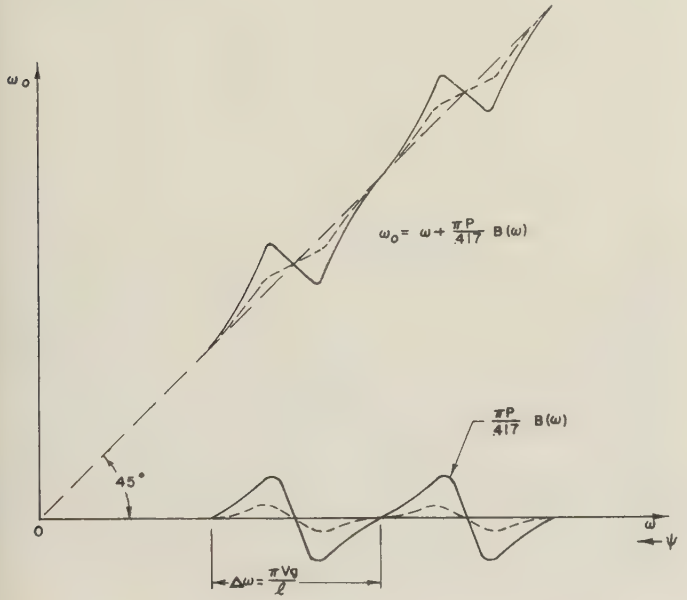

Fig. 4—Magnetron tuning curve.

For completely stable operation, regardless of the phase angle of the load, it is necessary that the curve of ω vs ω_0 be always single-valued. This critical condition is determined by setting the slope $d\omega_0/d\omega$ equal to zero at the points where $\omega_0 = \omega$.

$$\frac{d\omega_0}{d\omega} = 1 + \frac{\pi P}{.417}\left[\frac{1 + \frac{\rho^2+1}{\rho^2-1}\cos\psi}{\left(\frac{\rho^2+1}{\rho^2-1} + \cos\psi\right)^2}\right]\left[\frac{4\pi}{c}\frac{\lambda_g}{\lambda} l\right]\left[\frac{1}{2\pi}\right],$$

letting $\psi = \pi$, $3\pi \cdots$ and $d\omega_0/d\omega = 0$, we solve for l to get

$$l_c = \frac{\frac{.417}{\pi P}\frac{\lambda}{\lambda_g} c}{\rho^2 - 1}. \qquad (16)$$

l_c is the "skip length" and is the longest length of line for which completely stable operation is possible regardless of load phase angle. Note its dependence on vswr, pulling figure, and proximity to cutoff of the transmission line. Eq. (16) can be rewritten as

$$\frac{l_c}{\lambda_g} = \frac{k/\lambda_g}{\rho^2 - 1}, \qquad (17)$$

where

$$k/\lambda_g = \frac{.417}{\pi}\frac{f}{P}\left(\frac{\lambda}{\lambda_g}\right)^2.$$

Eq. (17) is plotted in Fig. 5 for representative values of the variable and parameters. It is important to note that the skip length for a particular vswr is longer at lower frequencies only because the pulling figure of lower frequency oscillators is generally lower and *not* because of the longer wavelength directly.

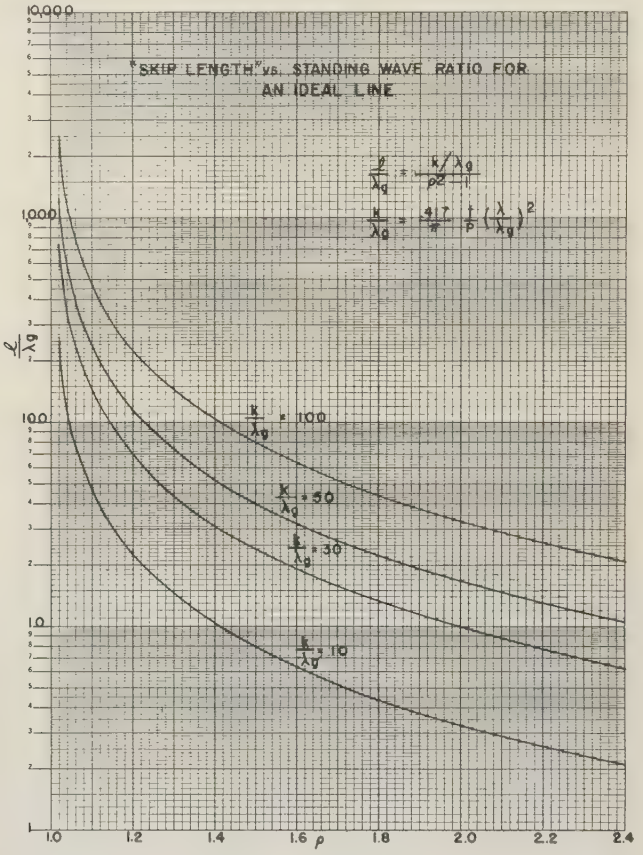

Fig. 5—"Skip length" vs standing wave ratio for an ideal line.

5. *Effect of Line Losses*

The preceding theory has been developed under the assumption that the line is lossless. The effect of loss is to reduce the vswr at the input of the line and hence increase the skip length. The problem can be handled theoretically by assuming that a lossy line is replaceable by a lumped attenuator and a lossless line. Let ρ_l and Γ_l represent the vswr and reflection coefficient of the load and ρ_0 and Γ_0 represent the vswr and reflection coefficient at the input end. They will be different from ρ_l and Γ_l because of the line attenuation α per unit length. We have the following relations from transmission line theory. (A is the total attenuation of a line of length l).

$$\rho_l = \frac{1+\Gamma_l}{1-\Gamma_l} \quad \rho_0 = \frac{1+\Gamma_0}{1-\Gamma_0} \quad \Gamma_0 = \Gamma_l/A^2 \quad A = \epsilon^{\alpha l}. \qquad (18)$$

Using the relations (18), we can write, after a little manipulating,

$$\rho_0^2 - 1 = \frac{4\Gamma_l}{(\epsilon^{\alpha l} - \Gamma_l \epsilon^{-\alpha l})^2} \tag{19}$$

or, in terms of hyperbolic functions,

$$\rho_0^2 - 1 = \frac{\rho_l^2 - 1}{(\cosh \alpha l + \rho_l \sinh \alpha l)^2}. \tag{20}$$

The value of $(\rho_0^2 - 1)$ is determined from (17) for the skip length, l_c, and substituted in (20). The result is a quadratic equation for ρ_l which can be solved and the solution written as

$$\rho_l = \frac{\sqrt{\frac{k/\lambda_g}{l_c/\lambda_g} + 1 + \frac{k/\lambda_g}{2l_c/\lambda_g} \sinh \left[(2\alpha\lambda_g) \frac{l_c}{\lambda_g} \right]}}{1 - \frac{k/\lambda_g}{l_c/\lambda_g} \sinh^2 \left[(\alpha\lambda_g) \frac{l_c}{\lambda_g} \right]}. \tag{21}$$

where k/λ_g has the same meaning as before. Eq. (21) is plotted in Fig. 6 for representative values of the parameters. Note that for any lossy line, no matter how low the losses, there is ultimately a length for which an infinite vswr can be tolerated. This length can be determined by setting the denominator equal to zero in (21) and solving for l_c. It is usually not of practical significance however, since the loss may be prohibitively high.

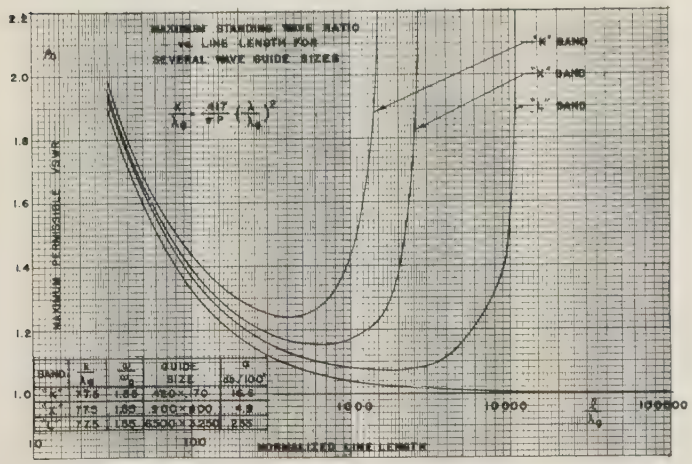

Fig. 6—Maximum standing wave ratio vs line length for several waveguide sizes.

III. Experimental Verification

Experimental verification of the theory developed in Section II was attempted by setting up a 2J42 magnetron (X Band), 10 or 40 feet of $1 \times \frac{1}{2}$ inch waveguide, and a mismatched load adjustable in magnitude and phase. The pulling figure is measured first by observing the total change in frequency when a load with a vswr of 1.5 is varied through all possible phases. This value of P is then used to compute the frequency of oscillation as a function of phase for various vswr's and for 10 feet of waveguide. Figs. 7 and 8 show the results of this computation [from (13)] along with the experimental results. The predicted changes in frequency follow the theoretical changes rather closely for all the values of vswr that were considered. The discrepancies are because of the simplified theory that has been used. A more precise theory, which would take into account the effects of line conductance on magnetron frequency, would probably be more accurate but too unwieldy to be useful practically. The principal purpose of the theory as developed here is to permit predicting unstable conditions and studying remedial measures. For these purposes the experiment shows it to be sufficient. Fig. 8 is the case where the vswr is high enough to cause frequency jumps. For $\rho_l = 2.5$ ($\rho_0 = 2.3$ when the correction for line loss is made) the normalized line conductance has also been plotted. The small numbers represent the phase angle of the load on both the frequency and conductance curves. Note that in the region where there are three possible frequencies of oscillation the magnetron will avoid the frequency where the conductance is high and oscillate at either of the two frequencies where the line conductance is low (cf. Fig. 4). The "high conductance" frequency corresponds to the frequency on Fig. 4 where $d\omega_0/d\omega$ is negative. This condition is not stable in the sense that the magnetron will not stay there with any incremental disturbance.

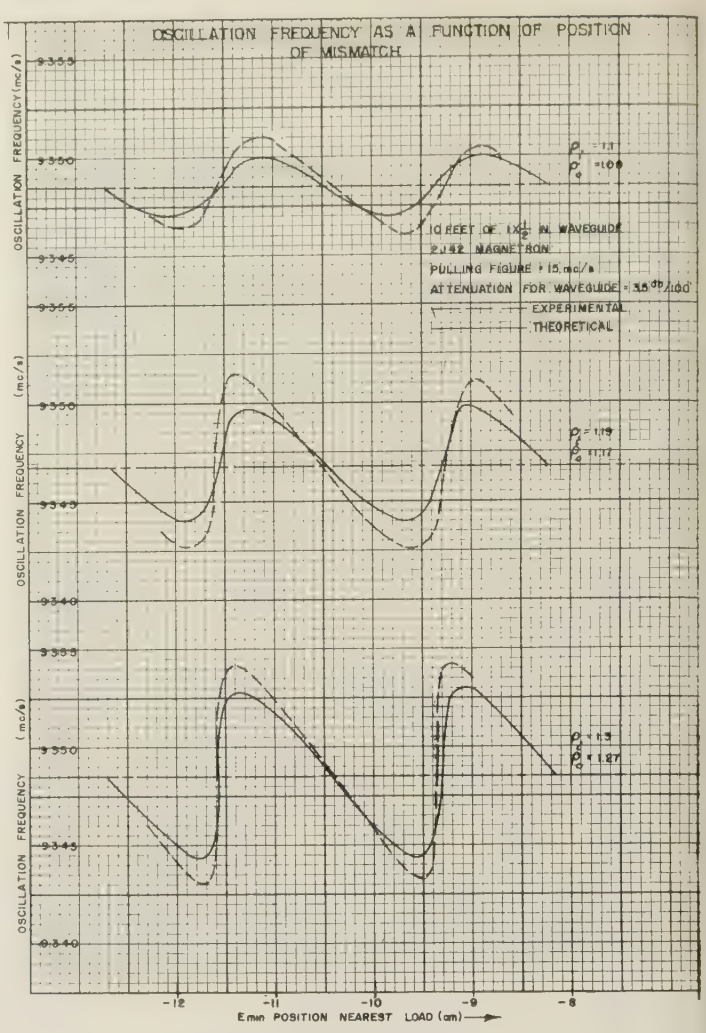

Fig. 7—Oscillation frequency as a function of position of mismatch.

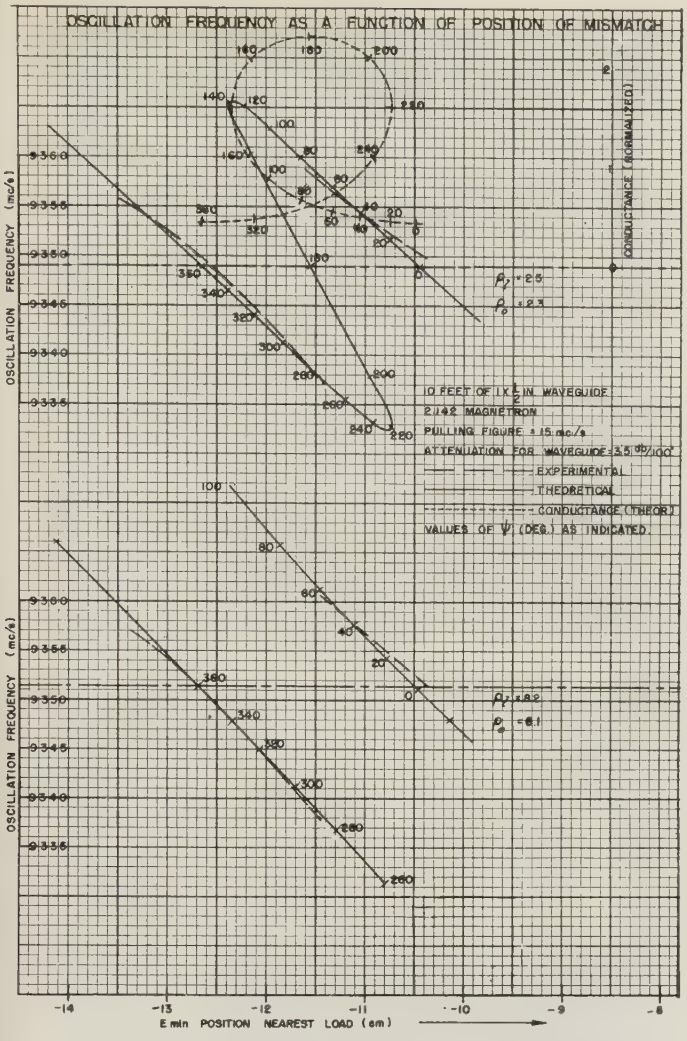

Fig. 8—Oscillation frequency as a function of position of mismatch.

Figs. 9–16 (pp. 38–45) are a series of photographs of rf envelope, spectrum, and instantaneous frequency of a pulsed magnetron under different load conditions. In each case ρ_l, the load vswr, and ρ_0, the vswr corrected for line loss, are shown. When the magnetron is operating stably, the rf spectrum is a single lobe and the instantaneous frequency is single valued. In an unstable condition the spectrum divides into two lobes, and the instantaneous frequency during the pulse becomes distinctly double valued. The two lobes of the spectrum will be separated by approximately the difference between the two principal instantaneous frequencies. Because of "pushing," the instantaneous frequency, even in a stable condition, shows variation during the pulse, but it is still easy to differentiate between incidental frequency modulation and true instability.

For 10 feet of line the critical vswr is 1.27, and reference to Figs. 10 through 13 shows that when ρ_0 is greater than this value, there exists the possibility for frequency jumping if the load phase is appropriate. Fig. 12 shows this clearly. Note also that for a vswr less than critical, but close to it, there is a distinct jitter in the frequency deviation during the pulse and a corresponding broadening of the spectrum. Fig. 14 shows the conditions with a very high vswr and Figs. 15 and 16 the conditions when a very long line (42 feet) is used.

When the load is greater than critical, it is still possible, by varying the phase, to achieve stable operation. Then we have a "quasi-stable" operation. The narrower the pulse (or broader the modulation spectrum) the more difficult it is to achieve quasi-stable operation with a given set of conditions. If the line is long enough, it may be impossible, since the period between skips can become less than the bandwidth needed for modulation.

This series of photographs, besides providing further verification of the theory, shows the deleterious effects of long-line skipping.

Corrective Measures

Long-line effect is best avoided by avoiding the long lines. For example, the transmitter can be located directly after the antenna, or occasionally a 45° mirror can be used instead of a transmission line. This is likely to be difficult if power loss is to be avoided. There still remain, however, many installations where a long transmission line is necessary. In this case, the ideal means to eliminate long-line skipping is a unilateral device which directs the reflected energy into a dummy load instead of returning it to the oscillator.

Several varieties of such devices have been developed using ferrities.[2,3] Most of them fall into two categories: one uses nonreciprocal Faraday rotation to divert the reflected energy into a load and the other uses resonant absorption of the energy returned from the antenna. They have been extremely successful at high frequencies and medium power levels, but materials are still not generally available for use at ultra-high frequencies and for very high average powers.

A brutal solution to the problem is the introduction of attenuation to lower the vswr at the transmitter below the critical value. Obviously, this is not desirable since the over-all efficiency of the system will also be lowered. However, with power to spare, it is often satisfactory. Frequently, a better approach is to decouple the magnetron (or other oscillator) and thus lower its pulling figure. For the usual magnetron coupling values, this will result in less over-all loss in efficiency for a given increase in skip length than will the insertion of loss. Reference to Fig. 2 shows that for high values of P only a very small reduction in η will produce a large reduction in P. In general there exists an optimum compromise between decoupling the oscillator and adding attenuation which will result in the least loss in over-all efficiency for the maximum increase in skip length. This optimum can be computed once the length of line that will be necessary and the best obtainable vswr are known. This calculation is best handled numerically

[2] C. L. Hogan, "The microwave gyrator," *Bell. Sys. Tech. Jour.*, vol. 31, p. 1; January, 1952.

[3] H. Chait and N. Sakiotis, "Properties of ferrites in waveguides," Trans. IRE, vol. MTT-2, pp. 11–16; November, 1953.

E_{min} position nearest load = -11.1 cm
Frequency = 9347 mc/s
a) Frequency spectrum
b) Same as (a) with gain increased

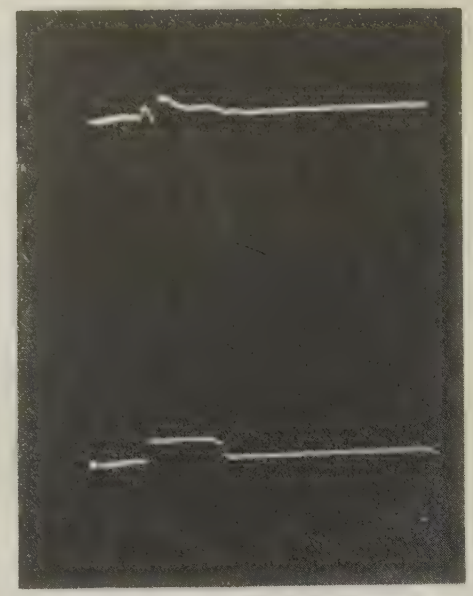

E_{min} position nearest load = -11.1 cm
Frequency = 9347 mc/s
a) Frequency deviation
b) RF envelope

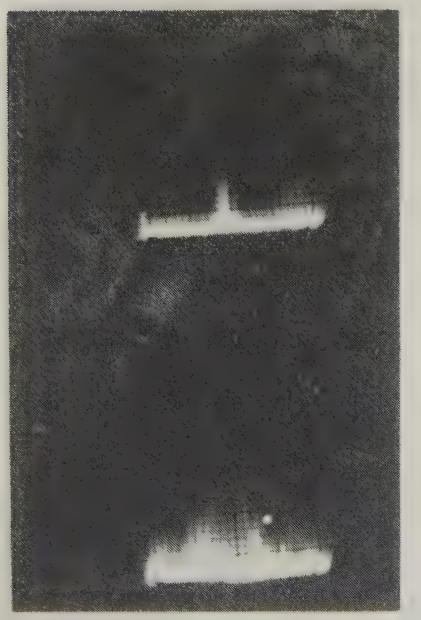

E_{min} position nearest load = -10.1 cm
Frequency 9350 mc/s
a) Frequency spectrum
b) Same as (a) with gain increased

Mismatch at magnetron
$\rho_1 = \rho_0 = 1.45$

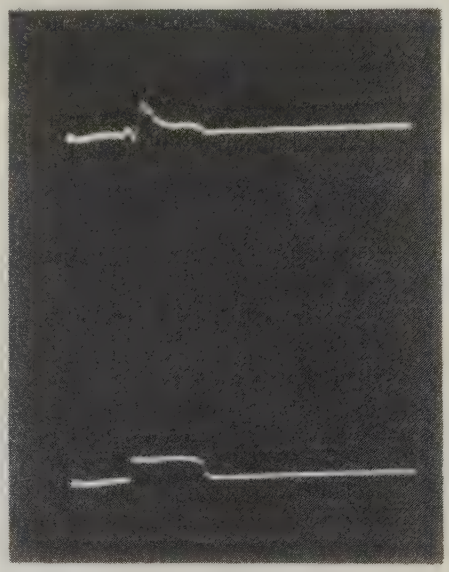

E_{min} position nearest load = -10.1 cm
Frequency 9350 mc/s
a) Frequency deviation
b) RF envelope

Load mismatch is shifted in phase by 80°

Fig. 9—RF envelope, spectrum, and instantaneous frequency of a pulsed magnetron under different load conditions.

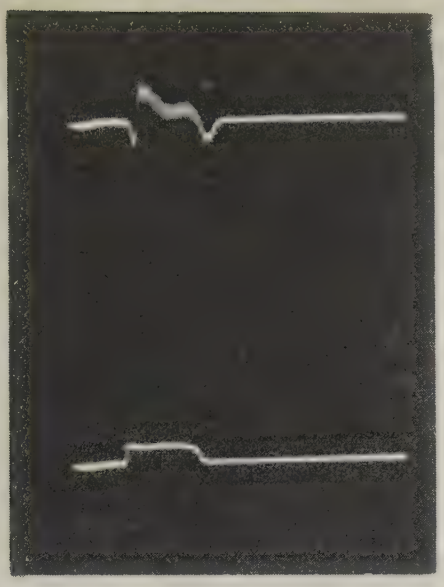

E_{min} position nearest load = -9.05 cm
Frequency = 9350.5 mc/s
a) Frequency deviation
b) RF envelope

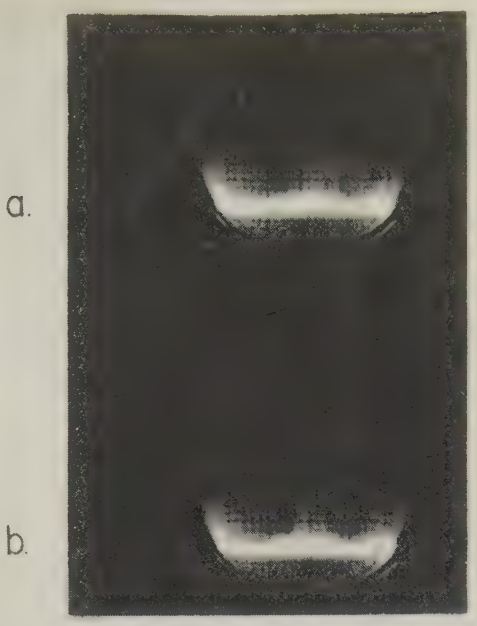

Frequency spectrum
a) E_{min} position nearest load = -9.05 cm
b) E_{min} position nearest load = -10.55 cm

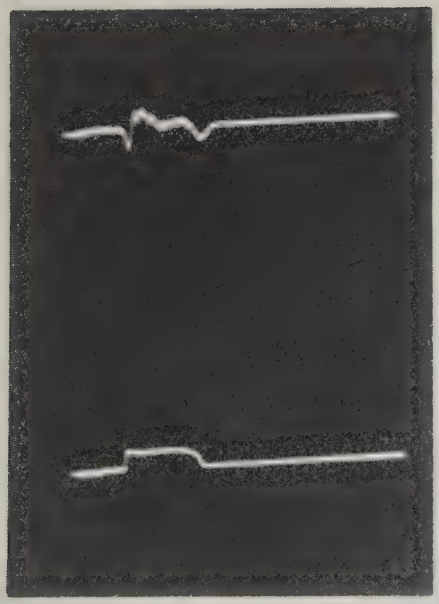

E_{min} position nearest load = -10.55 cm
Frequency = 9349.5 mc/s
a) Frequency deviation
b) RF envelope

10 feet of 1 x 1/2 in. wave guide

$\rho_1 = 1.1$

$\rho_0 = 1.08$

Load mismatch is shifted in phase by 120°

Fig. 10

a

b

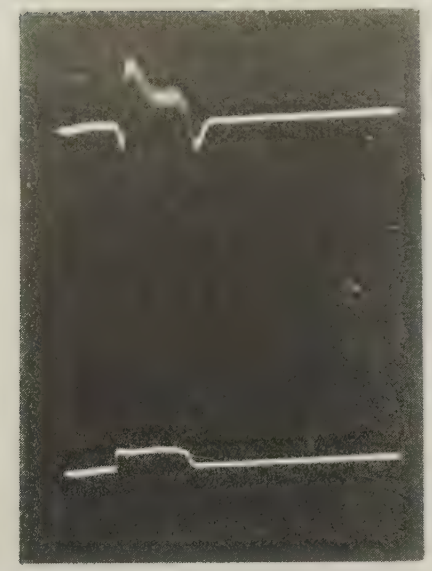

E_{min} position nearest load = -9.17 cm
Frequency = 9352 mc/s
a) Frequency deviation
b) RF envelope

a

b

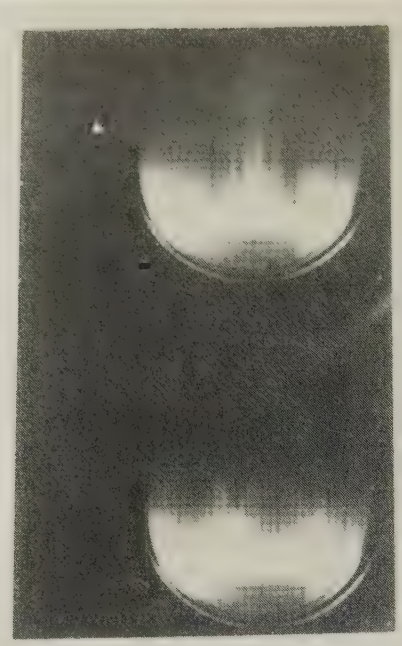

Frequency spectrum
a) E_{min} position nearest load = -9.17 cm
b) E_{min} position nearest load = -9.27 cm

a

b

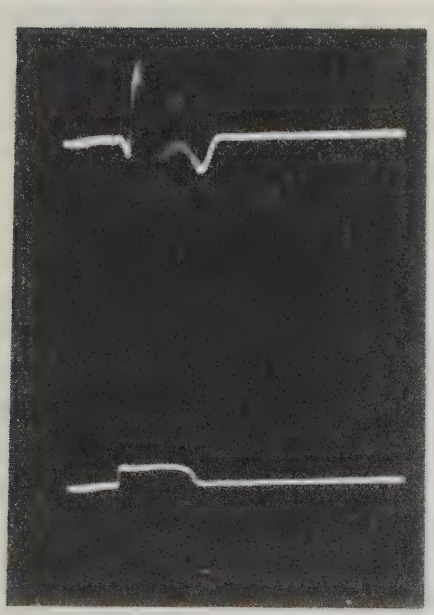

E_{min} position nearest load = -9.27
Frequency = 9350 mc/s (median)
a) Frequency deviation
b) RF envelope

10 feet of 1 x 1/2 in. wave guide

$\rho_1 = 1.19$

$\rho_0 = 1.17$

Load mismatch is shifted in phase by 9°

Fig. 11

a.

b.

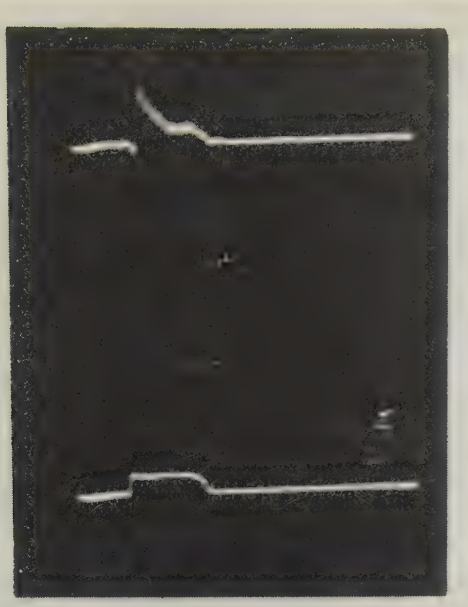

E_{min} position nearest load = -9.52 cm
Frequency = 9343 mc/s
a) Frequency deviation
b) RF envelope

a.

b.

Frequency spectrum
a) E_{min} position nearest load = -9.52 cm
b) E_{min} position nearest load = -9.41 cm
oscillation at two frequencies

a.

b.

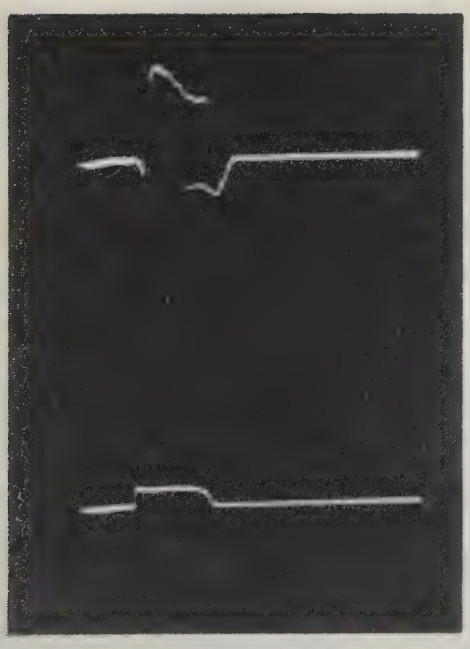

E_{min} position nearest load = -9.41 cm
Frequency = 9343 mc/s and 9353 mc/s
a) Frequency deviation
b) RF envelope

10 feet of 1 x 1/2 in. wave guide

$\rho_1 = 1.3$

$\rho_0 = 1.27$

Load mismatch is shifted in phase by 8.8°

Fig. 12

a

b.

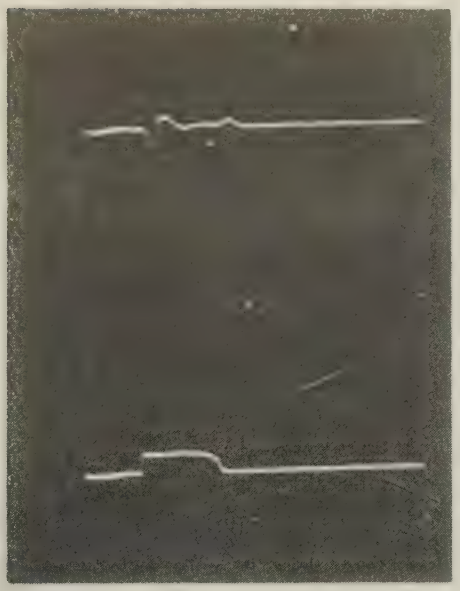

E_{min} position nearest load = -12.83 cm
Frequency = 9351 mc/s
a) Frequency deviation
b) RF envelope

a

b.

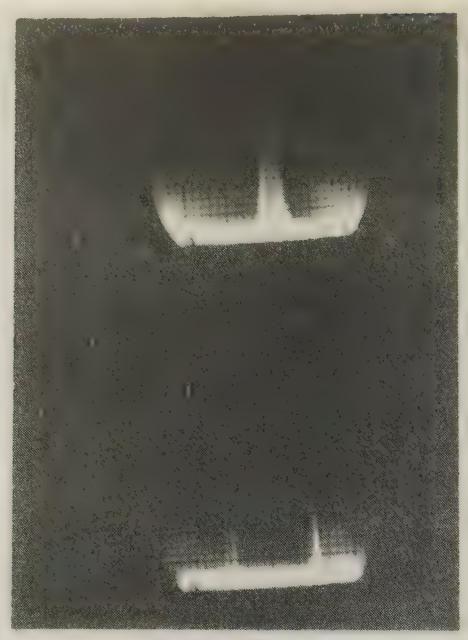

Frequency spectrum
a) E_{min} position nearest load = -12.83 cm
b) E_{min} position nearest load = -11.64 cm

a.

b.

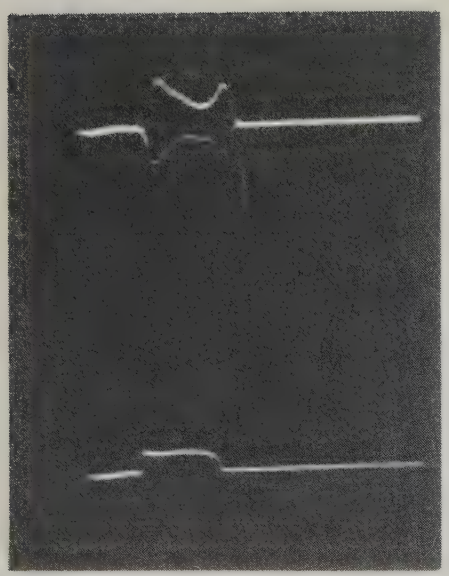

E_{min} position nearest load = -11.64 cm
Frequency = 9339 mc/s and 9360 mc/s
a) Frequency deviation
b) RF envelope

10 feet of 1 x 1/2 in. wave guide

$\rho_1 = 2.5$

$\rho_0 = 2.3$

Load mismatch is shifted in phase by 95.1°

Fig. 13

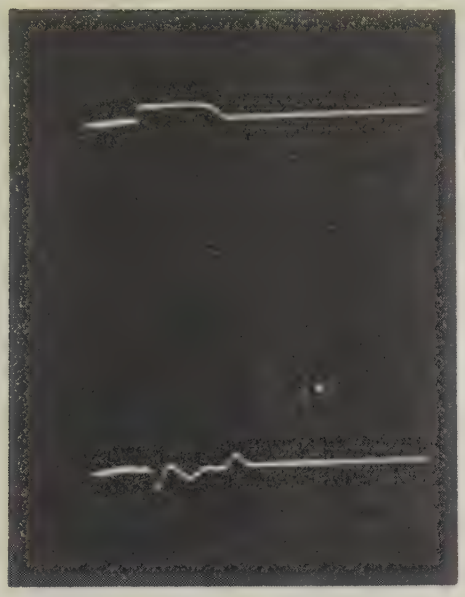

E_{min} position nearest load = -12.35 cm
Frequency 9368 mc/s
a) RF envelope
b) Frequency deviation

Frequency spectrum
a) E_{min} position nearest load = -12.35 cm
b) E_{min} position nearest load = -11.47 cm

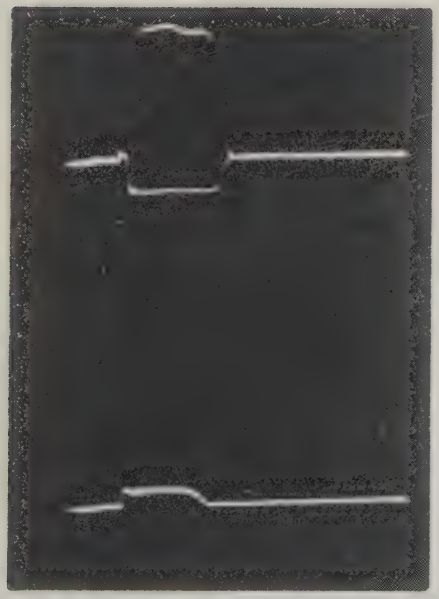

E_{min} position nearest load = -11.47 cm
Frequency = 9341 mc/s and 9361 mc/s
a) Frequency deviation
b) RF envelope

10 feet of 1 x 1/2 in. wave guide

$\rho_1 = 8.2$

$\rho_0 = 8.06$

Load mismatch is shifted in phase by 70.4°

Fig. 14

a.

b.

E_{min} position nearest load = -9.08 cm
Frequency = 9347 to 9350 mc/s
a) Frequency spectrum
b) Same as (a) with gain increased

a.

b.

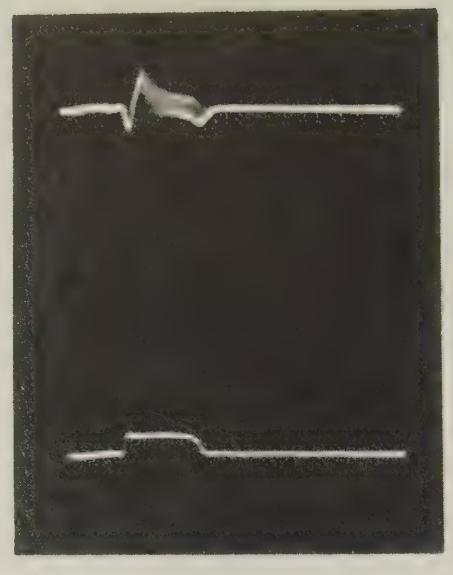

E_{min} position nearest load = -9.08 cm
Frequency = 9347 to 9350 mc/s
a) Frequency deviation
b) RF envelope

a.

b.

E_{min} position nearest load = -10.20
Frequency = 9348 mc/s
a) Frequency spectrum
b) Same as (a) with gain increased

41.5 feet of 1 x 1/2 in. waveguide.
$\rho_1 = 1.21$ $\rho_0 = 1.15$

a.

b.

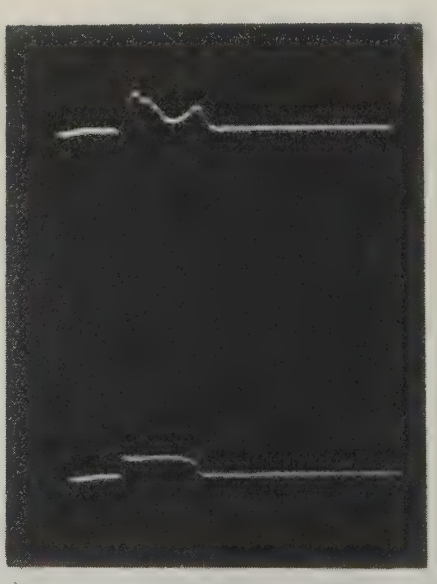

E_{min} position nearest load = -10.20 cm
Frequency = 9348 mc/s
a) Frequency deviation
b) RF envelope

Load mismatch is shifted in phase by 89.5°

Fig. 15

a.

b.

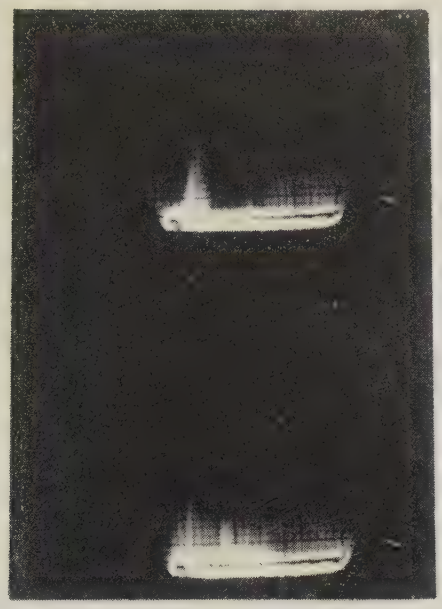

E_{min} position nearest load = -9.28 cm
Frequency = 9348 mc/s and 9353 mc/s
a) Frequency spectrum
b) Same as (a) with gain increased

a.

b.

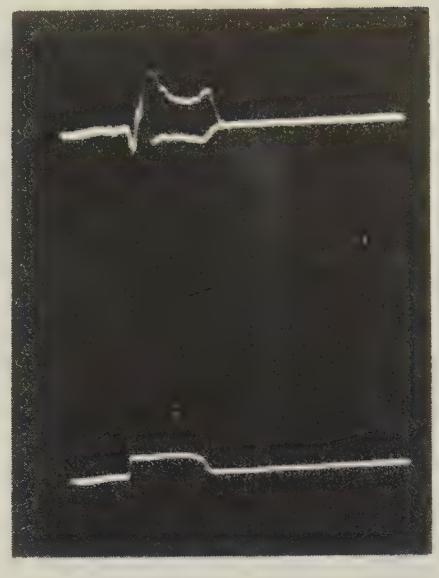

E_{min} position nearest load = -9.28 cm
Frequency = 9348 mc/s and 9353 mc/s
a) Frequency deviation
b) RF envelope

a.

b.

E_{min} position nearest load = -10.4 cm
Frequency = 9348 mc/s
a) Frequency spectrum
b) Same as (a) with gain increased

41.5 feet of 1 x 1/2 in. waveguide
$\rho_1 = 1.45$ $\rho_0 = 1.30$

a.

b.

E_{min} position nearest load = -10.4 cm
a) Frequency deviation
b) RF envelope

Load mismatch is shifted in phase by 89.5°

Fig. 16

by using (17) and (18). For a series of assumed values of P the permissible vswr, ρ, is calculated from (17) using a fixed value for l_c. Eq. (9) is then used to compute the magnetron efficiency. If ρ is higher than that which can be obtained with the given load, then (18) is used to compute the attenuation necessary to reduce the load vswr to the permissible value ρ_0. The over-all efficiency is then calculated from the magnetron efficiency and other loss values. The results, plotted vs P, are shown in Fig. 17. Note the maximum value of efficiency is rather broad, leaving some freedom in the tube design. Unfortunately many existing magnetrons are heavily overcoupled to increase the output power and reduce the back heating at the cost of making the over-all equipment design much more difficult.

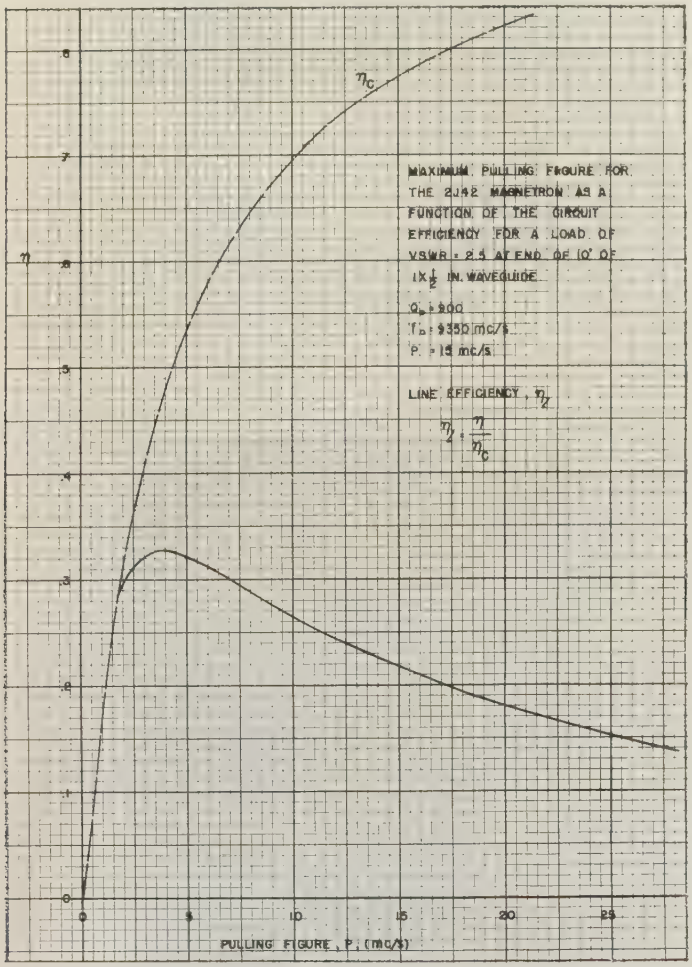

Fig. 17—Maximum pulling figure for the 2J42 magnetron as a function of the circuit efficiency for a load of vswr = 2.5 at end of 10 feet of 1×½ inch in waveguide.

If the vswr is not too high, then a phase shifter can be incorporated which will permit quasi-stable operation in between the points of frequency jumping, as discussed in Section III. The wider the modulation bandwidth, the less likely it is that this scheme will be successful. This is particularly true if the line is very long and the frequency separation between "skips" is small.

If magnetron operation is restricted to a narrow band of frequencies and the line length is too long to permit quasi-stable operation, even with a phase shifter, then there is another device which is sometimes successful. A rather large mismatch is introduced in the line considerably closer than the load. The period between skips for this mismatch is greater than the period between skips for the load (antenna). By phasing this mismatch, it will be possible to achieve quasi-stable operation at some reduction in output power. Effectively this is decoupling the magnetron by a cavity formed with a resonant line length. It is a useful and practical cure for long line effect when the system is only to be operated over a narrow frequency range.

List of Symbols

A Total attenuation of line of length, l.
B Input susceptance of transmission line.
B_m Susceptance of magnetron equivalent circuit.
c Velocity of light in appropriate dielectric.
C Shunt capacitance of magnetron equivalent circuit.
f Frequency.
f_1 Maximum oscillation frequency as B is varied.
f_2 Minimum oscillation frequency as B is varied.
G Shunt conductance of magnetron equivalent circuit.
k Parameter relating f, P, λ, and λ_g.
l Length of transmission line.
l_c Skip length.
n Transformer turns ratio.
P Pulling figure.
Q_E "External Q" of the magnetron.
Q_0 "Unloaded Q" of the magnetron.
Y Normalized input admittance of a lossless line.
Y_l Normalized load admittance.
α Line attenuation per unit length.
β Coupling factor for magnetron.
Γ Reflection coefficient of Y_l.
Γ_l Reflection coefficient at end of transmission line of length, l.
Γ_0 Reflection coefficient at input to transmission line.
η Over-all efficiency of power transmission to load.
η_c Coupling efficiency of magnetron.
θ Electrical length to resistive mismatch.
λ Wavelength of plane wave in appropriate dielectric.
λ_g Wavelength in waveguide in appropriate dielectric.
ρ vswr of load.
ρ_l vswr at end of transmission line of length, l.
ρ_0 vswr at input to transmission line.
ϕ Phase of reflection coefficient, Γ.
ψ $\phi - 2\theta$, phase of Y.
ω Angular frequency of oscillation.
ω_0 "Natural" resonant frequency of magnetron.
$\Delta\omega$ Change in ω between alternate positions where $\omega = \omega_0$.

Acknowledgment

The author wishes to thank Mr. Setsuo Dairiki of Raytheon Manufacturing Company for the experimental work and photographs.

The Use of Non-Euclidean Geometry in Measurements of Periodically Loaded Transmission Lines*

R. L. KYHL†

Summary—**The propagation characteristics of periodically loaded transmission lines can be deduced from impedance measurements taken with a series of different terminating configurations in a manner analogous to the "nodal shift" method of measuring microwave junction characteristics. The non-Euclidean properties of impedance transformations form a particularly simple approach for analyzing measurements in the case of the loaded line.**

I. Introduction

A NUMBER of techniques used in testing the disk-loaded guide for the large Stanford linear electron accelerator[1] are not only of interest to workers with similar structures, but also provide an interesting example of the use of the non-Euclidean properties of impedance or reflection coefficient charts which have been described by Deschamps.[2]

The basic property to be used in this discussion is that one can define a non-Euclidean geometry on the set of reflection coefficients or impedances, such that transformation through a nondissipative two-terminal-pair network constitutes a rigid displacement in this geometry. This concept is of general use in network problems, as illustrated in footnote reference 2. The ideas presented are valid for the interpretation of measurements made at a single frequency. No attempt is made to discuss frequency dependence. We shall plot our diagrams on the conventional Smith chart. A few properties of this representation are listed below. Let words in *italics* represent the description in the non-Euclidean system. Deschamps uses the adjective "hyperbolic" to denote quantities in this system. *Straight lines* are circles orthogonal to the edge of the chart. *Circles* are circles but with the *center* displaced from the Euclidean center. The *unit of length* is proportional to the logarithm of the voltage standing-wave ratio in the following sense: the *distance* between the center of the Smith chart and a given point is half the logarithm of the vswr (voltage standing-wave ratio) at the point in question; the *distance* between *two points* is the value that would be obtained by applying any *rigid displacement* which moves one of the points to the center of the chart. *Angles* between *intersecting straight lines* are equal to the angles between tangents at the point of intersection. For a description of additional properties of this geometry, the reader is referred to the references. The treatment used in this discussion is, from personal preference, entirely geometric. Use is freely made of the theorems of Euclid, care being taken not to use any that depend on the parallel axiom.

Fig. 1—Regular mosaic in a non-Euclidean geometry.

Many *ruler-and-compass* constructions carry over directly to the non-Euclidean system if practical methods are available for drawing a *straight line* through *two points*, and for drawing a *circle* with a given *center*. Deschamps[2] gives a useful method for the former which involves the "projective-chart" as well as the Smith-chart representation. In the work described in the present contribution, the lines of constant reactance on the printed Smith-chart were used as a set of French curves for drawing *straight lines* in conjunction with a tracing table. To draw *circles* use is made of the definition of *distance*. If a *circle* is to have its *center* at $(\text{vswr})_0$ and the *radius* is to be $\frac{1}{2}$ in $(\text{vswr})_R$, then the points on the *circle* will have vswr values lying between $(\text{vswr})_0 \times (\text{vswr})_R$ and $(\text{vswr})_0 \div (\text{vswr})_R$. The extremes will lie on a Euclidean diameter of the Smith chart drawn through the desired *center*. The two extremes also lie on a Euclidean diameter of the desired circle which may now be drawn at once. In order to give a graphic illustration of this geometry, Fig. 1 shows a mosaic pattern of congruent triangles and regular heptagons.

* This project was supported by the U. S. Atomic Energy Commission.

† Formerly at Microwave Lab., Stanford Univ., Stanford, Calif.; now at General Electric Res. Lab., Schenectady, N. Y.

[1] M. Chodorow, E. L. Ginzton, W. W. Hansen, R. L. Kyhl, R. B. Neal, and W. K. H. Panofsky, "Stanford high-energy linear electron accelerator (Mark III)," *Rev. Sci. Instr.*, vol. 26, p. 134; February, 1955.

[2] G. A. Deschamps, "Application of non-Euclidean geometry to the analysis of waveguide junctions," (summary) PROC. IRE, vol. 40, p. 743; June, 1952; also, *J. Appl. Phys.*, vol. 24, p. 1046; August, 1953; and "A hyperbolic protractor," Fed. Telecom. Labs., Nutley, N. J.; 1953. A more elegant and sophisticated treatment is given in the Proc. of the Symposium on Modern Network Synthesis, vol. 1, p. 277, Polytech. Inst. of Brooklyn.

II. Measurements on Periodically Loaded Lines

Fig. 2 shows a typical experimental situation. The coupling network is some device for connecting the loaded line to an ordinary transmission line. The measuring device is usually a probe and slotted section for measuring standing-wave ratio in a transmission line, but this is not essential to the argument; the same considerations would apply to a completely lumped network. The plunger can be used for terminating the loaded line in various impedances, either purely reactive or partly resistive, and generally unknown.

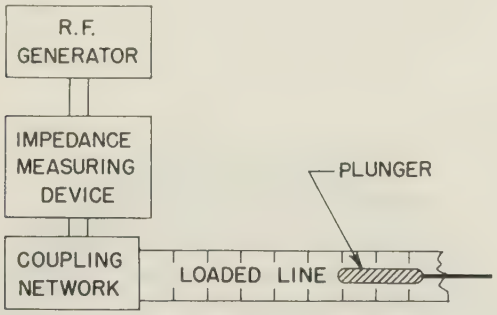

Fig. 2—A diagram of a typical experimental setup.

Since it is possible to generate in periodic structures waves which may be defined as "pure traveling waves," the entire structure of analysis developed for conventional transmission lines can be taken over directly to systems containing periodically loaded lines or combinations of these with ordinary lines, provided only that some care is taken in the interpretations.

The purpose of an experiment may be to measure the propagation constant of the loaded line, to check its uniformity, or to measure its characteristic impedance as seen through the coupling network. The concept of impedance and reflection coefficient in periodically loaded transmission lines has been discussed by Slater[3] and by Jaynes.[4]

III. Geometric Analysis

The *rigid displacement* corresponding to the transformation through one period (one disk) of the loaded line will have one fixed point at the characteristic impedance Z_0 of the structure. Within the pass band of the structure the characteristic impedance will lie inside the Smith chart (rather than at *infinity*). The only possible *displacement* is then a *rotation* about Z_0. Transformation through several sections must then consist of a succession of *rotations* about the same point. The total *angle of rotation* will be $N\theta$ where θ is the *angle of rotation* for a single period.

[3] J. C. Slater, "Microwave Electronics," D. Van Nostrand and Co., Inc., New York, N. Y., ch. 7; 1950.

[4] E. T. Jaynes, "The concept and measurement of impedance in periodically loaded waveguides," *J. Appl. Phys.*, vol. 23, p. 1077; October, 1952.

If we plot with Z_0 at the center of the Smith chart the *rotation* will appear Euclidean. Consider the experiment consisting in the placing of a purely reactive, totally reflecting termination successively in equivalent positions in cavities $a, b, c, d, \cdots$ of the loaded line. The resulting impedances as seen, for example, in cavity a and plotted on a Smith chart normalized to the characteristic impedance of the loaded line must appear as in Fig. 3 (though it is not yet clear from the discussion whether it is possible to make such measurements). Here ϕ is the phase shift per section in the line. Since the plunger is purely reactive the reflection coefficient has unit amplitude and all points lie on the edge of the chart if there are no losses present. (Loss in the structure will be considered later.) The factor 2 in 2ϕ is the usual one found on Smith-chart plots.

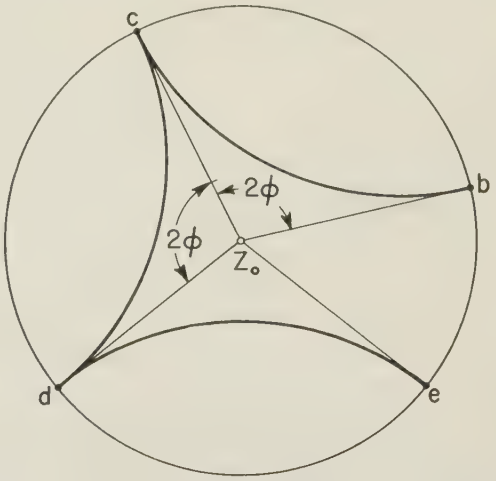

Fig. 3—Unclosed *regular polygon* with center at center of chart, sides of infinite *length*.

We may now ask what will be observed by an actual impedance measurement made through a non-lossy coupling network such as in Fig. 2. The plunger is again to be purely reactive as in the previous paragraph. First suppose the coupling network exactly matches the loaded line to the uniform line. This means by definition that Z_0 of the loaded line falls at the center of the Smith chart. It follows at once that we must again observe exactly Fig. 3 except for an arbitrary *rigid rotation*. In general, however, the coupling will not be matched. The observed points will fall in the manner indicated in Fig. 4. The first step in interpreting the measurements is to determine the position of Z_0. Connect points $b, c, d, e, \cdots$ with *straight lines*. These form a *regular polygon* (*unclosed*) in the sense that all vertices are equivalent and all sides are equivalent. It can be readily seen that it must be a *regular polygon* in Fig. 3. Since Fig. 4 represents a *rigid displacement* of Fig. 3, the figure must still be a *regular polygon*. Ordinarily, location of the center of a regular polygon is an elementary geometric construction. Unfortunately

in this case the *vertices* are at *infinity*, the *vertex angles* are vanishingly small, and the sides have *infinite length*.[5] We construct the *straight lines* (cZ_0 and Z_0d) which are the *loci of points equidistant* from two adjacent *sides* of the *polygon*. (It may not be at once clear how to perform such a construction, or even that the locus in question is a *straight line*. Fortunately, a simple construction is available.) This may be done on the Smith chart by superimposing the diagram on the printed Smith chart so that the *vertex* under discussion falls at the point $Z=\infty$. The adjacent *sides* then lie on lines of constant reactance X. The *line* of constant $X=(X_1+X_2)/2$ is the desired *locus*. The proof is left to an appendix.

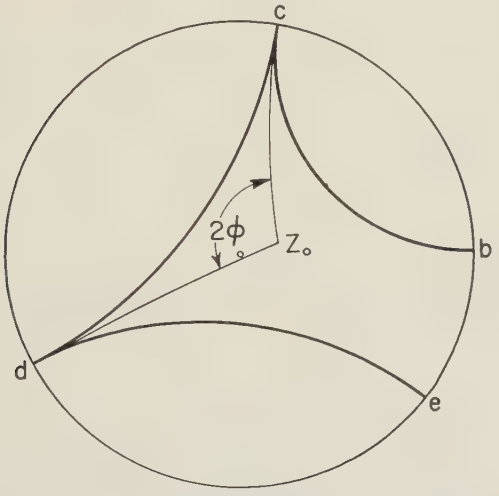

Fig. 4—Unclosed *regular polygon* with center displaced from center of chart. This figure is *congruent* to Fig. 3.

The intersection of all these loci determines the center Z_0 of the polygon. The reflection coefficient of the coupling network can be read off directly from the position of this *center*. Since we have already drawn the *lines* connecting the *center of the polygon* with the vertices, the *angles* 2ϕ can be measured at once as the *angles* formed by these *lines* at the *center of the polygon*.

If it should happen that point f falls upon point b as in Fig. 5, then the *polygon* reduces to a "*square*" and the *center* of the polygon can be determined by drawing the two *diagonals*. This is a special case of the type of nodal-shift[6] measurement suggested by Deschamps[2] for use with uniform lines. It can be used if the loaded line is transmitting in exactly the $\pi/4$ or $3\pi/4$ mode.

The $\pi/2$ mode is commonly used in traveling-wave linear accelerators. The method just described breaks down at or near this point. Fig. 6 shows measurements on a periodically loaded line very near the $\pi/2$ mode. In order to determine the Z_0 point with precision a second set of plunger positions can be measured giving rise to points b', c', d', e', etc.

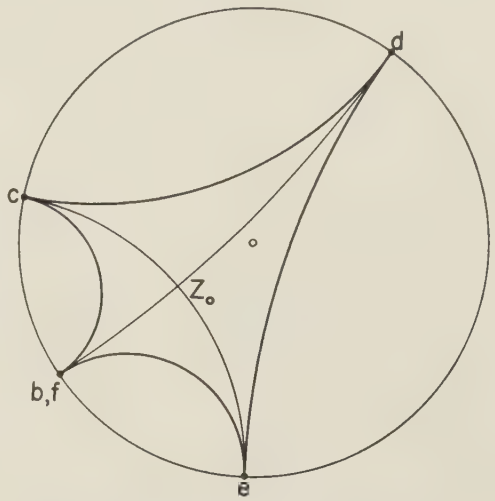

Fig. 5—*Square*, showing method of locating its *center* by drawing the *diagonals*.

These points determine another *polygon* which is also *centered* about Z_0. Unfortunately, in a disk-loaded structure (at least if the coupling holes are small), there is one set of points (say, b, c, d, e) which is insensitive to plunger position and corresponds to successive complete detuning of the set of cavities. All other points (like b', c', d', e') can be obtained only by positioning the plunger in the transition region between successive cavities with great precision. Fig. 6 indicates how the location of Z_0 is determined.

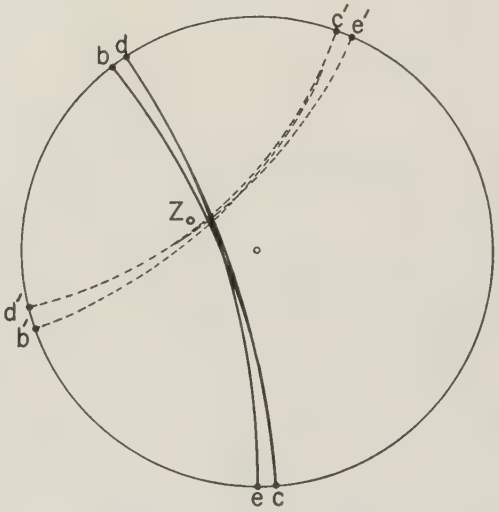

Fig. 6—Typical data obtained in a loaded line operating near the $\pi/2$ mode.

[5] If the reader is disturbed by a *regular polygon* with *vertices at infinity* he may consider this discussion as the limiting case of an experiment in which the plunger has a slight loss.

[6] E. Feenberg, "The relation between nodal positions and standing wave ratio in a complete transmission system," *J. Appl. Phys.*, vol. 17, pp. 530–532; June, 1946 and N. Marcuvitz, "On the representation and measurement of waveguide discontinuities," Proc. IRE, vol. 36, pp. 728–735; June, 1948.

Another method of determining the location of Z_0 which may give greater accuracy and is feasible near the $\pi/2$ mode involves the use of a lossy plunger. The *points* now fall inside the chart and the difficulties with points at *infinity* disappear. The Z_0 *point* may be determined as the intersection of the *perpendicular bisectors of the sides* or *bisectors* of the *vertex angles* as seen in Fig. 7. Ordinary "ruler-and-compass" constructions are suitable.

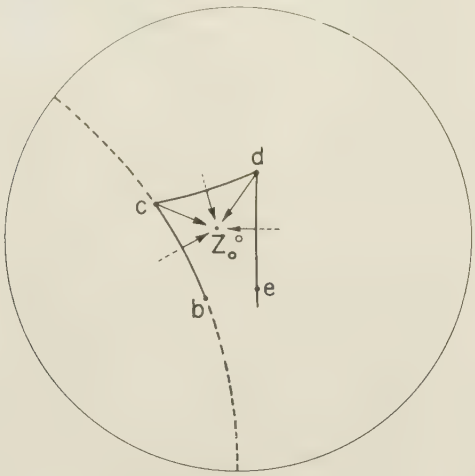

Fig. 7—Unclosed *regular polygon* constructed from data obtained with lossy plunger.

This method does not break down at the $\pi/2$ mode. It is not as accurate a method for measuring phase angles. It has been used at Stanford in conjunction with the totally reflecting plunger.[7] By a little trial and error, a lossy plunger has been manufactured with a vswr of less than 1.1 when placed appropriately in a cavity of the large Stanford linear accelerator. With such a plunger the Z_0 *point* can be located accurately by inspection.

Another method of analyzing lossy plunger data consists of drawing a *circle* through the data points. The points must fall on a *circle* because they form a *regular polygon*. A *circle* is always also a circle in the Euclidean plane so the construction can be made by conventional methods. The *center of the circle* coincides with the *center of the polygon*. Location of the *center of a circle* is one of the simplest constructions on a Smith chart. It is illustrated in Fig. 8. The diameter WXY of the chart through the Euclidean center O of the circle is drawn intersecting the circle at A and B. The *center* O' *of the circle* is given by vswr values from the center of the Smith chart according to the formula

$$\text{vswr}_{O'} = \sqrt{\frac{\text{vswr}_B}{\text{vswr}_A}},$$

or if the circle does not link the origin,

$$\text{vswr}_{O'} = \sqrt{\text{vswr}_B \times \text{vswr}_A}.$$

This is the reverse of the method of drawing a *circle* described in section I.

[7] Chodorow *et al*, *op. cit.*, p. 161.

IV. Reflections in Loaded Lines

A direct extension of the methods described above permits the determination of reflections which may occur within periodic structures. Such discontinuities may be the result of faulty manufacture or may be introduced intentionally. The experimental arrangement will be the same as before. The measurement will now consist of one set of plunger settings on the near side of the point of reflection and another set on the far side. The interpretation of each set will be made as usual; it is then possible by conventional microwave network methods to determine the nature of the impedance transformation which lies between the two sets.

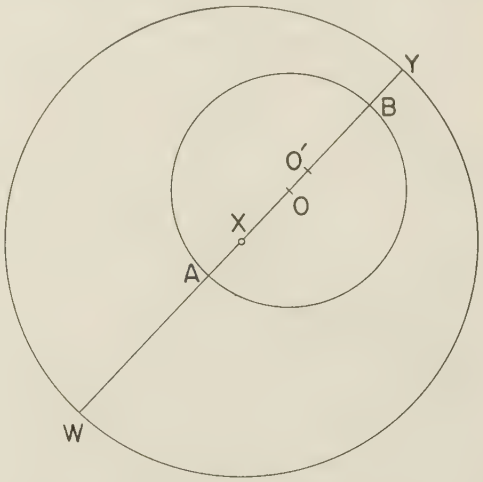

Fig. 8—Illustration of method of locating the *center* of a circle.

V. Lossy Loaded Lines

The impedance transformation through a general lossy network cannot be described as a *rigid displacement* in the non-Euclidean system. (All possible *displacements* already represent nondissipative transformations.) In the lossy case it is found that the Smith chart is mapped into a smaller circular region entirely within the Smith chart (possibly tangent to the boundary). All positions and sizes of the reduced circle are permitted, subject to the above restrictions. If the reduced circle is considered to be a new reduced size representation of the entire *plane*, then the lossy network transformation constitutes a *rigid displacement* within this region.

We shall consider only the case of sufficiently small attenuation constant so that the attenuation through a few cavities may be neglected. We may then assume that the result of an experiment with a reactive plunger as described in section III will be points lying on a circle (rigorously they fall on a spiral).

The entire analysis procedure described for nonlossy lines carried over unaltered to this case if we define the non-Euclidean quantities with respect to the region inside the reduced circle (measured for example with the use of the reactive plunger). The result is that we can establish the characteristic impedance and propagation

constant in the region of the reactive plunger, as seen through the lossy network. We have thus taken care of the periodic loading aspect of the problem and have reduced it to the corresponding problem with conventional transmission lines, for which methods of interpretation are available.[2] Fig. 9 shows a sample measurement for this case.

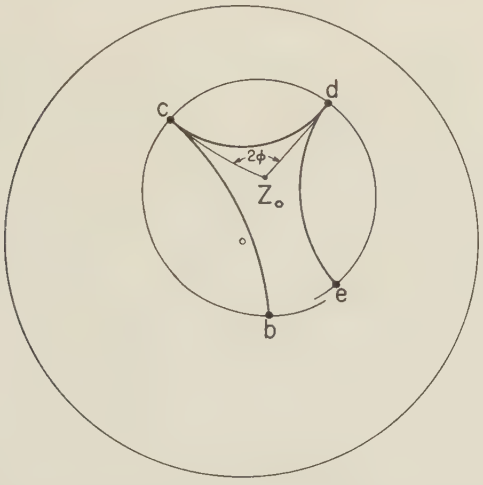

Fig. 9—Unclosed *regular polygon* constructed from data obtained with a lossless plunger some distance down a slightly lossy transmission line.

VI. Conclusion

We have shown how measurement of the various network properties of transmission line circuits can be extended to circuits containing periodically loaded transmission lines. The use of the non-Euclidean approach permits the analysis to be made with a minimum of mathematical complexity, and provides a convenient conceptual framework.

The methods here described are readily extended but with considerable complexity to the case where attenuation cannot be neglected even between two successive cavities.

Appendix: Location of the Center of a "Polygon" with Vertices at Infinity

It will be recalled that the existence of a "*regular*" *polygon* was based on physical arguments about the network under examination. These arguments also show that if a transformation is used to move the *center* of the *polygon* to the center of the Smith chart, then the figure will possess rotational symmetry about the center in the laboratory coordinates as well as in the hyperbolic. Under these conditions it is clear at once from symmetry considerations that the *center* of the *polygon* is located at the intersection of *lines* through the vertices (radii of the Smith chart) which have the property of being equidistant from the two adjacent sides of the figure in both the laboratory and the hyperbolic coordinates. The problem is now to obtain a formula for constructing these *lines* even when the *center* of the *polygon* does not happen to be at the center of the Smith chart.

If the *polygon* in question (not necessarily centered on the Smith chart) is superimposed on the printed Smith chart with the vertex in question at $Z=\infty$, then the two adjacent *sides* of the *polygon* will lie along lines of constant reactance jX. This follows at once, since the family of constant reactance lines on the chart are the family of all *straight lines* which can be drawn through the point $Z=\infty$. Call the reactance values X_1 and X_2. Then it is asserted that the curve of constant reactance equal to $(X_1+X_2)/2$ is the desired *line*. To see this let us apply the transformation which consists of adding a series reactance of $-j(X_1+X_2)/2$. This is certainly a permissible transformation since it is physically realizable and is nondissipative. The result is lines of constant reactance $j(X_1-X_2)/2$; 0; $j(X_2-X_1)/2$. The figure is symmetric about the curve $jX=0$, which has all the necessary symmetry properties to be the desired *line* through the center of the polygon. Since this is a property in the hyperbolic geometry it is invariant under transformation and is the desired *line* under all conditions.

The same construction can be applied to the other *vertices* to give two or more *lines* whose intersection defines the *center* of the *polygon*.

VII. Acknowledgment

The assistance rendered by K. B. Mallory and Charles Süsskind of Stanford University in the preparation of this paper is gratefully acknowledged.

A New Microwave Frequency Standard by Quenching Oscillator Control

N. SAWAZAKI† AND T. HONMA†

Summary—This paper shows that in this new frequency standard system the multiplication is made by synchronizing oscillation, which is achieved by quenching a microwave oscillator with a standard quartz-crystal oscillator. The output frequency spectrum of this synchronizing oscillator includes only integral multiple frequencies of a quartz-crystal oscillator. Each spectrum can be utilized as standard frequencies. Theoretical calculations and experimental results are also described here. And to avoid the influence of noise voltage on the build-up of the quenching control microwave oscillator, the double modulation system is used, which is controlled and intermitted simultaneously by both f_1 voltage (output of the low frequency standard) and $n_1 f_1$ voltage (n_1 is an integer).

By this double modulation method we can understand that the build-up and the stop of the microwave oscillation are exactly controlled by the constant phase of the waves from the standard generator, and also the experimental results of this are described. As an application of this new system, a method of precise frequency measurement is also described.

Introduction

FOR THE microwave communication industry, the technique of frequency measurement with high accuracy has become very important. As microwave frequency meters, cavity-type wavemeters are mostly used by reason of their simplicity, but their accuracy is not high. The fine measurement of the microwave frequency requires a frequency standard, and results of research on the subject have already been published, but the methods described are based on the principle of using vacuum-tube frequency multipliers of crystal oscillators to the vhf region, and using silicon crystal diodes as harmonic generators in the microwave region. In these systems the arrangements are considerably complicated and the microwave output power from the equipment is too small to calibrate the cavity wavemeters directly.

The authors have devised a new system for obtaining the standard frequencies by quenching the microwave oscillator at the low standard frequency.[1,2] This system can increase the member of the multiplication factor.

This paper describes the principle of the new system and the method for a fine measurement of microwave frequency as a new frequency standard, and also presents actual results of the tests obtained by an experimental device based on the system mentioned above.

† Matsuda Research Laboratory, Tokyo Shibaura Electric Co., Kawasaki, Japan.

[1] N. Sawazuki and T. Honma, "On a new frequency standard system at microwaves," *J. I. E. C.* (Japan), vol. 33, pp. 62–68; February, 1952.

[2] N. Sawazuki and T. Honma, "On a precise frequency measurement at microwaves," *J. I. E. C.* (Japan), vol. 35, pp. 69–73; February, 1952.

Basic Principles

This method is a microwave application of R. Golicke's method which was applied to a frequency multiplier in low-frequency range.[3] To understand the operation of such a device, consider first the simple system shown in Fig. 1. The oscillation of the Klystron microwave oscillator is controlled and intermitted by the output of the standard crystal controlled oscillator, where the frequency of the crystal oscillator $\doteqdot f_1$, the frequency of the microwave oscillator $\doteqdot f_2$, and the microwave oscillator output is applied to the high-Q cavity resonator which acts as a band pass filter. If it is possible to control the build-up time and stop time of the microwave oscillator by a constant phase of the control voltage from the standard frequency oscillator, then the microwave output of the standard frequency wave could be driven through the cavity resonator.

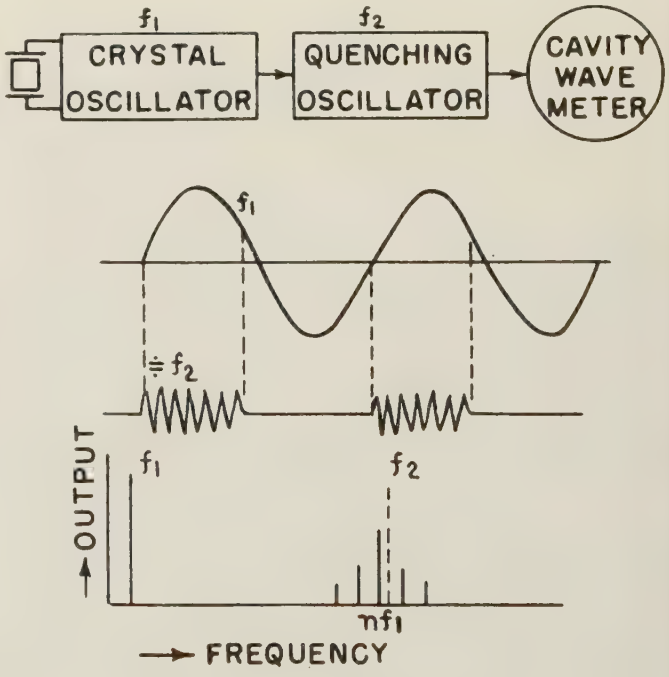

Fig. 1—Basic scheme of the system.

As far as the oscillation of f_2 repeats the same waveform in the period of $1/f_1$, the frequency spectrum of this microwave oscillator is expressed as shown in Fig. 1. We can see that the frequency spectrums of this oscillator are expressed only by the integer multiples

[3] R. Golicke, "Teilung und Vervielfachung von Frequenzen," *Elec. Nachr.-Tech.*, vol. 15, p. 134; March, 1938.

of f_1 and are independent of f_2. So we shall be able to pick up each spectrum one by one through a narrow bandpass filter, such as the Ho_{11}-type high-Q cavity resonator, which is coupled to the microwave quenching oscillator. For example, let us consider the case shown in Fig. 2, where

$n_0 \cdots f_2/f_1 \qquad t, \cdots$ time $\qquad \theta = 2\pi f_1 t$

$e \cdots$ voltage,

then the wave shapes are given by,

$$e = \epsilon \sin n_0\theta \qquad 0 \leqq \theta \leqq 2\pi\alpha$$

$$e = 0 \qquad 2\pi\alpha \leqq \theta \leqq 2\pi(\alpha - 1).$$

By Fourier's series, the following equations are obtained

$$e(\theta) = \frac{1}{2}\alpha_0 + \sum_{n=1}^{\infty}(a_n \cos n\theta + b_n \sin n\theta)$$

$$a_n = \frac{1}{\pi}\int_0^{2\pi} e \cos n\theta d\theta$$

$$= \frac{E}{2\pi}\left[\frac{1}{n+n_0}\{1 - \cos 2\pi\alpha(n_0+n)\} + \frac{1}{n-n_0}\{1 - \cos 2\pi\alpha(n_0-n)\}\right]$$

$$b_n = \frac{E}{2\pi}\left\{\frac{1}{n_0-n}\sin 2\pi\alpha(n-n_0) - \frac{1}{n_0+n}\sin 2\pi\alpha(n_0+n)\right\}.$$

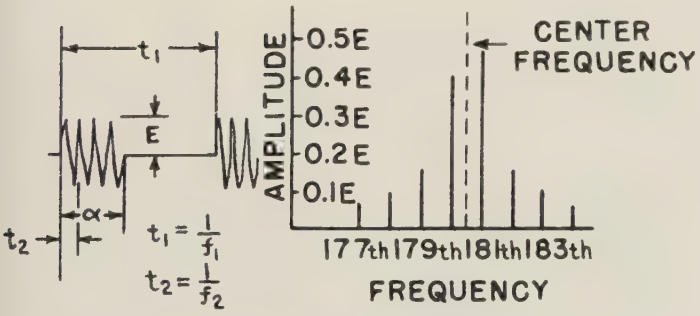

Fig. 2—Example of the calculation.

For example, putting $\alpha = 1/2$, $f_1 = 23$ mc, $f_2 = 4{,}150$ mc and, if the oscillator is controlled as shown in Fig. 2, and computing by the equation above, the frequency spectrums of the microwave output are obtained as shown in Fig. 2. In this figure, the maximum amplitude of the output spectrums is about one-half of the original amplitude of the oscillation voltage. Therefore, if we use a Klystron tube as an oscillator whose output power is about several tens of milliwatts, the output power of this equipment will be far greater than that of the crystal frequency multiplier.

Technical Problems in Frequency Multiplication by Quenching Oscillator at Microwave Range

If we are able to control the microwave oscillator by means mentioned above, it is theoretically possible to generate a standard frequency. Practically reflex Klystrons are used as microwave oscillators for measuring equipments. The high-frequency circuit of a Klystron is a cavity resonator, and the shunt impedance and also the loaded Q of the resonator are very high. We must consider the transient phenomena of the quenching oscillator. For a better understanding of the problems, let us consider the major assumptions by the simplest L, C, γ circuit, which is shown in Fig. 3.

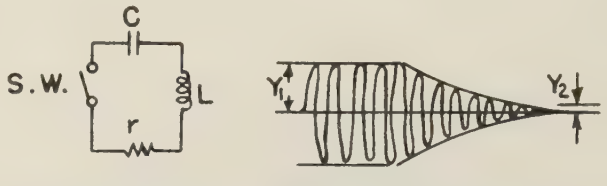

Y_2/Y_1	10^{-1}	10^{-2}	10^{-3}	10^{-4}	10^{-5}	10^{-6}
n_{12}	0.735Q	1.47Q	2.2Q	2.92Q	3.68Q	4.4Q

Fig. 3—Relations between Y_2 and n_2.

In the first place let us consider the decaying case of oscillation. If charge q_0 is applied initially to condenser C, the circuit equation when the switch is closed is written as

$$\frac{d^2q}{dt^2} + \frac{\gamma}{L}\frac{dq}{dt} + \frac{1}{LC}q = 0,$$

when the circuit loss is small; *i.e.*,

$$\gamma^2 < 4\frac{L}{C}$$

the solution is as follows,

$$q = \frac{2\sqrt{\frac{L}{C}}}{\sqrt{4\frac{L}{C} - \gamma^2}} q_0 e^{-\alpha t}\sin(\beta t + \phi);$$

where

$$\alpha = \frac{\gamma}{2L}, \qquad \beta = \frac{\sqrt{4\frac{L}{C} - \gamma^2}}{2L}, \qquad \phi = \cos^{-1}\frac{\alpha}{\beta}.$$

Describing q_0 in a voltage term, $q_0 = CE$, the circuit current equation will be derived as

$$i = \frac{2E}{\sqrt{4\frac{L}{C} - \gamma^2}} e^{-\alpha t} \sin \beta t.$$

The amplitude variations of the current or voltage with the time are shown in the form of $e^{-\alpha t}$ or $e^{-(\gamma/2L)t}$.

The number of the cycle of the alternating current (n_{12}), when amplitude y varies from Y_1 to Y_2, is described as

$$n_{12} = \frac{\omega}{2\pi}\int dt \qquad y = e^{-(\gamma/2L)t}$$

$$n_{12} = \frac{\omega}{2\pi}\cdot\frac{2L}{\gamma}\int_{Y_2}^{Y_1} dy$$

$$n_{12} = Q\cdot\frac{1}{\pi}\left[\log y\right]_{Y_2}^{Y_1}.$$

From this equation, the relations between Y_2 and n_{12}, where $Y_1 = 1$, are calculated as shown in Fig. 3.

The exciting voltage of the oscillator by the quenching voltage must be larger than that of the noise voltage, otherwise the build-up phase of the oscillator will be affected by the noise voltage, on the other hand, Y_2 must be smaller than the exciting voltage (which is the component voltage of harmonics of f_1 near the frequency of f_2), to control the quenching oscillation. By rough estimation, the value of Y_2 will be in the range, 10^{-5}–10^{-3}. Then

$$\text{if} \quad Y_2 < 10^{-5} \qquad n_{12} \doteqdot 3.68Q$$
$$\text{and} \quad Y_2 < 10^{-3} \qquad n_{12} \doteqdot 2.2Q.$$

The next problem is the build-up time of the oscillation. The voltage (transient waveform) at the start of oscillation is expressed as follows:

$E = E_0 e^{\alpha t} \sin \omega_0 t$, where E_0 is the exciting voltage.

The value of the α is expressed by the function of the circuit Q, the characteristics of the oscillator tube, and the oscillating amplitude. Studies have been done on the build up of the oscillation in the case of triodes by Dr. Usui,[4] and in the case of magnetrons by Mr. Lloyd P. Hunter.[5] We cannot apply these theories to the Klystron oscillators, but from these results we can see the same rule for a general case in the transient of the oscillation build up. Shown in Fig. 4 is the relation between the build-up time of the oscillator and the circuit Q.

In the case of high Q, the build-up time is large and it is proportionate to the value of Q, and in the case of small Q, the oscillation stops when $Q = Q_1$; in this condition the build-up time is infinite. We can see on the build-up time curve where there is a minimum point. The build-up time is shorted when $Q = Q_2$. And in this condition the build-up time of the oscillator having the circuit of Q_2 is, by the rough estimation, nearly equal to the decaying time of the circuit Q_2. Let us consider the building up of the oscillation on the case of the oscillator with the circuit of Q_2. The initial amplitude is $Y_1 = 10^{-3}$ when oscillation starts. We find also that for the time in building-up for the case of decaying, it is necessary to satisfy the following equation:

$$n_{12} \doteqdot 2.2Q_2 \text{ cycles.}$$

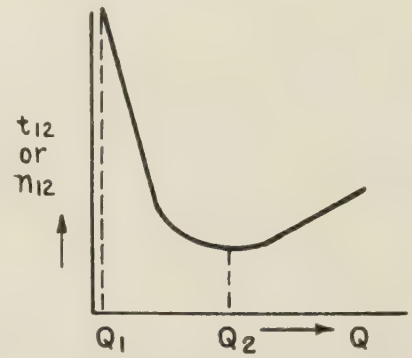

Fig. 4—Relations between Q and n_{12}.

It is also necessary at least nearly $4.4Q_2$ cycles to complete the start and the stop of the oscillation, and then frequency multiplication factor n_0 must be larger than $4.4Q_2$, or

$$f_2/f_1 = n_0 > 4.4Q_2.$$

For example,

$$f_2 = 4{,}000 \text{ mc} \qquad Q_2 = 100$$

then

$$n_0 > 440, \qquad f_1 < 9 \text{ mc}$$

So by the above reason, it is difficult to reduce the multiplication factor n_0 to a certain extent. But in the other point of view, if n_0 is too large, the f_2 component, by the quenching control voltage (f_1), in the beam current of the Klystron will be down lower than the noise level, then the build-up phase of the microwave oscillation (f_2) will be controlled by noise. It is very desirable to use a control voltage with large harmonic content and the square waveform for control voltage (f_1) is more desirable. But at the high radio frequencies, it is not so easy to generate a square waveform. To solve these difficulties, we applied the following methods. This is a double modulation method of which the schematic diagram and basic principle are shown in Fig. 5. In this system, two controlling voltages of f_1 and $n_1 f_1$ are applied simultaneously to the microwave oscillator. In this case, if n_1 is large number, or f_1 is of sufficiently low frequency, the system mentioned above would be used for a quenching control device with a standard oscillator, and the jittering of the build-up

[4] R. Usui, "Transient phenomena and the building up of oscillation amplitudes in triode oscillators," *Rep. Rad. Res. in Japan*, vol. 7; 1937.

[5] L. P. Hunter, "Energy build-up in magnetrons," *J. Appl. Phys.*, vol. 17, p. 833; October, 1946.

point by the noise is suppressed by the harmonics of the applied $n_1 f_1$ voltage. So by this system we can understand that the build-up and the stop of the microwave oscillator are exactly controlled by the constant phase from the standard generator.

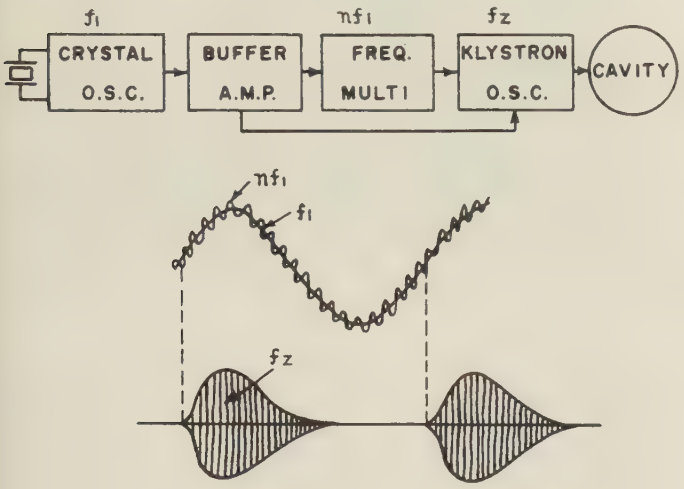

Fig. 5—The double modulation method.

For a example, if we put,

$f_2 = 4{,}000$ mc $\quad f_1 = 2$ mc, $n_1 = 40$, $\quad n_0 = 2{,}000$

$n_1 f_1 = 80$ mc, $\quad n_0/n_1 = 50$, $\quad Q = 100$,

then

$$n_0 > 440.$$

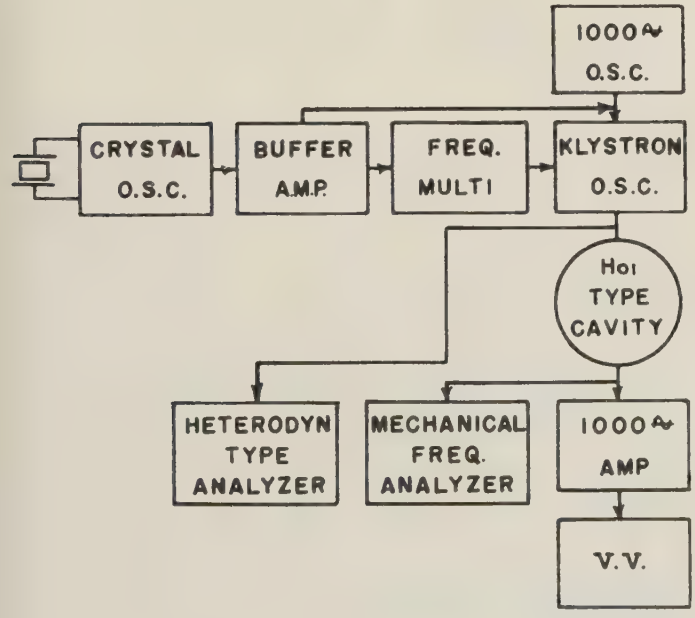

Fig. 6—Scheme of the double modulation method.

Experiments on the New System

The experiments are done using low power reflex Klystron oscillators in the frequency range of 3,500–4,500 mc and 9,000–10,000 mc. A block diagram is shown in Fig. 6. In the experiment, 2–6 mc standard quartz oscillator, and $n_1 = 4$–40 primary frequency multipliers were used, and the experiments were done both on the modulation method of single modulation and double modulation with the voltage of f_1 and $n_1 f_1$ as mentioned above. This double modulation circuit is shown in Fig. 7. Standard frequency microwave output is measured with a cavity reasonator and analyzed with the spectrum analyzers. Experimenting by the single modulation method, the following results are obtained: where

$f_1 = 5 - 40$ mc,	$f_2 \fallingdotseq 4{,}000$ mc
$f_1 \fallingdotseq 40$ mc	microwave output $\fallingdotseq 0$
$f_1 \fallingdotseq 30$ mc	microwave output is very weak
$f_1 \fallingdotseq 25$–20 mc	microwave nf_1 output was measured but very weak
$f_1 \fallingdotseq 15$ mc	microwave nf_1 output is measured but very noisy
$f_1 \leqq 10$ mc	noise output only and microwave nf_1 output is not measured.

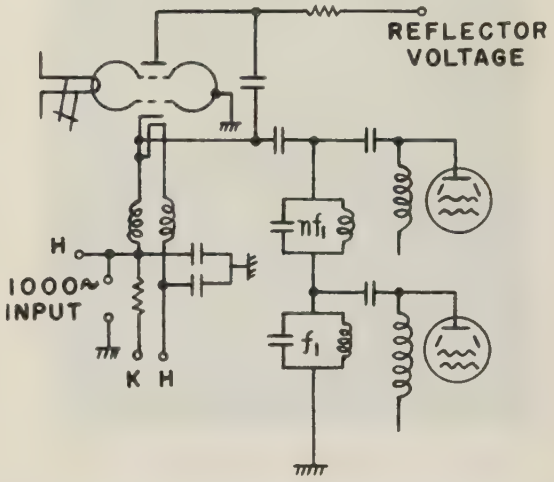

Fig. 7—Double modulation circuit.

As shown above, satisfactory operation was not obtained by this modulation method, and the signal was unstable and not free from noise.

But experiments by the double modulation method, satisfactory operation was obtained by frequency $f_1 = 5.7$ mc–2.8 mc, $n_1 = 16$–32. Under these conditions the microwave output which is frequency multiplied from a quartz crystal oscillator is very stable and relatively free from noise. Fig. 8 shows the experimental results of the double modulation, this figure obtained by a mechanical spectrum analyzer and Fig. 9 obtained by a heterodyne type spectrum analyzer. In this experiment when the modulation condition is changed by varying the control voltage $(n_1 f_1)$, the results are A, B, $\cdots$ E; in case A the modulation is complete single modulation, and in case B the modulation is complete double modulation. In case A the build-up of the microwave oscillator is controlled by noise only, and in case E, it is controlled by the $n_1 f_1$ voltage only

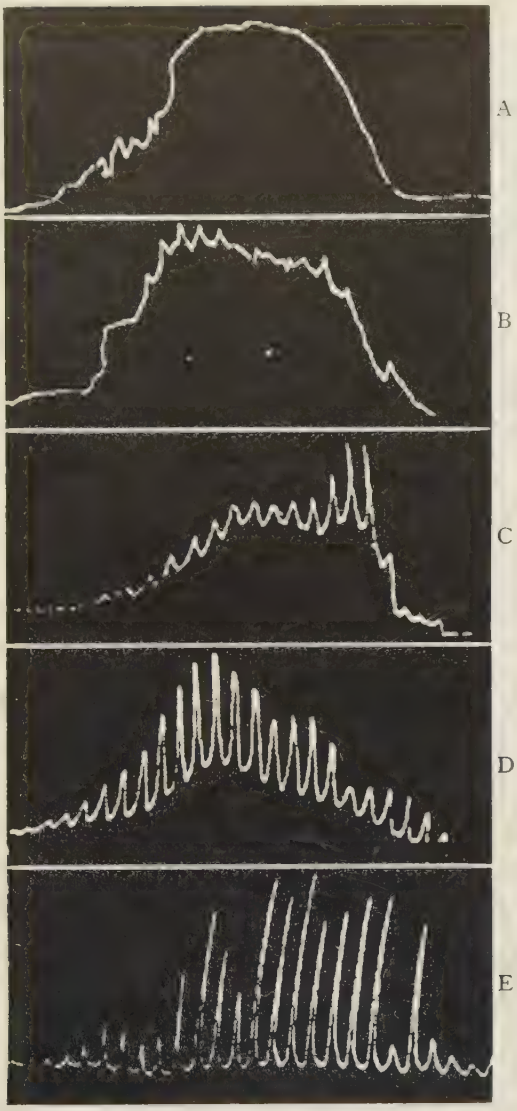

Fig. 8—Experimental results of the quenching control oscillator, obtained by the mechanical spectrum analyzer.

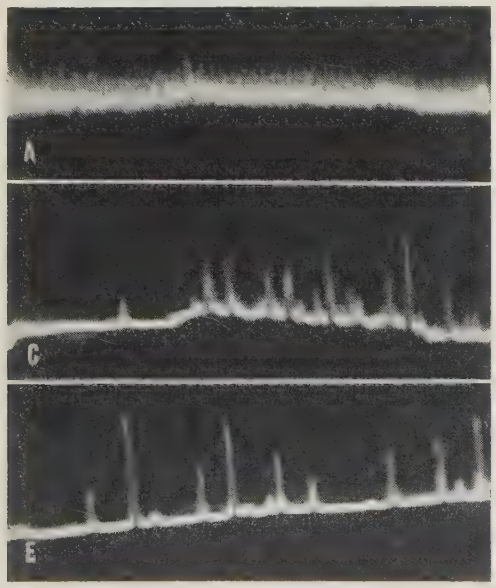

Fig. 9—Experimental results of the quenching control oscillator obtained by heterodyne type spectrum analyzer.

and is free from noise. Fig. 10 shows one of the examples measured at following conditions:

$f_1 = 5.1925$ mc $\quad n_1 f_1 \doteqdot 84$ mc $\quad n_1 = 16$

E_1 (control voltage of f_1) $\doteqdot 65$v

E_1 (control voltage of $n_1 f_1$) $\doteqdot 33$v.

The output power of nearly 1 mw at the standard frequencies are obtained by a 25 mw (cw power output) Klystron.

In these experiments, when the tuning of the Klystron cavity or the reflector voltage is varied slightly, position of the spectrums did not change and the amplitudes of them were only varied. Thus it is proved that the oscillation is perfectly synchronized by quenching control.

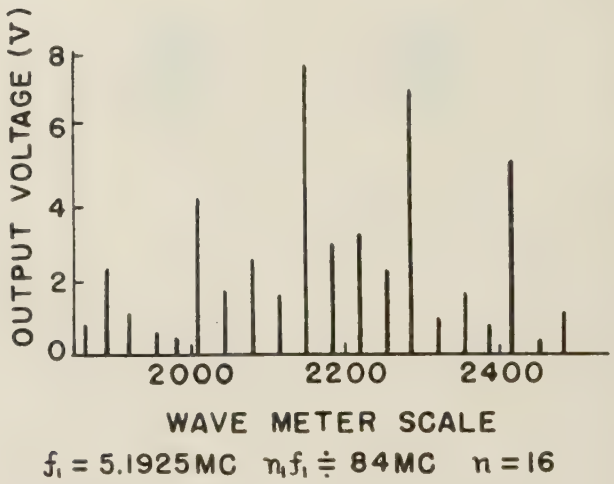

Fig. 10—Example of the measured spectrums.

Applications of the New Frequency Standard

When we compare the new system mentioned above with the previous one, the equipment of this new system is very simple, and its output power is considerably high. Fig. 11 shows the outside view of the microwave standard of this new system. Fig. 12 shows the comparison of output frequency spectrums of the new system with the previous crystal multiplier systems.

By applying the new system the authors have obtained a method of precise frequency measurement of microwaves. The basic principle is as shown in Fig. 13. The precise measurement is done by measuring the Δf (in Fig. 13) with the combination of the special cavity wavemeter as shown in Fig. 13, and the frequency standard by this principle.

Unknown frequency fx is measured in a form

$$fx = fs + \Delta f,$$

where fs is one of the spectrums of the standard frequency and Δf is measured with the cavity wavemeter by vernier rod B. Accuracy of this system is good, and

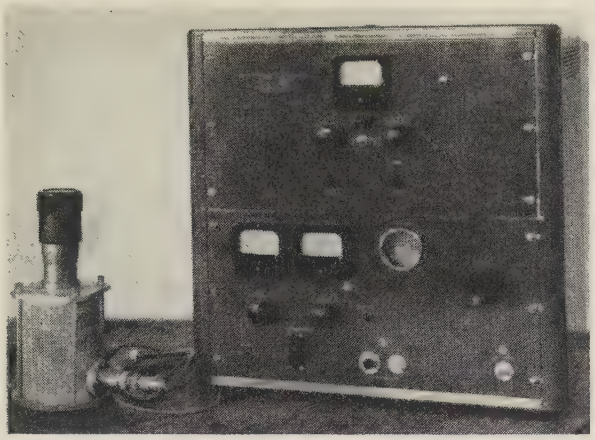

Fig. 11—Outside view of the new type microwave frequency standard.

over-all accuracy of 0.001 per cent or better is obtained. In the modified system of this principle, the measurement of Δf is done by the heterodyne principle. In this system, unknown frequency of fx is beaten down to Δf and then the frequency measurement of Δf is done with a heterodyne-type frequency meter of Δf range as customarily used, and the accuracy of 0.0001 per cent is obtained.

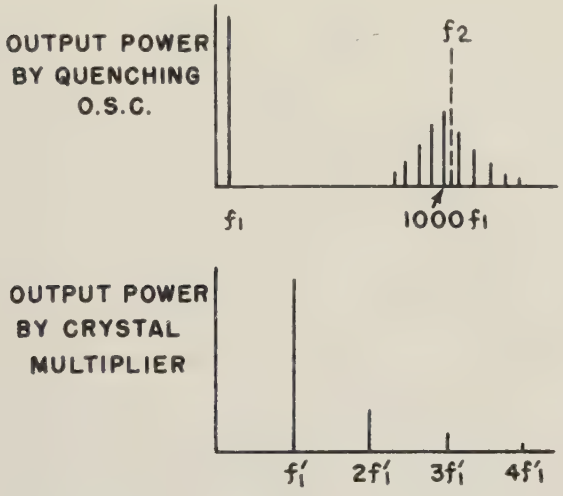

Fig. 12—Comparison of output frequency spectrums of the new system with the crystal multiplier system.

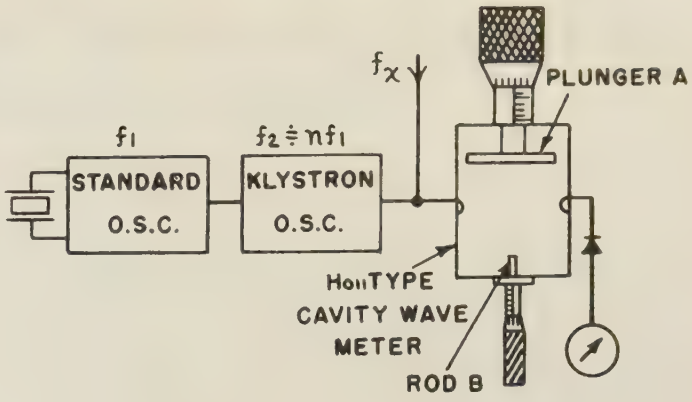

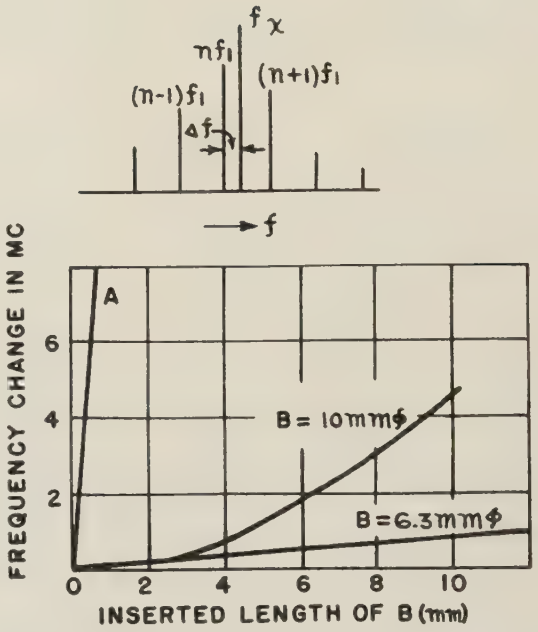

Fig. 13—The method of precise frequency measurement.

Conclusion

The equipment in this paper is one of the simplest and most economical for microwave frequency standards, and may possibly be the one for solving these problems by the precise measurements of the microwaves. They are now applied to commercial products. We consider that these methods will be applied to not only microwave region but also uhf or vhf regions.

Determining Attenuation of Waveguide from Electrical Measurements on Short Samples

A. F. POMEROY† AND E. M. SUÁREZ†

Summary—An improved method for accurately determining the attenuation of waveguide from measurements on very short samples is presented. First, two samples are measured separately and then in tandem. When the measurements are properly made, the sum of the attenuations when the samples are measured separately agrees with the attenuation when measured in tandem at each frequency of measurement. Second, the average effective resistivity is found over a band of frequencies. Using the average effective resistivity, the attenuation at any frequency in the band can be determined. Results for WR159 copper waveguide are shown.

Introduction

THIS PAPER presents an improved method for accurately determining the attenuation of waveguide, using two samples only a few feet long. Other methods have the disadvantages of: 1) using more total length of waveguide, 2) of requiring very precisely machined cavities, or 3) of lacking the required accuracy. This improved method consists of two parts. The first part is the insertion of a length of waveguide between a microwave measuring setup and a movable short and the measuring of the voltage standing-wave ratios (vswr) before and after the insertion. The two samples are inserted separately, then in tandem. An attenuation value, associated with the inserted waveguide is obtained from the vswr readings at each frequency of measurement. To prove-in the particular measuring equipment being used, the sum of the attenuations of the two samples measured separately, must agree with the attenuation of the two samples measured in tandem. The second part is finding an average effective resistivity over a band of frequencies. This may be done either by computations or by plotting the attenuation values found above, at each frequency, on computed attenuation-vs-effective-resistivity characteristics. The intersections of the average effective resistivity with the computed attenuation characteristics give accurate values of attenuation for the waveguide being measured. For the WR159 copper waveguide measured, the effective resistivity is 2.1×10^{-6} ohm-centimeter, and the attenuations are 0.0130 db per foot at 6,425 mc, 0.0135 db per foot at 6,175 mc, and 0.0138 db per foot at 5,925 mc. The samples were $3\frac{1}{2}$ feet long.

Factors Affecting Attenuation

The two principal factors which affect the attenuation of waveguide are the internal dimensions of the waveguide, and the effective resistivity of the conducting surfaces. The internal dimensions of the waveguide are principally controlled by the drawing plug used in manufacture. The effective resistivity depends on the roughness of the conducting surfaces, the direct-current (dc) resistivity of the metal, and the extent and nature of the metal in the conducting surfaces. The roughness of the conducting surfaces is important because of the increased path length due to the roughness, since current at microwave frequencies travels essentially on the surface. The dc resistivity can be computed from dc and dimensional measurements or by making a chemical analysis and comparing the analysis with others for which the dc resistivities have already been determined [26]. The dc resistivity places a lower limit on the value of the attenuation that may be expected. In the samples tested, corrosion is not thought to be important.

Previous Methods of Measurement

Attenuation of waveguide has been measured by many methods. Five of the most commonly used methods are the following:

1) A length of waveguide is inserted in a microwave measuring setup and the loss is measured by comparing attenuator settings, before and after the insertion. The comparison attenuator may be in the microwave path or in an intermediate-frequency path if a double- or triple-detection measuring set is used. The result is the average attenuation for the total length. A long run (several hundred feet) of waveguide is required for accurate determination. Reflections from waveguide flanges may cause an error due to the interaction factor [28].

2) A length of waveguide is inserted between a microwave measuring setup and a short and the power returned from the short is measured by comparing attenuator settings before and after the insertion. The same comments apply to this method as to method 1) except that the length of waveguide under test needs to be only half as long. In addition, voltages reflected from waveguide flanges may cause small errors by adding vectorially to the voltage reflected from the short.

3) A length of waveguide is made into a cavity by shorting the section at both ends. The frequency at which maximum power is absorbed in the cavity formed by the shorts and the sample of waveguide, is determined, as is the frequency interval between the lesser and greater frequencies at which the power absorbed is half as much. The attenuation calculated from the readings is the average attenuation for a few inches of waveguide.

4) A length of waveguide is inserted between a slotted section and a short, and the vswr is measured. The attenuation due to the length of waveguide is determined

† Bell Telephone Labs., Murray Hill N. J.

by subtracting the computed attenuation of the slotted section between the movable probe and the short from the attenuation calculated from the vswr reading. The result is the average attenuation for the total length. Great reliance is placed on computed values of attenuation in the slotted section and in the short. A run of waveguide 10 to 60 feet long is required. Reflections from waveguide flanges can cause large errors.

5) A length of waveguide is inserted between a slotted section and a short and the vswr is measured before and after the insertion. The attenuation calculated from the readings is the average attenuation for the total length. As in method 4), 10 to 60 feet of waveguide can be measured. Reflections from waveguide flanges can cause large errors.

Theory of Measurement for the Improved Method

If a microwave frequency is applied to the near end of a waveguide section that is shorted at the far end, a standing wave is set up. Voltage standing-wave ratio, vswr, the ratio of the value of the maximum voltage to the value of the minimum voltage, is infinite for the quarter-wave length section nearest the short, if the short is lossless, because the minimum voltage is zero. For quarter-wave length sections nearer the generator, both the maximum and minimum values of voltage increase. Since the minimum value is increasing faster than the maixmum value, the vswr decreases. The higher the loss per unit length in the waveguide, the faster the vswr decreases. Reflections from waveguide flanges can cause large errors. The sources of error are discussed later.

In order to obtain good accuracy in the measurement of very large vswr's, the 3 db method of evaluation of vswr is used. In this method, two distances are measured. The first distance is that between successive minimums, P and P', on the standing-wave characteristic shown in Fig. 1. This distance is exactly one-half wavelength in waveguide, $\lambda_G/2$. The ordinate of the standing-wave characteristic in Fig. 1 is $|V/A|^2$, where V is the voltage at a distance x from the short, and A is a constant.

The second distance, y in Fig. 2, is that between points O and Q at which the power is twice the power W at point P. The measurements of power at O, P, and Q must not be affected appreciably by noise. Let S be the letter symbol for vswr. Then

$$S = \frac{\lambda_G}{\pi y}. \tag{1}$$

A derivation of this equation by E. M. Purcell is shown on page 505 of reference [18].

For large vswr's, the distance y is very small. In the measurements reported herein, this distance varies between 0.008 and 0.017 inch. Because it is difficult to obtain accurate measurements of this sort using a slotted section, E. G. Morton of the Bell Telephone Laboratories, Inc., suggested in 1945, the use of a movable short and a fixed sampling orifice. In this method, the movable short moves the standing wave past a sampling orifice which acts as a probe. The slotted-section method, described in the section on "Previous Methods of Measurement (5)," moves a probe along a slotted waveguide to sample the standing wave.

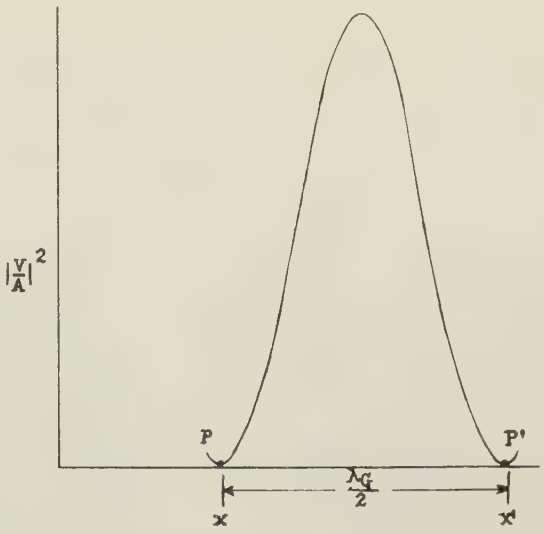

Fig. 1—Determining a half wavelength.

$$\left|\frac{V}{A}\right|^2 = \frac{\cosh 2\alpha x}{2} - \frac{\cos 2\beta x}{2}$$

V = Voltage at distance x from short
A = Constant
α = Attenuation per unit length
x = Length from the short
β = Radians per wavelength

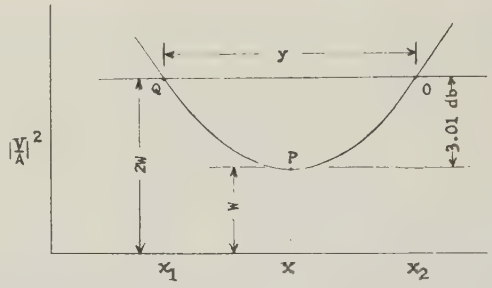

Fig. 2—Determining the displacement y between 3 db points. (Portion of Fig. 1 expanded around point P.)

Attenuation is obtained by substituting the value of S obtained from (1) into (2).

$$\alpha x = 10 \log_{10} \frac{S+1}{S-1}, \tag{2}$$

where

α = attenuation per unit length in db,

and

x = distance from the short.

A derivation of this equation by E. Weber is shown on page 818 of reference [18].

One source of error which should be noted here is the effect of noise in measuring at or near a voltage minimum. A common method of minimizing this error is to increase the length of the waveguide between the orifice and the short. Another way proposed by J. H. Vogelman [5] is to use a lossy short. Still a third way, using a lossy shunt, is described by J. M. Altschuler and A. A. Oliner [2]. The method described herein uses a pad attached to the front of a movable short. The loss in the pad takes the place of the equivalent loss in a length of waveguide and raises the voltage minimums out of the noise, so that accurate 3 db changes can be measured. The choice of a value for the pad is considered later in the sections "Noise," and "Difference Between Numbers" under "Discussion of Errors." The value does not have to be known.

The attenuation calculated from (2) includes the loss in the short, if any, and in all connected waveguide from the short to the sampling orifice.

In order to eliminate the extraneous losses that are measured along with the loss of the sample, it would appear that only two sets of readings are required at each frequency. The first set of readings would be made to determine the attenuation of the waveguide parts located between the orifice of the voltage-sampling orifice and a movable short. The second set would be made with the sample of waveguide inserted between the orifice and the movable short. The difference should be the attenuation of the sample of waveguide.

Unfortunately, there are many sources of error that may affect the accuracy of the above measurements. In order to prove-in the particular measuring equipment being used, at each frequency, two additional sets of readings, 2) and 3), are required as follows:

1) A measurement, made with one test sample inserted;
2) A measurement, made with another test sample inserted; and
3) A measurement, made with both test samples inserted in tandem.

The sum of the attenuations of the two test samples measured separately, and in tandem, should be the same, within reasonable limits. If this criterion is not met, the measuring equipment, or technique, or both, need to be improved. The possible sources of error will be considered later under "Discussion of Errors." The average of the sum of the attenuations of the two samples measured separately and the attenuation of the two samples measured in tandem will be called the "measured attenuation."

The surface roughness factor might be defined as the ratio of the length of a profile path over a rough surface to the length of a path over an ideal surface. The surface roughness factor has been measured by the use of microphotography by F. A. Benson [7]. The correlation with microwave determinations has been good.

For the $TE_{10}\square$ mode, Benson has found cases in which the factor was as great as 1.4 for current paths transverse to the axis of transmission. It is generally much less. He found that the factor was about unity for the path in line with the axis of transmission. For the purposes of this paper, it is assumed that an average surface roughness factor can be used and that it can be combined with the dc resistivity to give a resultant "effective resistivity."

Suppose now that the attenuations of hollow conducting waveguides are computed using (3) and (4) in the Appendix. The resultant attenuation, at any one frequency, varies as the square root of the effective resistivity. Using frequency as a parameter, it is possible to plot attenuation-vs-effective-resistivity characteristics for as many frequencies as is desired. These characteristics are straight lines on log-log paper. Usually three frequencies in each band will suffice. Such characteristics are shown in Fig. 3.

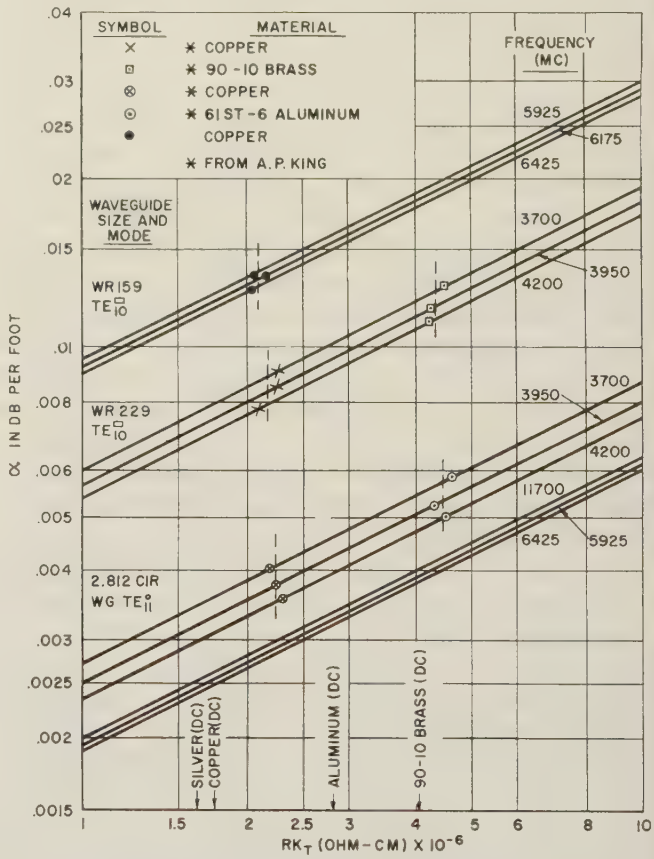

Fig. 3—Measured attenuation plotted on calculated attenuation (α)-vs-effective resistivity (R) characteristics.

The "measured attenuations" as found above can be plotted, frequency by frequency, on the characteristics as shown in Fig. 3. In general, they will not fall on a common abscissa. The causes may be inherent in the measuring equipment.

It might be expected that the effect of surface roughness would be greater at the higher microwave frequencies than at the lower microwave frequencies. However, this effect would not ordinarily vary much over a small band of frequencies. For the purposes of this

discussion, it is assumed that there is no change in this effect over the small band of frequencies of interest. Consequently, an attempt can be made to increase the accuracy by finding an arithmetic-average effective resistivity that best represents the "measured attenuation" data.

The intersections of the average effective resistivity and the attenuation characteristics will determine the attenuation of the sample waveguide, for as many frequencies as there are plotted characteristics.

The differences between this improved method and previous methods using a slotted section and a short can be summarized as follows:

1) An orifice is used as a voltage sampler.
2) A movable short is used to move the standing wave past the orifice.
3) A pad is used instead of a long length of waveguide or a lossy short, to prevent noise from affecting the accuracy of the measurements.
4) The particular measuring equipment used is proved-in by measuring the attenuation of two samples separately, then measuring the two samples in tandem.
5) Accurate attenuation per foot at any frequency is determined by using the value of an arithmetic-average effective resistivity that best represents the data.

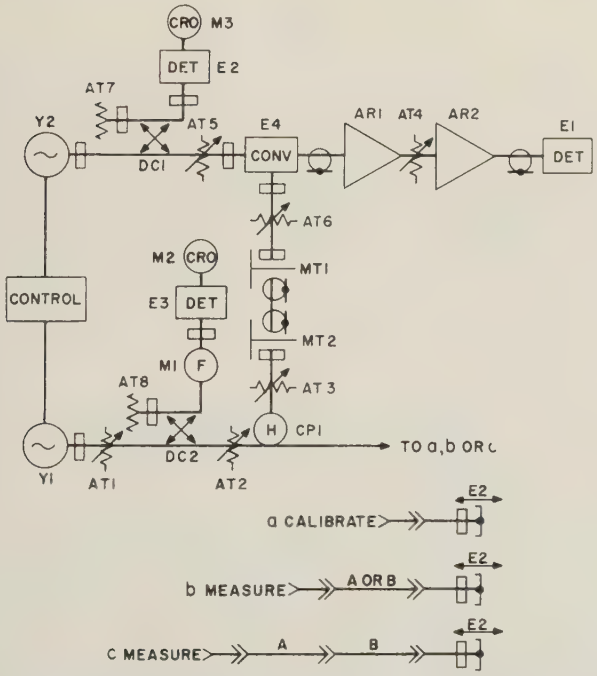

Fig. 4—Schematic drawing of test setup for measurement of attenuation.

Description of Measuring Equipment

The circuit schematic of the equipment used in making these measurements is shown in Fig. 4. The physical layout is shown in Fig. 5. The setup consists of waveguide parts and an associated heterodyne measuring set. The signal and beat-frequency oscillators *Y1* and *Y2*, mounted in shielded containers, are shown at the extreme left end of the waveguide setup. A klystron power supply and control panel for the oscillators is located in the bottom of the cabinet shown at the extreme left in Fig. 5. Attenuators AT1 and AT2 are used to pad the signal oscillator Y1 in order to prevent pulling. A directional coupler DC2 is used to connect

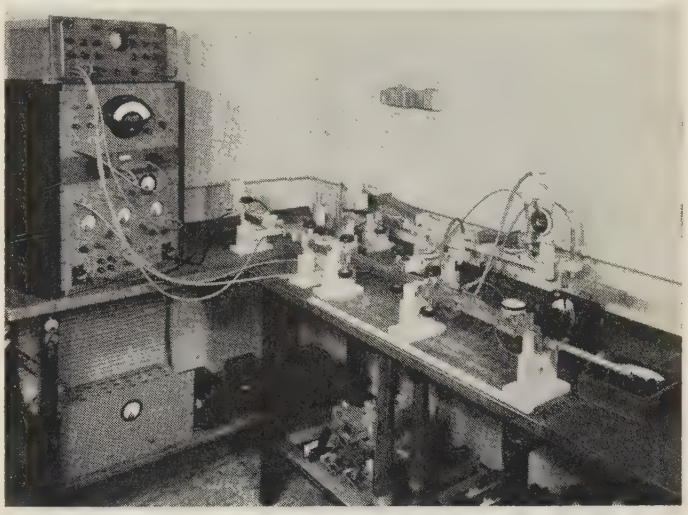

Fig. 5—Test setup for "calibrate" measurement.

equipment which continuously monitors the frequency of Y1. The sampling orifice CP1 consists of an 18-inch length of WR159 waveguide with a hole on one side as shown in Fig. 6. The waveguide test samples A and B consist of 42-inch sections of WR159 waveguide. A movable short E2 and associated pad are mounted on a

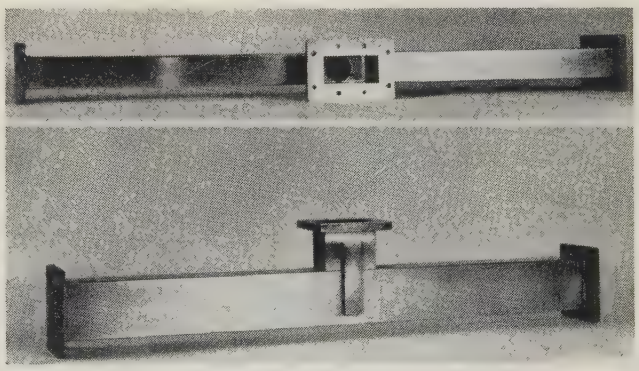

Fig. 6—Two views of the assembly containing the voltage-coupling orifice.

carriage, as shown in Fig. 7. The carriage holds the short in the same relative position with respect to the sides of the waveguide as the carriage is moved. The pad, mounted on the face of the movable short E2, consists of a small, triangular piece of lossy Synthane. A dial indicator measures the distance y between 3 db points. A closeup of the dial indicator, as mounted to measure the y distance, is shown in Fig. 8. A close-up of the micrometer, as mounted to measure the distance between half-wavelength points, is shown in Fig. 9. A battery and meter are used to indicate that the micrometer spindle is just touching. Connected to the sam-

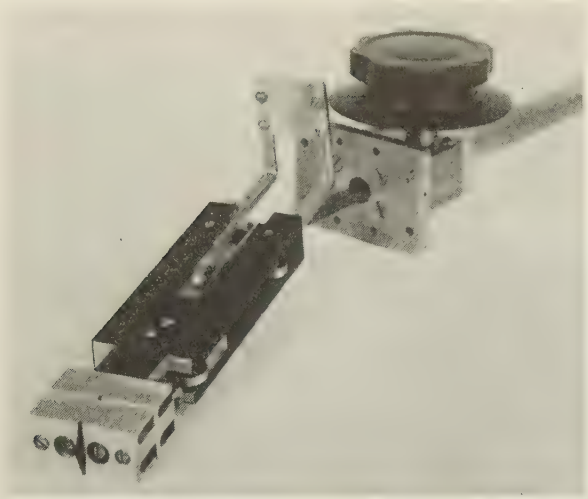

Fig. 7—Movable shorting piston and pad.

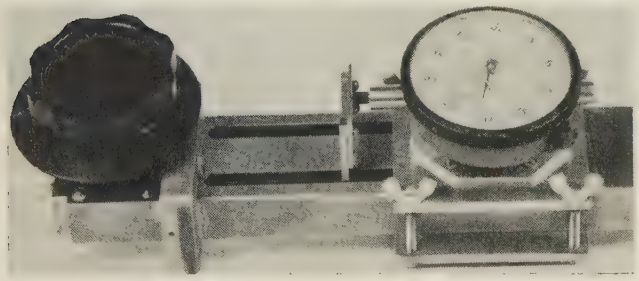

Fig. 8—Dial indicator mounted to measure the distance y.

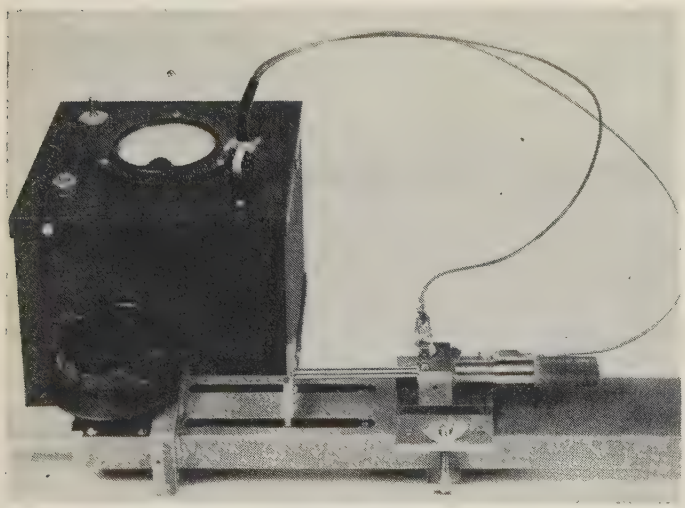

Fig. 9—Micrometer mounted to measure a half wavelength.

pling orifice are the pads AT3 and AT6 and a converter E4, which consists of a hybrid junction and a crystal detector. A coaxial cable connects the converter to the 70 mc equipment, consisting of a preamplifier AR1 and an amplifier-detector (AR2 and E1) shown on the extreme left-hand side of Fig. 5. The power supply for the 70 mc equipment is shown on the bottom of the bench. AT4 is the 70 mc precision attenuator used to measure accurately a change of 3 db.

Preparation of Waveguide Assemblies

Flanges on the two test samples, on the section of waveguide in which the movable short is located, and on the section of waveguide in which the sampling orifice is drilled, are finished so that the waveguide assemblies meet a 45 db return-loss requirement. The return loss is measured over the 500 mc band of frequencies between precision "standard" flanges that have a 60 db return loss, or better, when measured as a pair.

Attenuations Obtained From Measurements

In determining the attenuation of WR159 waveguide, four sets of data were recorded at each frequency (5,925, 6,175, and 6,425 mc): 1) data with no waveguide test sample inserted between the orifice and the section in which the movable short is mounted, the setup for which is shown in Fig. 4 and 5; 2) data with test sample A inserted between the orifice and the section in which the movable short is mounted; 3) data with test sample B; and 4) data with test samples A and B in tandem. The data recorded for each set consists of distances between 3 db points and the distances between adjacent minimums. The distances between 3 db points ranged from 0.025 centimeter to 0.043 centimeter. The vswr's corresponding to these values ranged from 88 to 42. The attenuations obtained from the above vswr's ranged from 0.099 to 0.205 db and are shown in Table I.

TABLE I

Attenuation of WR159 Waveguide

Row	Frequency (mc)	Attenuation (db)		
		5925	6175	6425
1	Section A (42.0 inches long)	0.0488	0.0483	0.0462
2	Section B(42.0 inches long)	0.0471	0.0466	0.0444
3	Sections A and B in tandem	0.0955	0.0952	0.0901
4	Sum of sections A and B Row 1+Row 2	0.0959	0.0949	0.0906
5	Average of Row 3 and Row 4	0.0957	0.09505	0.09035
6	Per cent difference between Row 3 and Row 4	0.4	0.3	0.6

Finding Average Effective Resistivity and Determining Attenuation Values

The second part of this improved method is finding the average effective resistivity over a band of frequencies. One way is to use the results from the previous section, and to find the calculated effective resistivity (RK_T) at each frequency by using (3) of the Appendix. An easier way is to plot in Fig. 3 the values of attenuation per foot shown in Row 1 of Table II, then to determine the average effective resistivity as shown by the dashed line. The intersections of this dashed line with the attenuation characteristics lead to values of 0.0138 db per foot at 5,925 mc, 0.0135 db per foot at 6,175 mc, and 0.0131 db per foot at 6,425 mc. These are the accurate answers sought.

TABLE II

ATTENUATION OF WR159 WAVEGUIDE DETERMINED FROM AVERAGE EFFECTIVE RESISTIVITY

Row	Frequency (mc)	Attenuation (db per foot)		
		5925	6175	6425
1	Calculated attenuation from Row 5, Table I	0.01367	0.01358	0.01291
2	Effective resistivity from Fig. 3 for values in Row 1 ($\times 10^{-6}$ ohm-cm)	2.06	2.17	2.03
3	Determined attenuation from Fig. 3 using average effective resistivity (dashed line)	0.0138	0.0135	0.0131
4	Per cent difference between Row 1 and Row 3	1.1	0.9	1.5

Data from A. P. King[1] of the Bell Telephone Laboratories, Inc., has been similarly plotted on the proper attenuation characteristics and dashed lines drawn to show average effective resistivity values. These data are included to show that measurements made by other methods also show about the same spread in effective resistivity values.

SURFACE ROUGHNESS FACTORS

If we know the dc resistivity and the average effective resistivity, division of the second by the first leads to the surface roughness factor. H. T. Wilhelm[1] of the Bell Telephone Laboratories, Inc., reports that the dc volume resistivity of the material in the WR159 waveguide measured had a value of 1.756×10^{-6} ohm-centimeter at 25°C (equivalent to 1.703×10^{-6} ohm-centimeter at 20°C). The values of dc resistivities of silver, copper, aluminum, and 90-10 brass are also indicated in Fig. 3.

As shown in Table III, the effective resistivities derived for the copper waveguides in Fig. 3 lead to surface roughness factors of: 1.32 for the 2.812 circular waveguide, 1.29 for the WR229 waveguide, and 1.23 for the WR159 waveguide.

TABLE III

SURFACE ROUGHNESS FACTORS

Row	Waveguide	WR159	WR229	2.812 CIR
1	DC resistivity for copper ($\times 10^{-6}$ ohm-cm)	1.703	1.703	1.703
2	Effective resistivity from Fig. 3 ($\times 10^{-6}$ ohm-cm)	2.1	2.2	2.26
3	Surface roughness factor K_T	1.23	1.29	1.32

In order to compute factors for the 2.812 circular waveguide and the WR229 rectangular waveguide, it is assumed that the copper in these waveguides has the same dc resistivity as that in the WR159 waveguide.

[1] Unpublished work.

A. P. King[1] measured waveguide runs with lengths of 150 to 200 feet in order to determine the attenuations of WR229 and 2.812 circular waveguide, plotted in Fig. 3.

Benson [7] reports factors that average 1.11 for a 60-foot length of WR90, drawn to loose tolerances, and 1.034 for a 15-foot length of WR90, drawn to tight tolerances. A comparison of (5) with (3) shows that the factors reported by Benson must be squared to compare with the surface roughness factors derived in this paper, as the factor given herein is under the radical and his is not. Squaring the Benson factor leads to the following results: 1.23 for WR90 waveguide (loose tolerances) [7] 1.07 for WR90 waveguide (tight tolerances) [7].

DISCUSSION OF ERRORS

Nine of the major factors affecting the accuracy of the determinations are discussed below.

Dimensions of the Waveguide

Table IV shows the effect of a 0.001-inch change in both wide and narrow dimensions of a waveguide on the attenuation. This effect is computed to be 0.2 per cent. The WR159 waveguide from which the samples described in this paper were made was within the specification tolerances of $1.590 \pm 0.002 \times 0.795 \pm 0.002$ inches.

TABLE IV

EFFECT OF WAVEGUIDE TOLERANCE ON ATTENUATION OF WR159 WAVEGUIDE AT A FREQUENCY OF 5925 MC [CALCULATED USING (3) IN THE APPENDIX]

Wide Dimension (inches)	Narrow Dimension (inches)	R (ohm-cm)	Attenuation (db per foot)
1.590	0.795	2.1×10^{-6}	0.013756
1.589	0.794	2.1×10^{-6}	0.013782

Impedance Mismatch

Impedance mismatches at the waveguide flanges [9] have been made very small by careful preparation of the waveguide assemblies.

Purcell [18] states that the error due to orifice susceptance is very small for this method of measurement.

The error due to change in impedance presented by the pad and the short has been made very small by a mechanical design that assures that the impedance presented will be the same for all positions axially in the waveguide. Over the years, many types of supports for movable shorts have been tried. The design of the carriage used in these tests was chosen after trials had shown that previous designs would not meet the stringent requirements for change of impedance vs movement axially in the waveguide. The change in impedance is checked by measuring y, the distance between the 3 db readings, at two or three minimums and checking that the values of y do not differ by more than

2 per cent for the calibrate measurements, or by more than 1 per cent for the remaining measurements.

The effect of the leakage of the short has been minimized by using two choke-type shorts in tandem, and fastening lossy Synthane to the sides and top of the supporting carriage. This reduces the behind-the-carriage resonance effects to a negligible value.

Distance Measurements

The determination of the 3 db change is done by using a calibrated 70 mc attenuator, making use of the calibration corrections to 0.01 db, and interpolating to 0.005 db on the 1.5-inch-per-db output meter. The distance y between the 3 db points is measured by a sensitive dial indicator.

Half wavelength in waveguide is determined accurately by using a long micrometer spindle, with battery and meter to indicate when the spindle is just touching the bracket as shown in Fig. 9.

Noise

Two checks are made to avoid errors due to noise. First, the input-output characteristic of the converter-preamplifier is checked for linearity. Input signals must be kept in the linear range, since the IF attenuator is connected after the preamplifier. Second, the loss of the pad attached to the movable short is chosen to lift the voltage, at a minimum, out of the noise by about 20 db in order to have 0.1 db accuracy in attenuator readings.

Difference Between Numbers

Since the method depends upon subtracting a "calibrate" attenuation from a "measure" attenuation, the smaller the value of the "claibrate" attenuation, the better the accuracy, in general. This means keeping the value of the pad attached to the movable short as small as possible.

Frequency Drift

Frequency drift of the signal oscillator is minimized by making the measurements in a temperature-controlled room. The sort of measuring setup used is essentially a very sensitive frequency meter [19] and care must be taken to minimize errors due to drifts of the oscillator frequency and to changes in length of the waveguide due to temperature changes.

Two or More Signal Frequencies

On occasions, a klystron produces more than one signal frequency. An error introduced by more than one signal frequency being detected at the same time will make the calculated attenuation for that reading too small.

If the signal oscillator produces sufficient power in harmonics, an error will be introduced that will make successive distances between the 3 db points different.

Crosstalk

In a heterodyne-type measuring set, such as the one used, crosstalk between the signal oscillator and the converter will cause errors in the measurements. This was the reason for the complete shielding of both the signal- and beat-frequency oscillator mounts and the power leads to them.

Approximate Formulas

Computations, carried out to 5 significant figures show no appreciable error due to the use of the approximation in (1).

Conclusions

The method reported in this paper leads to a precise determination of the attenuation of waveguide in short or long samples equipped with flanges, without destroying the commercial value of the samples.

It avoids the use of a precise slotted section, substituting instead a precise movable short which, in the opinion of the authors, is much easier to build.

It incorporates a check on the effect of noise on the accuracy of measurement. The check is accomplished by measuring the samples separately, then in tandem.

This method takes account of small inaccuracies in measurements, shown by scattering, by finding an average effective resistivity, then uses this resistivity in order to determine the accurate attenuations.

Appendix

Formulas for Calculation of Attenuation

Rectangular Waveguide (TE_{10}□)

$$\alpha = \frac{5.963\left[\frac{RK_T}{\lambda}\right]^{1/2}\left[\frac{1}{b}+\frac{\lambda^2}{2a^3}\right]}{\sqrt{1-\frac{\lambda^2}{4a^2}}}. \qquad (3)$$

Circular Waveguide (TE_{11}○)

$$\alpha = \frac{11.932}{d}\left[\frac{RK_T}{\lambda}\right]^{1/2} \cdot \left[\frac{1.419}{\sqrt{1-\left[\frac{\lambda}{1.71d}\right]^2}} - \sqrt{1-\left[\frac{\lambda}{1.71d}\right]^2}\right]. \qquad (4)$$

α = attenuation in db per foot.
R = dc resistivity of conducting surface in ohm-centimeters.
a = wide dimension of waveguide in inches.
b = narrow dimension of waveguide in inches.
λ = free-space wavelength in inches.
d = diameter of waveguide in inches.
K_T = surface roughness factor.
RK_T = effective resistivity of conducting surface in ohm-centimeters.

Rectangular Waveguide (TE_{10}□)

Taking Account of Surface Roughnesses: A formula derived by Benson [3] from Kuhn [21] for the TE_{10}□ mode is:

$$\alpha = \frac{\lambda_G}{b(\lambda_e)^{3/2}}\left[\frac{c}{\sigma}\frac{\mu_1}{\mu}\left[\frac{\epsilon}{\mu}\right]^{1/2}\right]^{1/2} \cdot\left[\left(K_{T2}+\frac{a}{2b}K_{T1}\right)\frac{\lambda_e{}^2}{\lambda_c{}^2}+Kp\frac{a}{2b}\left(1-\frac{\lambda_e{}^2}{\lambda_c{}^2}\right)\right] \qquad (5)$$

where

α = attenuation produced by wall metal
a = wide dimension of waveguide
b = narrow dimension of waveguide
c = velocity of light = 2.99776×10^{10} centimeters per second
σ = conductivity of wall metal
μ_1 = permeability of wall metal
λ_G = guide wavelength
λ_e = wavelength in unbounded dielectric
λ_c = critical guide wavelength
ϵ = dielectric constant of dielectric
μ = permeability of dielectric
K_{T1} = ratio of length of actual surface to that of an ideal surface for wide face of waveguide transverse to tube axis
K_{T2} = corresponding factor for narrow face
Kp = factor for longitudinal direction.

Bibliography

[1] Lending, R. D., "New Criteria for Microwave Surfaces." National Electronic Conference Proceedings; October, 1955.
[2] Altschuler, H. M., and Oliner, A. A., "A Shunt Technique for Microwave Measurements." Transactions of the IRE, Vol. MTT-3 (July, 1955), p. 24.
[3]* Allison, J. and Benson, F. A. "Surface Roughness and Attenuation of Precision-Drawn, Chemically Polished, Electropolished, Electroplated and Electroformed Waveguides." *Proceedings of the IEE*, Vol. 102 (March, 1955), Part B, p. 251.
[4]* Benson, F. A., "Attenuation in Nickel and Mild-Steel Waveguides at 9,375 mcs. *Proceedings of the IEE*, Vol. 101 Part III, (January, 1954), p. 38.
[5] Vogelman, J. H., "Precision Measurement of Waveguide Attenuation." *Electronics*, Vol. 26 (December, 1953), p. 196.
[6]* Benson, F. A., "Attenuation and Surface Roughness of Electroplated Waveguides." *Proceedings of the IEE*, Vol. 100, Part III (July, 1953), p. 213.
[7]* Benson, F. A., "Waveguide Attenuation and Its Correlation with Surface Roughness." *Proceedings of the IEE*, Vol. 100, Part III (March, 1953), p. 85.
[8] Miller, S. E., and Beck, A. C., "Low-Loss Waveguide Transmission." Proceedings of the IRE, Vol. 41 (March, 1953), p. 348.
[9] Pomeroy, A. F., "Improved Contact Flange for Waveguides." *Bell Laboratories Record* (March, 1953), p. 104.
[10] Simms, G. D., "The Influence of Bends and Ellipticity on the Attenuation and Propagation Characteristics of the H_{01} Circular Waveguide Mode." *Proceedings of the IEE*, Vol. 100, Part IV (January, 1953), p. 25.
[11] Chambers, R. G. and Pippard, A. B., "The Effect of Method of Preparation on the High-Frequency Surface Resistance of Metals." Institute of Metals Monograph No. 13 (1953), p. 281.
[12] Beck, A. C. and Dawson, R. W., "Conductivity Measurements at Microwave Frequencies." Proceedings of the IRE, Vol. 38 (October, 1950), p. 1181.
[13] Beck, A. C., "Conductivity Measurements at Microwave Frequencies." *Bell Laboratories Record*, Vol. 28 (1950), p. 433.
[14] Millership, R. and Webster, F. V., "High-Frequency Permeability of Ferromagnetic Materials." *Proceedings of the Physical Society, B*, Vol. 63 (1950), p. 783.
[15] Vivian, A. C., "Superficial Conductivity of Metallic Conductors for Waveguides." Telecommunications Research Establishment Technical Note No. 45 (1949).
[16] Morgan, S. P., "Effect of Surface Roughness on Eddy Current Losses at Microwave Frequencies," *Journal of Applied Physics*, Vol. 20 (1949), p. 352.
[17] Simon, I., "Measurement of permeability and ferromagnetic resonance at microwave frequencies," *Casopis pro Pestovani Mathematiky a Fysiky*, Vol. 73 (1948), p. 41.
[18] Purcell, E. M. (Chapter 8) and Weber, Ernst (Chapter 13), Vol. 11, Radiation Laboratory Series, Technique of Microwave Measurements. New York, McGraw-Hill Book Company, 1947.
[19] Frantz, G. R. and Pomeroy, A. F., U. S. Patent No. 2, 419,208, Ultra High Frequency Wavemeter, 1947.
[20] Maxwell, E., "Conductivity of Metallic Surfaces at Microwave Frequencies," *Journal of Applied Physics*, Vol. 18 (1947), p. 629.
[21] Kuhn, S., "Calculation of Attenuation in Waveguides" *Journal of the IEE*, Vol. 93, Part IIIA (1946), p. 663.
[22] Kittl, C., "Theory of Dispersion of Magnetic Permeability in Ferromagnetic Materials at Microwave Frequencies." *Physical Review*, Vol. 70 (1946), p. 281.
[23] Simon, I., "Magnetic Permeability of Nickel in the Region of Centimetre Waves." *Nature*, Vol. 157 (1946), p. 735.
[24] Allanson, J. T., "The Permeability of Ferromagnetic Materials at Frequencies Between 10^5 and 10^{10} cs." *Journal of the IEE*, Vol. 92, Part III (1945), p. 247.
[25] Hoag, J. B. and Gottlieb, N., "The Inner Initial Permeability of Iron and Nickel from 98/410 Megacycles." *Physical Review*, Vol. 55 (1939), p. 410.
[26] L. L. Wyman, "Copper and Oxygen." *General Electric Review* (March, 1934), p. 120.
[27] Hoag, J. B. and Jones, H., "Permeability of Iron at Ultra-Radio Frequencies." *Physical Review*, Vol. 42 (1932), p. 571.
[28] Johnson, K. S., "Transmission Circuits for Telephone Communications." New York, D. Van Nostrand Company, 1924

* The Benson papers list additional references.

Correspondence

Planar Transmission Lines—III*

The general theory of planar transmission lines developed earlier[1] allows one to show that there is only a certain range of dimensions within which the line will be mechanically stable and reproducible. Within this range, very simple approximate formulas for the attenuation and characteristic impedance can be given. The optimal line, with respect to both stability and attenuation, has its central conductors in the form of very narrow strips.

In the earlier communication we showed how one can compute the operating parameters (characteristic impedance, Z_0, and attenuation, α) of transmission lines made of thin conducting strips supported by dielectric slabs, as shown in cross section in Fig. 1. The study resulted in a number of more or less complex formulas in which the physical relationships were much obscured, and the question was subsequently raised whether there was at least some criterion which can be set up for a satisfactory line, accompanied by practical simplifications of the basic formulas. It has become clear what the main criterion is. This note will describe it and exhibit simple approximations to α and Z_0 for lines which satisfy the criterion.

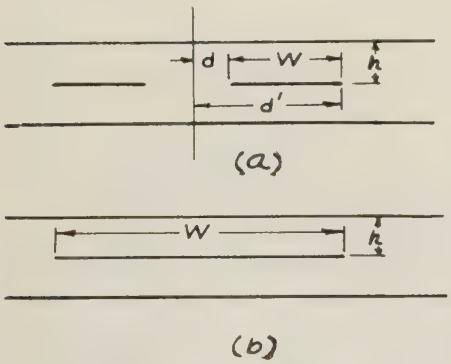

Fig. 1—Cross sections of two planar transmission lines.

If one examines Fig. 4 of I and the associated formulas, it becomes clear that the line parameters depend very sensitively on the quantity k, defined by

$$k = \frac{\sinh d/b}{\sinh d'/b} \qquad (b = 2h/\pi) \tag{1}$$

when k is in the neighborhood of 0 or 1. In such a case, a very small change in any of the dimensions of the line may result in totally different operating characteristics. Such a line is unsuitable for practical use; for stability we must require that

$$0.1 < k^2 < 0.9, \tag{2}$$

or some similar restrictive condition.

Suppose that the line has $d \geqq b$. Then it follows from (1) that to reasonable accuracy[2]

$$k^2 \approx e^{-2w/b} \tag{3}$$

and putting this into (2) results essentially in

$$0.03 < w/h < 0.75. \tag{4}$$

Thus the primary requirement on the strips is that they be relatively narrow. If the dielectric is rather thin, then the strips must be narrow ribbons, and can of course be laid at any distance apart. It seems likely, however, that convenience of manufacture would require the inequality $d \geqq b$ to be satisfied by quite a comfortable margin, and so we shall assume it to be true throughout.

If k^2 is in the middle range (2), then the complicated function $f(k^2)$ may for practical purposes be replaced by a straight line (cf. *I*, Fig. 4). One readily finds that, to within a few per cent,

$$K'/K \approx 1 - 0.91(k^2 - \tfrac{1}{2})$$

where

$$0.1 < k^2 < 0.9, \tag{5}$$

so that the characteristic impedance becomes

$$Z_0 \approx \frac{260}{\sqrt{\kappa(1 - \frac{5}{8}k^2)}} \text{ ohms} \tag{6}$$

where κ is the dielectric constant of the insulating sheets.

The attenuation in the line is given by

$$\alpha = \frac{1}{8}\eta\frac{\epsilon}{\mu}\frac{Z_0}{K^2}J, \quad \eta = \sqrt{(\pi f\mu/\sigma_c)} \tag{7}$$

for the double-strip line and four times as much for the single-strip one, where f is the frequency, σ_c is the conductivity of the conductors, and J is an integral over the boundaries of the conductors which gives the dissipation. If one calculates J under the above restrictions from (26) and (28) or (29) of *I*, one finds that the integrals simplify to

$$J_1 \approx \frac{4w}{b^2k'^2}, \quad J_2 \approx \frac{4}{b^2k'^2}\left(\ln\frac{2w}{t} - \frac{w}{2b}\right) \tag{8}$$

where t is the thickness of the inner strips. Thus, for the two types we have

$$J = J_1 + 2J_2 \approx \frac{8}{bk'^2}\ln\frac{2w}{t} \quad \text{(double strip)} \tag{9a}$$

and

$$J = J_1 + J_2 \approx \frac{4}{bk'^2}\left(\ln\frac{2w}{t} + \frac{w}{2b}\right) \quad \text{(single strip)}. \tag{9b}$$

To continue, one has to approximate the value of k'^2K^2 in the range of values we are considering. To do so we can use the highly convergent series[3]

$$\sqrt{(2k'K/\pi)} = 1 - 2q + 2q^4 + 2q^9 - \cdots,$$

where q (cf. I) is given for our purposes by $k^2/16$. Thus,

$$k'^2K^2 \approx \tfrac{1}{2}\pi(1 - \tfrac{1}{8}k^2)^4. \tag{10}$$

The figure for the attenuation thus involves the factor

$$(1 - \tfrac{1}{8}k^2)^{-4}(1 - \tfrac{5}{8}k^2)^{-1} \approx 1 + k^2 + \tfrac{5}{8}k^4 + \cdots$$

where the coefficients are only approximate. Since there is usually no necessity for an exact evaluation (especially since we have omitted the dissipation in the dielectric material), we shall write the attenuation in the two cases as

$$\alpha \approx 9\cdot3\cdot10^{-4}\eta\sqrt{\kappa}(1 + k^2)\ln(2w/t) \quad \text{(double strip)} \tag{11}$$

and

$$\alpha \approx 1\cdot9\cdot10^{-3}\eta\sqrt{\kappa}(1+k^2)[\ln(2w/t + w/2b] \quad \text{(single strip)}. \tag{12}$$

For the stable lines, these replace the approximations given in *I*.

Both formulas state that the attenuation will be decreased by decreasing w (down to rather small values). Thus, criteria both of stability and of attenuation demand that the lines be made with w very small (*i.e.* of the order of $\frac{1}{2}h$ or less) which may well conflict with considerations of technical convenience if the strips are made of foil. On the other hand, if the current to be carried is not large, it is indicated by these results that the best lines are exactly those most easily constructed by the use of printing techniques.

I would like to thank Mr. Norton Cushman for his comments on this subject.

D. Park
Fulbright Lecturer
University of Ceylon
Colombo, Ceylon

* Supported by the Sprague Electric Co., North Adams, Mass.

[1] D. Park, "Planar transmission lines," Trans. IRE, vol. MTT-3, pp. 8–12; April, 1955. This will be referred to as I. It contains the following nontrivial errors: p. 11, end: J_2 is the dissipation from both sides of one strip; p. 12, line 5: $e^{-2d/b}$ should be $e^{-2d'/b}$; p. 12, 2 lines after (34): the voltage across the two-strip line is $2K$, not K. None of the subsequent conclusions are altered. One should note also that there are two quantities denoted by w. Both are fully explained; w has one meaning prior to (17) and the other thereafter.

[2] If $d = b$, the error is about 10 per cent, decreasing rapidly as d increases.

[3] E. T. Whittaker and G. N. Watson, "Modern Analysis," Cambridge University Press, Cambridge, Eng., 4th ed., p. 479; 1927.

Phase Shift and Attenuation in a Transmission Line

Circular transmission line charts, *i.e.* Carter (Z-θ) and Smith (R-X) charts, can be used to determine the phase shift and attenuation in a uniform transmission line, or waveguide, which may be lossy and which is not terminated in a matched load. The procedure discussed here is based on the simple properties of these charts. The procedure can be extended to symmetrical four-terminal networks.

A uniform transmission line may be described by its characteristic impedance Z_0, propagation constant $\gamma = \alpha + j\beta$, and length d. The units for α and β are nepers and radians per unit length, respectively. When the transmission line is terminated in a matched load, the efficiency of power transfer is

$e^{-2\alpha d}$ and the phase shift is βd. These simple expressions for the efficiency and phase shift are not valid when the transmission line is not terminated in a matched load.

The load voltage E_L, load current I_L, input voltage E_A, and input current I_A are given by the equations

$$E_L = E_L^+(1 + K_L), \tag{1}$$

$$I_L = (E_L^+/Z_0)(1 - K_L), \tag{2}$$

$$E_A = E_L^+(e^{\gamma d} + K_L e^{-\gamma d}) = E_L^+ e^{\gamma d}(1 + K_A), \tag{3}$$

$$I_A = (E_L^+ e^{\gamma d}/Z_0)(1 - K_A); \tag{4}$$

where E_L^+ is the component of voltage at the load associated with the wave traveling toward the load, the voltage reflection coefficient K_L at the load is

$$K_L = \frac{(Z_L/Z_0) - 1}{(Z_L/Z_0) + 1}, \tag{5}$$

and the voltage reflection coefficient K_A at the input is

$$K_A = K_L e^{-2\gamma d}. \tag{6}$$

It follows from (1)–(4) that

$$\frac{E_L}{E_A} = \frac{1 + K_L}{1 + K_A} e^{-\gamma d} \tag{7}$$

and

$$\frac{I_L}{I_A} = \frac{1 - K_L}{1 - K_A} e^{-\gamma d}. \tag{8}$$

The input impedance Z_A is

$$Z_A = \frac{E_A}{I_A} = Z_0 \frac{1 + K_A}{1 - K_A}. \tag{9}$$

The efficiency η of power transfer is

$$\eta = \frac{E_L I_L \cos\theta_L}{E_A I_A \cos\alpha_A} = \frac{I_L^2 R_L}{I_A^2 R_A}$$

$$= \frac{|1 + K_L||1 - K_L| \cos\theta_L}{|1 + K_A||1 - K_A| \cos\theta_A} e^{-2\alpha d}$$

$$= \frac{|1 - K_L|^2 R_L}{|1 - K_A|^2 R_A} e^{-2\alpha d}, \tag{10}$$

where θ_L and θ_A are the angles of Z_L, and Z_A, and R_L and R_A are the resistance components of Z_L and Z_A, respectively. The efficiency can be converted into attenuation.

Circular transmission line charts provide a convenient graphical method for evaluating (7)–(10). First the normalized load impedance $Z_L' = Z_L/Z_0$ is plotted on a transmission line chart as shown in Fig. 1. This point is rotated about the center C of the chart through the angle $2\beta d$, which corresponds to d/λ, where λ is the wavelength in the transmission line. The new point is designated Z_A''. The distance $\overline{CZ_A''}$ is measured with any convenient scale and is multiplied by $e^{-2\alpha d}$. The point Z_A' is located on the line CZ_A'' at the distance $\overline{CZ_A''}e^{-2\alpha d}$ from C. (If the transmission line is lossless, $Z_A' = Z_A''$.) Lines are drawn through the points Z_L' and Z_A' as shown in Fig. 1.

Now (7)–(10) can be written

$$\frac{E_L}{E_A} = \frac{\overline{OZ_L'}}{\overline{OZ_A'}} e^{-\alpha d}, \tag{7'}$$

$$\text{angle of } \frac{E_L}{E_A} = -\left(\frac{d}{\lambda} - \frac{a}{\lambda}\right)360° \tag{7''}$$

$$\frac{I_L}{I_A} = \frac{\overline{BZ_L'}}{\overline{BZ_A'}} e^{-\alpha d} \tag{8'}$$

$$\text{angle of } \frac{I_L}{I_A} = -\left(\frac{d}{\lambda} + \frac{b}{\lambda}\right)360°, \tag{8''}$$

$$Z_A = Z_0 Z_A', \tag{9'}$$

and

$$\eta = \frac{(\overline{OZ_L'})(\overline{BZ_L'})\cos\theta_L}{(\overline{OZ_A'})(\overline{BZ_A'})\cos\theta_A} e^{-2\alpha d}$$

$$= \frac{(\overline{BZ_L'})^2 R_L}{(\overline{BZ_A'})^2 R_A} e^{-2\alpha d}. \tag{10'}$$

The distances $\overline{OZ_L'}$, $\overline{OZ_A'}$, $\overline{BZ_L'}$, and $\overline{BZ_A'}$ are measured with any convenient scale. In (7''), the sign of a/λ is positive if the point Z_L' is above the line OZ_A'; otherwise it is negative. In (8''), the sign of b/λ is positive if the point Z_L' is above the line BZ_A'; otherwise it is negative.

If Z_0 and γd are not known, their values can be determined experimentally. Let Z_{sc} and Z_{oc} denote the values of Z_A when $Z_L = 0$ and ∞, respectively. Since

$$Z_{sc} = Z_0 \frac{1 - e^{-2\gamma d}}{1 + e^{-2\gamma d}} \tag{11}$$

and

$$Z_{oc} = Z_0 \frac{1 + e^{-2\gamma d}}{1 - e^{-2\gamma d}}, \tag{12}$$

it follows that

$$Z_0 = \sqrt{Z_{sc} Z_{oc}} \tag{13}$$

and

$$\sqrt{\frac{Z_{sc}}{Z_{oc}}} = \frac{1 - e^{-2\gamma d}}{1 + e^{-2\gamma d}}. \tag{14}$$

For convenience in notation, let $D = \sqrt{Z_{sc}/Z_{oc}}$. Now

$$e^{-2\gamma d} = \frac{1 - D}{1 + D}. \tag{15}$$

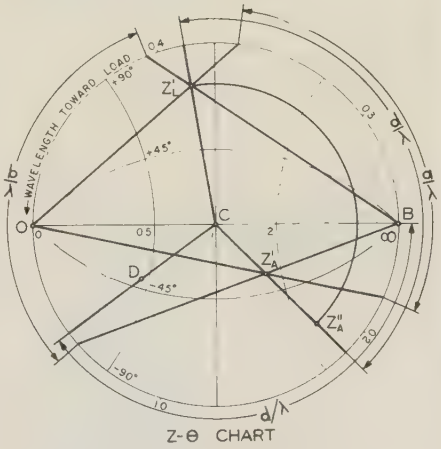

Fig. 1—Graphical construction.

When the point D is plotted on a transmission line chart as shown in Fig. 1, d/λ is measured as indicated and

$$e^{-2\alpha d} = \frac{\overline{CD}}{\overline{OC}}. \tag{16}$$

The values of the parameters for the construction shown in Fig. 1 are $Z_0 = 100/\underline{-10°}$, $Z_L = \underline{85/65°}$, $d = 0.2\lambda$, and $e^{-\alpha d} = 0.707$. The results are $E_L/E_A = 0.63/\underline{-19°}$, $I_L/I_A = 1.24/\underline{-126°}$, $Z_A = 168/\underline{-42°}$, and $\eta = 0.45$.

H. F. Mathis
Goodyear Aircraft Corp.
Akron, Ohio

A Novel Technique for Making Precision Waveguide Twists

In a recent issue of the IRE Transactions on Microwave Theory and Techniques, Wheeler and Schwiebert[1] described step-twist waveguide components having good performance over a full waveguide band. These step-twist components are composed of a few short sections of straight rectangular waveguide, twisted about their common axis at their junction faces. Typically the length of each short section of the step-twist is the order of $\frac{1}{8}$ to $\frac{1}{4}$ of a guide wavelength, while the twist angle between sections may be as much as 30 degrees.

The technique[2] described here for constructing precision waveguide twists makes use of a large number of very short adjoining sections of waveguide. Hence it can be considered as the limiting case of Wheeler's and Schwiebert's step-twist technique. The twists constructed of these short sections of waveguide can easily be made to assume very complicated shapes that would be practically impossible to construct in any other manner. Furthermore, their electrical properties, such as vswr, attenuation, and power-handling capacity, are essentially the same as those of straight sections of waveguide.

The short lengths of waveguide used in these twists are stampings formed by a precision punch and die, and consequently can be inexpensively mass produced. Fig. 1 shows two typical stampings of 0.005-inch brass sheet suitable for X-band components.

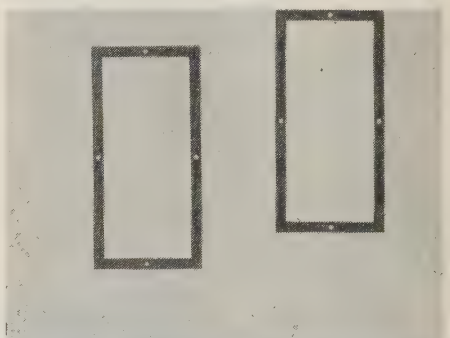

Fig. 1—Stampings used for constructing X-band precision twists.

One convenient method for aligning the stampings is to string them together on wires by means of the small holes shown in the figure. When the stampings are strung on the wires, the complete stack can then be twisted and one end translated with respect to the other in any desired manner, keeping the

[1] H. A. Wheeler and H. Schwiebert, "Step-twist waveguide components," Trans. IRE, vol. MTT-3, pp. 45–51; October, 1955.

[2] This construction technique was evolved by R. R. McPherson of Stanford Res. Inst. when called upon by the authors to make the multiple waveguide twist section described later in this letter.

two ends parallel to each other. The stack can then be compressed to assure good electrical contact between stampings. Good electrical contact can also be insured by soldering the stack, forming a solid unit which does not require continuous compression.

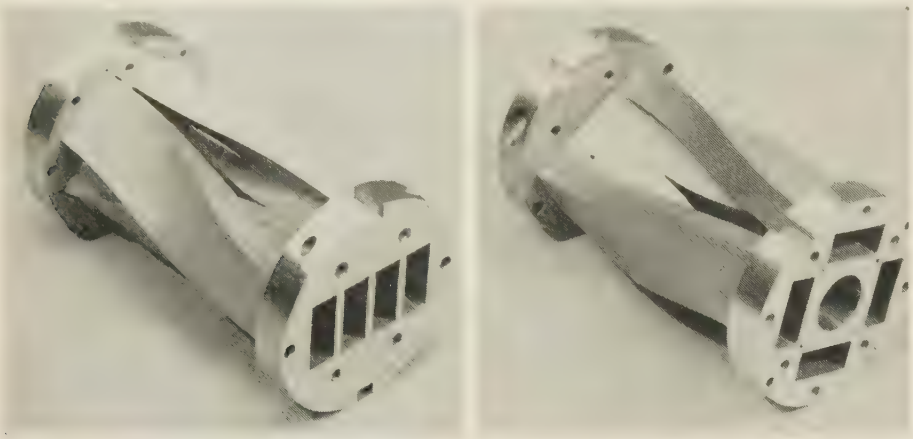

Fig. 2—Two views of a multiple waveguide twist section.

Fig. 2 shows two views of a very complex multiple waveguide twist section that was easily constructed of 0.005-inch thick brass stampings in the manner described above. In this case the assembly was soldered together in an electric oven. For the application in which this twist section was used, it was necessary that all the waveguides have the same electrical lengths to a high degree of precision. Initial measurements showed that over the 1.5 to 1 waveguide frequency range the electrical lengths of the four guides differed by as much as eight degrees due to their slightly different physical lengths. Therefore the widths of the appropriate individual guides were increased, by honing with an abrasive piston until all guides had electrical lengths within one degree of each other over this frequency range. The vswr of each guide was less than 1.02 over the full waveguide frequency range.

E. M. T. Jones and R. C. Honey
Stanford Res. Inst.
Menlo Park, Calif.

On Symmetrical Matching

It is sometimes desirable to use symmetrical matching for a symmetrical lossless discontinuity in a transmission line or waveguide. A convenient form of such matching is two equal shunt susceptances placed across the transmission line, or waveguide, at positions which are symmetrical with respect to the discontinuity. The following procedure can be used to determine the positions and value of the shunt susceptances. 1) The position P and the value B of the shunt susceptance for one-sided matching is determined. (The susceptance may be inductive or capacitive; therefore, there are two possible pairs of P and B. Either of these pairs may be used.) 2) A shunt susceptance whose value is $B/2$ is placed at the position P. 3) The second shunt susceptance is placed on the other side of the discontinuity so that symmetry is restored.

It can be shown that no other positions or values of shunt susceptance can be used for this type of matching. When symmetry is not required, two unequal shunt susceptances may be used at the positions indicated by the above procedure if their sum is B.

The above procedure is not strictly valid unless it is assumed that the discontinuity, transmission line or waveguide, and shunt susceptances are lossless. However, this procedure can often be used to obtain satisfactory matching when the losses are small.

H. F. Mathis
Goodyear Aircraft Corp.
Akron, Ohio

Contributors

J. T. Bolljahn (A'43–SM'53) was born in Oakland, Calif., in 1918. He received the B.S. and Ph.D. degrees from the University of California in 1941 and 1950, respectively. From August, 1941, until January, 1946, he was employed by the Naval Research Laboratory in Washington, D. C. From February, 1946, until September, 1949, he was a member of the staff of the University of California Antenna Laboratory.

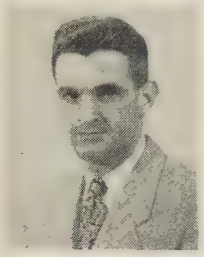

J. T. Bolljahn

Dr. Bolljahn joined the staff of the Stanford Research Institute in September, 1949, and his present position is manager of the Antenna Systems Laboratory.

He is a member of Sigma Xi, Tau Beta Pi and Eta Kappa Nu.

❖

E. H. Bradley (A'51–SM'55) was born on December 8, 1927, in Hampton, Va. He received the B.S. degree in electrical engineering, summa cum laude, from Duke University in 1949 and the M.S. degree in electrical engineering in 1950 from the Massachusetts Institute of Technology.

E. H. Bradley

Since 1950, Mr. Bradley has been employed by Melpar, Inc., of Falls Church, Va., in the development of missile guidance and submarine and aircraft detection systems. He is currently serving as section head in charge of the development of microwave components, receivers, and other electronic equipment.

He is a member of Phi Beta Kappa, Tau Beta Pi and Sigma Xi.

❖

E. K. Damon (S'50–A'52) was born in Concord, Mass., on January 3, 1928. He received his B.S. in physics in 1949 from Bowdoin College, and his M.S. in physics in 1954 from the Ohio State University. He has been with the Ohio State Research Foundation in Columbus, Ohio since 1950, and during that time has been engaged in the study of microwave filters, mixers, and ferrites.

E. K. Damon

Mr. Damon is an associate of the American Institute of Physics and Sigma Xi.

H. N. Dawirs (S'49–A'52) was born in Colorado, on July 10, 1920. He received his B.S. in electrical engineering in 1942 from Colorado State College of Agriculture and Mechanic Arts, and his M. S. in mathematics from Ohio State University in 1952.

H. N. Dawirs

From 1942 to 1946 Mr. Dawirs worked in the engineering departments of a number of Westinghouse plants. From 1946 until 1948 he worked in the research department of the Curtiss Wright Corp., Columbus plant; and since 1948 he has been with the Antenna Laboratory of the Ohio State University Research Foundation, in Columbus, Ohio.

He is a member of Pi Mu Epsilon.

❖

T. Honma was born in 1923 in Yamagata-ken, Japan. He graduated from Yamagata University in 1942 and served in the armed forces in the war.

T. Honma

After the war Mr. Honma worked at the research section of the Matsuda Research Laboratory, Tokyo Shibaura Electric Co., and has engaged in research connected with microwave measurement and microwave relay systems.

He is a member of the Institute of Electrical Communication Engineers of Japan.

❖

E. M. T. Jones (S'46–A'50) was born in Topeka, Kans., in 1924. He received the B.S. degree in Electrical Engineering from Swarthmore College in 1944 and the M.S. and Ph.D. degrees in Electrical Engineering from Stanford University in 1948 and 1950, respectively. Dr. Jones was a radar maintenance officer in the U. S. Navy from 1944 to 1946. From 1948 to 1950 he was a research associate at Stanford University, working on the Microwave Local Oscillator project. Dr. Jones joined the staff of Stanford Research Institute in 1950 where he is a senior research engineer in the microwave group of the Antenna Systems Laboratory.

E. M. T. Jones

He is a member of Sigma Tau.

For a photograph and biography of D. D. King, see p. 64 of the December, 1955 issue of Transactions of the PGMTT.

❖

R. L. Kyhl was born in Omaha, Neb., on July 27, 1917. He received the B.S. degree from the University of Chicago in 1937, and his Ph.D. in physics from M.I.T. in 1947. He has been associated with the M.I.T. Radiation Laboratory, Laboratory for Insulation Research, and Research Laboratory of Electronics, as well as the Stanford University Microwave Laboratory. He is now at the General Electric Research Laboratory.

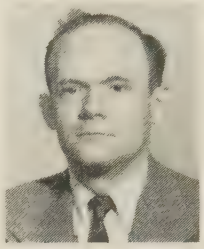

R. L. Kyhl

He is a member of the American Physical Society and Sigma Xi.

❖

B. J. Leon (S'51–A'54) was graduated from the University of Texas in January, 1954 with a B.S. in Electrical Engineering. Since February, 1954 he has been a staff member of Lincoln Laboratory. Mr. Leon is at present on leave from Lincoln in order to carry on advanced study as a teaching assistant in the Electrical Engineering Department of M.I.T. Mr. Leon is a member of Tau Beta Pi, and Eta Kappa Nu.

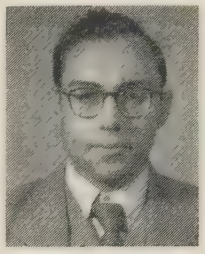

B. J. Leon

❖

E. Maxwell was graduated from Columbia University with the B.S. in Electrical Engineering. He received the Ph.D. degree in physics from M.I.T. and worked in applied geophysics for four years with Shell Oil Co., Inc. In 1941, he joined the M.I.T. Radiation Laboratory where he worked on test equipment and K band development. From 1945 to 1948 he was a research associate in physics at M.I.T. in the field of microwave superconductivity. He was a physicist in low temperature research at the National Bureau of Standards from 1948 to 1953. Since 1953 he has been a staff member of Lincoln Laboratory.

E. Maxwell

Dr. Maxwell is a member of Sigma Xi, Tau Beta Pi and is a Fellow of the American Physical Society.

A. F. Pomeroy (A'42–SM'43) was born at Buffalo, N. Y. in 1905. He graduated from Brown University with a B.S. degree in Engineering in 1929, and joined the Bell Telephone Laboratories in the same year.

A. F. Pomeroy

Mr. Pomeroy has developed various measuring sets and has investigated the properties of many types of transmission lines. Among the types of measuring equipment which he has developed are: phase, envelope-delay, attenuation, and return-loss measuring sets; power meters and current analyzers. He has studied the transmission properties of lines ranging from those used for voice frequencies to those used for microwave frequencies. His cooperation with manufacturers has led to the development of hollow, flexible waveguides and precision-drawn hollow, rigid waveguides with improved transmission qualities. He is working on ferrite structures in waveguides.

He was elected to Sigma Xi in 1929.

✣

W. L. Pritchard (A'45–M'48–SM'52) received the B.E.E. degree from the City College of the City of New York in 1943, and did further graduate study at M.I.T. between 1948 and 1951. From 1943 to 1946 Mr. Pritchard was an engineer with the Philco Radio and Television Corp., where he was engaged first in development of airborne radar systems and later of home radios and phonographs. From there he joined the Raytheon Manufacturing Co. as senior engineer, where he was engaged in developing microwave relay systems from 1946–48, in charge of rf component design from 1948–49, section head of the Microwave and Antenna Section of the equipment Engineering Division from 1949–54. During this latter time he was responsible for all rf and antenna design on Raytheon's government and commercial radars, beacons, relay systems, and microwave cooking equipment. At present he is manager of the Microwave and Transmitter Branch.

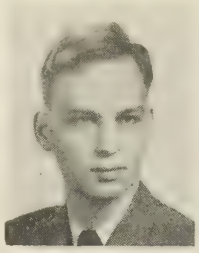

W. L. Pritchard

Mr. Pritchard is Chairman of the RETMA Committee on Waveguides and Fittings.

✣

N. Sawazaki was born in Wakayama-ken, Japan, on April 16, 1913. He graduated from Waseda University in 1938, and received the Doctor of Engineering degree in 1952.

N. Sawazaki

During the war he designed and developed radio altimeter and radar equipment at the Research section of the Tokyo Shibaura Electric Co. After the war Dr. Sawazaki engaged in research connected with the microwave measurement and microwave relay system at the research section of the Matsuda Research Laboratory, Tokyo Shibaura Electric Co., Kawasaki, Japan. He presently is chief of the research section of communication of this laboratory.

Dr. Sawazaki is secretary of the Institute of Electrical Communication Engineers of Japan, and a member of the Institute of Electrical Engineers of Japan.

✣

E. M. Suárez was born in Kingston, New York on November 8, 1929. He completed a two year course in Electrical Technology at the New York City Community College in 1950.

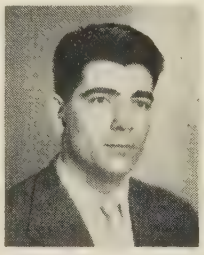

E. M. Suárez

After graduation he was employed by the Pennsylvania Railroad until he joined the Army in 1951. He attended Officers' Candidate and Officers' Radar schools at Fort Monmouth, N. J. As radar officer he was sent to Fort Sill, Oklahoma, in charge of a radar countermortar platoon.

In 1953 he joined the Bell Telephone Laboratories and is engaged in the development of broadband microwave radio relay equipment.

Mr. Suárez is presently attending evening school at Newark College of Engineering, studying electrical engineering.

INSTITUTIONAL LISTINGS (Continued)

MARYLAND ELECTRONIC MANUFACTURING CORPORATION, College Park, Md.
Development and Production of Microwave Antennas and Waveguide Components

MEASUREMENTS CORPORATION, Box 180, Boonton, N. J.
Specialists in the Design and Development of Electronic Test Instruments

MICROWAVE DEVELOPMENT LABS., INC., 92 Broad St., Babson Park, Mass.
Design, Development & Production of Waveguide Components & Complete RF Assemblies

NATIONAL INSTRUMENT CO., INC., 23 E. 26 St., New York, N. Y.
Wide-Band Microwave Equipment, Simulated Flight Instruments, Lobe Switches, Custom Built Precision Apparatus

RAYTHEON MANUFACTURING CO., 148 California St., Newton, Mass.
Microwave Communications Systems, Radar, Missiles, Cooking Equipment, Tubes & Components

WEINSCHEL ENGINEERING CO. INC., Kensington, Md.
Attenuation Standards, Coaxial Attenuators and Insertion Loss Test Sets

WHEELER LABORATORIES, INC., 122 Cutter Mill Road, Great Neck, N. Y.
Consulting Services, Research & Development, Microwave Antennas & Waveguide Components

The charge for an Institutional Listing is $50.00 per issue or $140.00 for four consecutive issues. Applications for Institutional Listings and checks (made out to the Institute of Radio Engineers) should be sent to Mr. L. G. Cumming, Technical Secretary, Institute of Radio Engineers, 1 East 79th Street, New York 21, N. Y.

INSTITUTIONAL LISTINGS

The IRE Professional Group on Microwave Theory and Techniques is grateful for the assistance given by the firms listed below, and invites application for Institutional Listing from other firms interested in the Microwave field.

AIRCRAFT RADIO CORPORATION, Boonton, N. J.
Airborne Electronic Equipment, Associated Test Equipment

AIRTRON, INC., 1102 W. Elizabeth Ave., Linden, N. J.
Microwave Mixers, Duplexers, Ferrite Devices, Flexible Guides, Castings, Antenna Components; Design & Production

CASCADE RESEARCH CORPORATION, 53 Victory Lane, Los Gatos, Calif.
Res., Dev., & Prod. Microwave Ferrite Devices, Backward Wave Oscillators & Microwave Test Equip.

COLLINS RADIO CO., Cedar Rapids, Iowa
Complete Industrial Microwave, Communication, Navigation and Flight Control Systems

ESPEY MFG. CO., INC., Congress and Ballston St., Saratoga Springs, N. Y.
Mfgrs. of X-Band and S-Band Wavemeters, Attenuators, Thermistor Mounts and Signal Generators

GENERAL PRECISION LABORATORY INCORPORATED, 63 Bedford Road, Pleasantville, N. Y.
Research, Development and Production of Microwave, Radar, Computers, Airborne Electronic Systems

GORHAM MANUFACTURING CO., Bronze Div., Dept. 781, Providence, R.I.
Waveguide Components, Rotary Joints, Mixers, Antenna Feeds, Duplexers, Plaster Cast Waveguides

(Please see inside back cover for additional names.)